Short Fatigue Crack Behaviour of a Submarine Hull Steel in Inert and Aggressive Environments

Xiaojun Wu

A Dissertation Submitted to the University of Sheffield
for the Degree of Doctor of Philosophy
in the Faculty of Engineering

Department of Mechanical and Process Engineering
University of Sheffield
January 1995

Preface

This thesis is based on the findings of research carried out in the Department of Mechanical and Process Engineering, University of Sheffield.

The content of this thesis is original, except where specific references are made to other work.

No part of this thesis has been submitted for a degree or other qualifications at any other University.

Acknowledgements

I am deeply indebted to my supervisor, Dr. R. Akid, for his valuable guidance, constant support and encouragement during the course of this project. I am sincerely thankful to Prof. K.J. Miller for his help, providing the opportunity to study in Sheffield and for many inspiring discussions.

I wish to express my gratitude to the Defence Research Agency for providing financial and technical support for this work, in particular to Mr J. C. Galsworthy and Dr. R. Jones. I am also thankful to the head of the Department of Mechanical and Process Engineering for the use of the laboratory and other departmental facilities.

I am grateful to all members of technical staff, in particular Mr J.P. Clarke, Mr J.M. Smith, Mr J.V. Goodliffe, Mr R.J. Cummins and Mr K.A. Rotchell for their assistance with the design and manufacture of equipment and specimens. I am also grateful to Dr U.S. Frenando, Dr M.W. Brown, Dr E.R. de los Rios, Dr Yi Liu, Prof. Jian Yu and all fellow research staff and students who contributed with their kind help and welcome advice.

I would like to express my gratitude to my Wife, Wei, not only for her sacrificing valuable family time for me to complete this thesis, but also for her complete support and useful discussions.

Finally, my deepest thanks must go to my parents for their endless support and patience from thousands miles away, giving me the strength to overcome every difficulty I encountered.

Summary

During the operational life of offshore structure numerous components experience the combination of seawater exposure and applied cyclic loading. As a consequence, corrosion fatigue, which consists of crack initiation and propagation has become one of the main causes of the numerous catastrophic accidents associated with offshore structures. This thesis reports on a study of the short crack growth behaviour of Q2N steel, designated for warship hulls, submarine hulls, deck railings and other offshore structural applications.

Within this thesis three main aspects of fatigue have been conducted. They are as follows;

1. **Evaluation of Short Fatigue Crack Growth in Air**

   Three-point-bend fatigue crack growth tests were conducted at various stress levels using smooth polished specimens in laboratory air. In the initial stages of the tests, short cracks were observed and found to propagate at much faster rates than those of long cracks when correlated with the linear elastic fracture mechanics (LEFM) parameter ΔK. Furthermore a period of crack growth retardation was observed at crack lengths around 50 μm. The theory of the interaction between short cracks and grain boundaries fails to predict the occurrence of this deceleration at these crack lengths. In this respect a new short crack deceleration mechanism has been considered and studied. Observation of the characteristic behaviour of short cracks, using an optical microscope and an Scanning Electron Microscope (SEM) allowed a short crack growth model to be developed based on microstructural fracture mechanics analyses.

2. **Seawater Effect on Short Fatigue Crack Growth Behaviour**

   Results obtained from a series of corrosion fatigue tests using smooth specimens in artificial seawater show that the first evidence of damage on a specimen surface is the formation of corrosion pits from which short cracks develop during the early stages of tests. Corrosion pitting is considered to play a major role during the early stages of corrosion fatigue damage. Models incorporating corrosion pitting and environment - assisted short crack growth regimes are proposed and discussed for this material - environment system.

3. **Frequency Effect on the Behaviour of Short Crack Growth**

   Frequency effects on short crack growth behaviour have been studied by conducting fatigue tests in both air and artificial seawater at cyclic load frequencies of 10, 1, 0.1 and 0.01 Hz. Experimental data obtained from tests conducted in air reveal that the fatigue lifetime, which includes both the initiation and propagation of short fatigue cracks, is little effected by changes in the applied test frequency. However fatigue strength and short crack growth behaviour within seawater appears to be heavily time dependent with fatigue lifetime decreasing significantly as the cyclic test frequency is reduced. Detailed effects of the influence of frequency on the development and growth of short cracks have been studied. Quantification of frequency effects on short crack growth behaviour is made through the introduction of a time - dependent parameter. In addition to these effects the initiation of multiple cracks, crack-crack interactions and crack coalescence have been investigated and discussed.

Nomenclature

a	=	half surface crack length
a_d	=	dominant crack length
a_p	=	pit size
c	=	half crack length plus plastic zone size
d	=	average crack length for an MSC - PSC transition
$D(s)$	=	dislocation density
da/dN	=	crack growth rate per cycle
da_d/dN	=	dominant crack growth rate per cycle
f	=	cyclic load frequency
f_c	=	crack closure factor
n	=	the number of cracks
N	=	number of loading cycles
N_f	=	fatigue lifetime in terms of number of loading cycles
P	=	applied load
r_p	=	plastic zone size
R	=	stress ratio (minimum stress / maximum stress)
S	=	length of moment arm
T	=	thickness of specimen
t	=	time
t_f	=	fatigue lifetime in terms of time
W	=	width of specimen
Y	=	stress intensity geometry factor

ΔK	=	stress intensity factor range
ΔK_{th}	=	fatigue crack growth threshold
Δr_p	=	cyclic plastic zone size
$\Delta\sigma$	=	stress range
$\Delta\sigma_{fl}$	=	fatigue limit
$\Delta\sigma_{th}$	=	stress range corresponding ΔK_{th}
σ	=	applied stress
σ_I	=	friction stress for a MSC type crack
σ_{II}	=	friction stress for a PSC type crack

Contents

Preface i

Acknowledgment ii

Summary iii

Nomenclature v

Contents vii

1 Introduction 1

1.1 General 1

1.2 Thesis Layout 2

1.3 References 4

2 Literature Review **6**

2.1 Introduction 6

2.2 Fracture Mechanics Characterization of Fatigue Crack Growth . . 7

2.3 Short Crack Problems 11

2.3.1 Short Crack Initiation 11

2.3.2 Short Crack Propagation 12

2.3.3 Modelling of Short Fatigue Cracks 14

2.4 Environment-assisted Short Fatigue Crack Growth 17

2.4.1 The Influence of Corrosive Environments on Short Crack Growth 17

2.4.2 Effect of Loading Frequency 19

2.4.3 Mechanisms of Corrosion Fatigue Short Crack Growth . . 20

2.4.4 Environment-Assisted Crack Growth Models 24

2.5 References 28

3 Material and Test Facilities **37**

3.1 Material 37

3.2 Microstructure 38

3.3 Fatigue Specimens 39

3.4 Fatigue Test Facilities 40

3.5 Crack Growth Monitoring 41

3.5.1 Plastic Replication Technique 41

3.5.2 Image Analysis System 42

3.6 Environment Control 43

3.7 References 44

4 Short Fatigue Crack Growth Behaviour in Air **45**

4.1 Introduction 45

4.2 Experimental Procedure 46

4.2.1 Long Crack Growth Tests Using a Pre-cracked Specimen . 46

4.2.2 Fatigue Lifetime and Short Crack Growth Testing 47

4.2.3 Method of Analysis 48

4.3 Experimental Results 49

4.3.1 Long Fatigue Crack Results 49

4.3.2 $S-N$ Curve 51

4.3.3 Short Fatigue Crack Growth Results 52

4.4 Modelling of Short Fatigue Cracks 54

4.4.1 Short Crack Regimes and the Crack-Tip Plastic Zone . . . 54

4.4.2 Crack Closure Effect 58

4.4.3 Short Crack Growth Rate 59

4.4.4 Fatigue Lifetime Estimation 60

4.5 Discussion 61

4.6 Summary of Air Fatigue Results 63

4.7 References 65

5 Seawater Effects on Short Crack Growth Behaviour **67**

5.1 Introduction 67

5.2 Experimental Procedure 68

5.3 Results 70

5.3.1 $S-N$ Curve 70

5.3.2 Corrosion Fatigue Crack Growth Behaviour 71

5.4 Modelling of Corrosion Pitting and Short Crack Growth 72

5.4.1 Modelling of Corrosion Pit Growth 72

5.4.2 Modelling of Corrosion Short Fatigue Crack Growth 74

5.4.3 Fatigue Lifetime Estimation 74

5.5 Discussion 76

5.6 Summary 77

5.7 References 79

6 Frequency Effects on the Growth of Short Fatigue Cracks 81

6.1 Introduction 81

6.2 Experimental Procedure 84

6.2.1 Fatigue and Short Crack Growth Tests 84

6.2.2 Method of Analysis 85

6.3 Results 86

6.3.1 Fatigue Life Results 86

6.3.2 Development of Short Fatigue Cracks 87

6.3.3 Crack Coalescence 90

6.4 Modelling of Frequency Effect on Short Crack Growth in Seawater 91

6.5 Discussion 93

6.6 Summary 94

6.7 References 97

7 Conclusions and Possible Future Work 100

7.1 Introduction 100

7.2 Conclusions 101

7.2.1 Air Fatigue Crack Growth Results 101

7.2.2 Modelling of Short Crack Growth in Air 101

7.2.3 Corrosion Fatigue Lifetime and Crack Growth Results . . . 102

7.2.4 Modelling of Corrosion Pitting and Short Crack Growth . 103

7.2.5 Influence of Test Frequency on Fatigue Behaviour 103

7.3 Recommendations for Future Work 104

Chapter 1

Introduction

1.1 General

Q2N, a quenched and tempered high strength offshore and marine structural steel has been selected as a suitable material to replace low strength structural steels, such as Q1N, for offshore applications where improved strength is required. The mechanical test data of this steel exhibits improved tensile strength properties and retains good toughness when compared to Q1N [1]. In service a submarine pressure hull and other offshore structures experience the combination of seawater exposure and cyclic stresses. This combination of alternating stress and exposure to seawater may promote fatigue crack initiation and growth, *i.e.* Corrosion Fatigue, a phenomenon which has been the cause of numerous catastrophic accidents associated with offshore structures [2].

Conventional approaches to fatigue design involve the use of $S-N$ curves, representing the total life resulting from a given stress (or strain) amplitude, suitably

adjusted to take into account effects of mean stress; effective stress concentrations at notches; variable amplitude loading; and so forth. In this method the fatigue damage fraction related to 1 cycle at a specified stress or strain level is defined by the life fraction $1/N_f$ derived from the $S - N$ curve.

The crack growth predictions based on a linear elastic fracture mechanics (LEFM) approach are related to a physically measurable damage quantity, that is, the propagating crack length. The LEFM relationship established for a particular material is derived from experimental data obtained from laboratory tests where test pieces containing pre-existing cracks of the order of 10 - 20 mm are used. However many component defects encountered in service are far smaller than this and it is often the case that a large proportion of the total fatigue life of a component is taken up in the development of short cracks. Numerous results recently obtained show that those cracks whose sizes are comparable to the material microstructure dimensions grow at much higher rates than those predicted from the LEFM relationship established for long cracks [3] [4] [5] [6]. Furthermore short cracks having an initially high growth rate are observed to decelerate or even partially arrest before attaining growth rates of typical long crack data obtained from pre-cracked specimens. The consequence of this retardation in growth has been rationalized as a result of crack interactions with microstructural features, for example grain boundaries [7] [8] [9].

1.2 Thesis Layout

The main objectives of this study are to characterize the short fatigue crack growth behaviour of Q2N steel and to propose short crack growth models for both inert, *i.e.* air, and aggressive environments. In addition, the effect of loading

frequency on both fatigue lifetime and short crack growth behaviour has been studied.

This thesis consists of 7 chapters. Chapter 2 presents a literature review on background material relating to this research project. The material, specimen design, basic test facilities and techniques are explained in Chapter 3. Short crack growth results obtained at various stress levels in laboratory air are given in Chapter 4 in which a short crack growth model based on the application of a microstructural fracture mechanics approach is also proposed. Chapter 5 presents the results of the effects of seawater on fatigue strength and short crack development and growth. Short crack growth models for predicting corrosion fatigue lifetime are proposed and discussed. The influence of test frequency on the behaviour of short fatigue cracks is given in Chapter 6. Additionally the initiation of multiple cracks, crack-crack interactions and crack coalescence are investigated and discussed. The main conclusions drawn from the present work and suggestions for possible future work are given in Chapter 7. Where figures and references are cited within a chapter, details of these are presented at the end of each chapter.

1.3 References

[1] Galsworthy J.C. (1990) Low frequency corrosion fatigue behaviour of Q2N steel. Admiralty Research Establishment, Holton health, Poole, Dorset, Report No ARE TM(UMM) 90419.

[2] Smith R.A. (1984) Thirty years of fatigue crack growth - an historical review. Proceedings of a conference on fatigue crack growth (Eds. R.A. Smith), Pergamon Press, pp1-16.

[3] Pearson S. (1975) Initiation of fatigue cracks in commercial aluminium alloys and subsequent propagation of very short cracks. Engng Fract. Mech., 7, 235 - 247.

[4] Tanaka K., Hojo M. and Nakai Y. (1983) Fatigue crack initiation and early propagation in 3% silicon iron. In: Fatigue Mechanisms - Advances in Quantitative Measurement of Physical Damage, ASTM STP 811 (Eds. J. Lankford, D. L. Davidson, W. L. Morris and R. P. Wei) Amer. Soc. Test. Mat., Philadelphia, PA, 207 - 232.

[5] Hudak S.J. (1981) Small crack behaviour and the prediction of fatigue life. J. Eng Mat. Tech., 103, 26 - 35.

[6] Lankford J. (1983) The effect of environment on the growth of small fatigue cracks. Fatigue Fract. Eng. Mat. Struct., 6, 15 - 31.

[7] Miller K.J. (1987) The behaviour of short fatigue cracks and their initiation. Part II - A general summary. Fatigue Fract. Engng. Mater. Struct., 10, 93 - 113.

[8] Morris W.L. (1979) Microcrack closure phenomena for Al 2219 - T851. Metall. Trans., 10A, 5 - 11.

[9] Tanaka K., Nakai Y. and Yamashita M. (1981) Fatigue growth threshold of small cracks. Int. J. Fract., 17, 519 - 533.

Chapter 2

Literature Review

2.1 Introduction

For more than a century, metal fatigue has been the subject of numerous research studies conducted by mechanical engineers, materials scientists and structural engineers from which a large number of papers have been published concerning aspects of damage mechanisms, lifetime prediction and failure analysis. The literature review presented here contains those studies closely related to this research program. A brief review is first given to the fracture mechanics characterization of fatigue crack growth. This is followed by recent developments concerning short fatigue crack studies. Finally, the effect of environment on short crack growth behaviour is reviewed.

2.2 Fracture Mechanics Characterization of Fatigue Crack Growth

The Linear Elastic Fracture Mechanics (LEFM) approach to correlating fatigue growth problems begins with characterizing the local stress and deformation fields at the crack tip. This was achieved through continuum mechanics analysis. For the linear elastic behaviour of a stationary mode I crack, the local crack tip stresses σ_{ij} can be characterized in terms of the K_I singular field [1]:

$$\sigma_{ij}(r,\theta) = \frac{K_I}{(2\pi r)^{1/2}} f_{ij}(\theta) + O(r^{1/2}) + ... \tag{2.1}$$

Where K_I is the mode I stress intensity factor; r is the distance ahead of the crack tip; θ is the polar angle from the crack plane; and f_{ij} is a non-dimensional function of θ. $O(r^{1/2})$ approaches zero when $r \rightarrow 0$.

According to the original analysis by Paris [2], for cracks subjected to cyclically varying loads, the crack growth rate, da/dN, can be described in terms of a power law function of the stress intensity factor range ΔK, that is

$$da/dN = C(\Delta K)^m \tag{2.2}$$

Where C and m are experimentally determined constants. This relationship has been viewed as a major breakthrough, for the assessment of the integrity of a structure, when compared to the use of conventional $S - N$ curve total life analyses [3]. It is important to note that Equation 2.2 is a continuum mechanics characterization and does not require a quantitative knowledge of the microscopic behaviour of individual fracture events, and thus the analysis is independent of

the specific micro-mechanism of crack growth.

For safety-critical structures, there has been a growing awareness that the presence of defects, below a certain size, in a material must be assumed and considered at the design stage. In this case the integrity of a structure will depend on the lifetime spent in crack propagation. This consideration has led to the adoption of the so-called 'defect tolerant' approach, which has been used for various applications for example in the aerospace industries. To account for different service conditions experienced by components and structures this technique has been modified to incorporate effects such as mean stress effects, variable amplitude loading and different environments. Such methods are based on the original Paris power law Equation 2.2, and thus belong to the so-called Paris long crack fracture mechanics regime.

The relation between fatigue crack growth rate, da/dN, and the stress intensity factor range ΔK is shown in Figure 2.1. It should be noted that the form of Equation 2.2 holds over only a limited range of crack propagation rates. The diagram derived from experimental data shows three regimes; the central linear part of the curve, *i.e.* stable fatigue crack growth, is represented by the Paris power growth law as described above. Experimental values of da/dN in this region are weakly dependent on microstructure, mean stress and environment. Below this region, *i.e.* at lower ΔK values, crack growth is dependent on the material's microstructure. There exists a threshold stress intensity factor, ΔK_{th}, below which no crack growth occurs. The upper region at high ΔK values represents rapid crack growth at increasing growth rates. Final fracture occurs when $K \geq K_c$, the fracture toughness.

Fatigue life can be estimated by integrating the Paris Equation 2.2 as shown in

Equation 2.3

$$\int_0^N dN = \int_{a_1}^{a_2} \frac{da}{C(\Delta K)^m} \tag{2.3}$$

Where N is number of cycles and a_1 and a_2 are initial and final crack lengths respectively.

ΔK can be expressed in terms of a geometry factor, stress and crack size as

$$\Delta K = Y \Delta\sigma\sqrt{\pi a} \tag{2.4}$$

Where Y is a function of the geometry of the test specimen and of the instantaneous crack size, a.

An important attribute of fracture mechanics, as applied to fatigue, is that Equation 2.3 can be applied to defects contained within most engineering components, assuming a knowledge of ΔK values is available.

One of the principle limitations of this approach, specifically of the adoption of ΔK_I as a valid description of the crack tip stress - strain field, is that a state of small scale yielding must exist. Calculation of the extent of this region varies according to the mode of applied loading and the geometry of the body [5]. An approximate estimate of the plastic zone size (r_p) ahead of a monotonically loaded crack is given by:

$$r_p = \frac{1}{2\pi}(\frac{K_I}{\sigma_y})^2 \tag{2.5}$$

where σ_y is the yield strength. The condition of small scale yielding requires that the extent of local plasticity is small compared to the extent of the K_I field and thus the K_I field can be assumed to dominate the region around the crack tip.

Following the analysis by Rice [5], the cyclic plastic zone size (Δr_p) is about a quarter of the size of the monotonic zone:

$$\Delta r_p = \frac{1}{2\pi}(\frac{K_I}{2\sigma_y})^2 \tag{2.6}$$

Elastic-Plastic Fracture Mechanics (EPFM) methods may be applied when the small scale yielding condition does not apply, *i.e.* when the plastic zone at the tip of the fatigue crack itself is comparable in size with the crack length. Since the use of the K_I singular field is no longer appropriate alternative analyses have been developed to define the crack tip stress and strain fields in the presence of extensive local plasticity. A significant development in characterizing these local fields is given by the Hutchinson, Rice and Rosengren (HRR) singularity based on the deformation theory of plasticity[6][7]. The important parameter in the HRR theory is the so-called J-integral [7] which is analogous to K_I and characterizes the crack tip field under elastic-plastic conditions. Some authors [8] have proposed a power law correlating the fatigue crack growth rate, under plastic conditions, to the applied J range:

$$da/dN = C'(\Delta J)^{m'} \tag{2.7}$$

Where C' and m' are material constants. An alternative method of analysis to that of the J-integral is one which adopts the concept of crack tip opening displacement, CTOD(δ_t) [9], where CTOD can be taken as a measure of the intensity of the elastic-plastic crack tip field and may be correlated with fatigue crack growth rates, *i.e.*:

$$da/dN \propto \Delta\delta_t \qquad (elastic-plastic) \tag{2.8}$$

2.3 Short Crack Problems

2.3.1 Short Crack Initiation

Studies concerning crack initiation have primarily focused on explaining the mechanisms of fatigue crack formation and, as such, are still predominantly qualitative.

Initiation of fatigue cracks has been observed to occur along slip bands, in grain boundaries and at discontinuities such as second phase particles, inclusions and voids where the mode of initiation appears to depend upon which process occurs most easily. In general, the weak points in a material and/or high strain localisations are more likely to serve as nucleation sites for cracks.

The mechanism of crack initiation in high strength or brittle metals may not involve slip band formation. Microcracks are often formed directly at inclusions or voids [10][11]. In ductile materials slip often occurs. Morris *et al* [12] indicated that for non-defective ductile metals, which are subjected to low or intermediate stress amplitudes, the initiation of cracks is generally related to the development of slip bands which results from the movement of dislocations.

The surfaces of engineering components, even the best prepared surfaces, invariably have micronotches to a depth of 2 - 3 μm and unavoidably contain microstructural discontinues such as grain boundaries, triple points and surface breaking inclusions. These machining marks and microstructural defects can lead to the initiation of cracks which can occur within the first few loading cycles. For most practical cases, at stress levels above and just below the fatigue limit, microcrack initiation in polycrystalline metals can therefore be assumed to occur almost immediately. From an engineering standpoint it appears appropriate that

attention should to be given to the nature of engineering surfaces rather than to a more detailed study on dislocation structures associated with extrusion - intrusions developing from very smooth surfaces [22].

More recent studies [14][15] have involved the initiation behaviour of multiple short cracks. The results of such studies are of increasing interest since the mechanism of fatigue damage is changed from that of the growth of a single crack to that of multiple crack coalescence.

2.3.2 Short Crack Propagation

In order to appreciate the behaviour of short cracks, detailed crack type demarcation is shown in Figure 2.2 [22] in which crack growth behaviour was separated into three regimes, namely:

1. Microstructurally short cracks (MSC), $a < d_3$.
2. Physically small cracks (PSC), $d_3 < a < l$
3. Long LEFM cracks, i.e. $\Delta\sigma < 2/3\Delta\sigma_y$.

Extensive experimental studies have revealed that short cracks propagate in a manner that is 'anomalous' to long crack behaviour. Furthermore this anomalous growth occurs in both the microstructurally short crack and physically small crack regimes.

Microstructurally short crack growth behaviour was first reported by Pearson [16] in his study of precipitation hardened aluminium alloys. The results showed that,

for a nominally identical stress intensity factor range ΔK, microstructurally short cracks grow at a rate several times greater than those of long cracks. Other workers [17] [18] [19] [20] have also noticed the lack of correlation between data for long and for microstructurally short cracks, as shown for example in Figure 2.3 which presents crack growth data for peak aged 7075 aluminium alloy [20]. Cracks with an initially higher growth rate were also observed to decelerate or, in certain cases, show momentary arrest before merging with the long crack data, see Figure 2.3.

The consequence of this 'anomalous' crack growth behaviour has been rationalized as a result of the interactions between short cracks and the texture of a given material [21][22][23][24] [25]. Textural effects include crystallographic orientation, size and shape of grains, the size and distribution of second phases and inclusions and cyclically induced micro- and macro-anisotropy. It is now widely recognised that the implementation of microstructural fracture mechanics (MFM) is necessary to quantify the crack growth behaviour of cracks having sizes of the order of the microstructural dimensions of the material.

Physically small cracks are those cracks having a size comparable to the scale of the local plasticity. Unlike MSC growth which is mainly dependent upon microstructural features, as described above, PSC growth is more dependent upon stress level and crack length since stress levels must be higher if crack growth is to continue above the fatigue limit stress. The growth rate of PSC was also found to be much higher than the equivalent long crack growth rates based on LEFM analyses [26][27][28]. A reason postulated for this anomalous behaviour is the greater degree of plasticity induced at the crack tip which is a significant factor in determining crack propagation.

2.3.3 Modelling of Short Fatigue Cracks

Considerable effort has been made concerning the modelling of short cracks and in this respect various models have been proposed. As previously discussed short fatigue cracks often propagate more rapidly than crack growth rates predicted from LEFM analyses. This 'anomalous' behaviour has led to a number of models adopting a 'modified' LEFM approach. For example, El Haddad *et al.* [27] hypothesized that short cracks behave as if they were a length a_0 longer than their true length and proposed the following relationship;

$$\Delta K = Y\Delta\sigma\sqrt{\pi(a + a_0)} \tag{2.9}$$

where a_0 is a constant for a given material and material condition and is related to material texture. As described by El Haddad *et al.*, the value of the intrinsic crack size a_0 can be calculated from the threshold stress intensity and the alloy fatigue endurance limit. For steels, a_0 increases with alloy grain size and decreases with alloy yield strength [27]. This expression frequently provides a good description of the relationship of crack length to ΔK, but there is no physical insight into its explanation or a limiting condition, for example, when a tends to zero.

In view of the consideration that stresses must be higher if short cracks are to grow above the threshold level more elaborate methods of elasto - plastic fracture mechanics (EPFM) have been considered. Using EPFM analyses four parameters have been developed and applied to characterize short fatigue crack growth namely; the strain intensity factor ,ΔK_ϵ, [29], cyclic J integral, ΔJ, [8], crack tip opening displacement, δ, [30], and the plastic zone size, r_p, [9][31]. it is suggested that these models provide a suitable approach for describing physically small cracks however for microstructurally short cracks such deterministic treatments may simply not apply.

In order to consider the influence of microstructure on short crack growth, as mentioned in Section 2.2, Hobson and Brown [32] suggested a crack growth model based on two equations; one for MSC growth and one for PSC growth. Miller *et al* [13] formulated crack growth equations in terms of the plastic shear strain range, γ_p. For constant stress amplitude test data, the short crack growth regime could be described by:

$$da/dN = C_1(d-a) \qquad MSC \quad growth \tag{2.10}$$

$$da/dN = C_2 a - D \qquad PSC \quad growth \tag{2.11}$$

where

$$C_1 = A(\Delta\gamma)^{\alpha} \qquad C_2 = B(\Delta\gamma)^{\beta} \tag{2.12}$$

A, B, α, β are material constants, d represents the distance to the major microstructural barrier affecting crack growth and D represents the threshold condition. The crack growth behaviour described by this model is shown schematically in Figure 2.4.

Yates and Grabowski [33] and Zhang [34] found in their experimental study on Waspaloy that a grain boundary caused deceleration in crack growth not only in the first grain, but also extended to subsequent grains, hence they proposed a model taking multiple grain boundary barriers into consideration for the microstructurally short crack growth, *i.e.*

$$da/dN = C_1(d_i - a) \tag{2.13}$$

where $C_1 = f(\Delta\sigma, R)$ and d_i is the distance from the initiation site to the next barrier.

Navarro and de los Rios [35] [36] concerned themselves with the elastic - plastic interface coinciding with a grain boundary at every instant, and solved in a single equation the distributed dislocation function either bounded or unbounded. This model describes the whole fatigue process, including the difference between the short and long crack regimes and their transition. Here crack growth rate is assumed as

$$da/dN = f\phi \tag{2.14}$$

where f is the fraction of dislocations on the slip band which participate in the process of crack extension and is a function of stress. ϕ is the crack tip plastic displacement and is expressed as

$$\phi = \frac{2k}{G}\frac{\sqrt{1-n^2}}{n}\sigma a \tag{2.15}$$

where G is the shear modulus, k equals 1 for screw dislocation motion and $1-\nu$ for edge dislocation motion, σ is the applied stress, n is the ratio of a/c where c is the crack length plus the plastic zone size. Modification of this model to quantify the strength of microstructural barriers [37] and involve strain hardening [38] has recently been achieved.

Since short crack growth rates usually show a degree of scatter probabilistic models of short fatigue crack growth have been developed. Cox *et al* [39][40] and Wang *et al* [41] draw a direct link between stochastic microstructure and the statistics of measured short crack growth rates. These models are formulated as semi-Markov and non-stationary Markov processes respectively. Statistical investigations involving the problem of multiple small cracks have also been conducted [42] [43] [44] and Monte Carlo simulation analyses have been applied to the prediction of fatigue lifetime [45] [46]. These statistical models assume that microstructure - related mechanisms control growth rates in a given material.

However a requirement of these models is the incorporation of a parameter describing the microstructure and quantitative relationships describing the effects of grain boundary blockage and closure effects upon crack propagation. Such models should be based on a physical understanding of short crack behaviour.

2.4 Environment-assisted Short Fatigue Crack Growth

2.4.1 The Influence of Corrosive Environments on Short Crack Growth

A review of the literature shows that, in comparison to data available on short crack behaviour in air, experimental results concerning crack size effects within deleterious environments is limited to a small number of research studies.

Existing work concerning experimental investigations of corrosion fatigue short crack behaviour has been focused almost exclusively on structural and alloy steels stressed in aqueous chloride solutions with a composition approximating that of seawater. A recent review [47] concluded that small corrosion fatigue cracks grew at rates faster than expected and that the magnitude of the crack size effect, in terms of the increase in crack growth rates of short cracks over long cracks, varies from 50% to several hundred percent depending on the steel yield strength and electrochemical variables.

For high strength 4130 steel in 3% NaCl solution, experimental results indicate that the effect of the environment on the growth of short cracks can be sub-

stantially larger than that for long cracks, even when the crack is long in the mechanical and metallurgical sense. The crack growth rate for short cracks was about ten times faster than that of long cracks at the same nominal ΔK level and in the same bulk environment. The effects of stress-level on the environmental enhancement of short crack growth were also recorded[48].

For medium strength alloy steels exposed to aggressive environments short corrosion fatigue cracks grow faster than long cracks for identical environmental conditions. However, the magnitude of the effect is small compared to those in high strength steel [47]. Experimental result for HY130 in 3.5 % NaCl obtained by Tanaka and Wei [49] shows that short cracks grow twice as fast as long cracks in the same bulk environment. When the crack length exceeded 1.1 mm crack growth rates become equal to those of long cracks. The additional enhancement of the growth rate of short cracks in 3.5% NaCl, having lengths less than 1.1 mm, is ascribed to the local crack-tip chemistry which is different not only from the bulk solution but also from the local crack - tip chemistry of a long crack subjected to the same stress intensity range.

For low strength steels the effect of crack size and shape on crack growth rate has to-date not been fully understood. Bardal *et al* [50] reported that small edge cracks which lie between 1 and 3 mm in length grow up to three times faster than long cracks (3 to 7 mm) during exposure to seawater in the freely corroding condition. Cathodic polarization has little effect on the growth rates of deep cracks in seawater however the kinetics of shallow cracks are significantly reduced relative to corrosion and grow at rates less than the long crack case. Very recent work for BS4360 50D low strength steel in 0.6 M NaCl solution by Akid [51] shows that there is significant difference between the "in air " and "environmental" fatigue lifetimes and short crack growth behaviour of specimens tested at stress

levels around and below the "in air " fatigue limit. This difference is ascribed to the difference in initial defect development where localized corrosion processes such as pitting and dissolution - assisted shear crack development provide a major contribution to overcoming microstructural barriers to fatigue crack development and growth. However for high stress levels and/or long crack lengths ($> 1mm$), experimental crack growth results show there to be little effect of the environment when compared to equivalent tests in air.

2.4.2 Effect of Loading Frequency

Frequency effects on corrosion fatigue crack growth rates have received extensive attention as corrosion fatigue is essentially a time-dependent process. Low frequency loading , especially at low stress amplitudes, provides more time for the interaction of the environment with the fatigue crack causing greater damage. Conversely, high frequencies, particularly when a high stress amplitude is involved tend not to affect fatigue lifetime.

Holroyd *et al* [52] reported that crack growth the rate of a 7017 - T651 aluminium alloy in seawater at frequencies from 0.1 to 70 Hz are significantly influenced by loading frequency, *i.e.*, crack growth rate increased when the loading frequency is decreased, see Figure 2.5. The effect of loading frequency were also reported by Pao *et al* [53]. Their results, obtained on AISI 4340 steel at room temperature and at a water vapour pressure of 585 MPa for various loading frequencies, are shown in Figure 2.6. This figure clearly shows that the rate of fatigue crack growth, below K_{ISCC}, increases to a greater extent at low frequencies than at higher test frequencies in the presence of water vapour.

From the literature review conducted to-date only a limited amount of data on the effects on loading frequency on small cracks have been found. From the study conducted by Gangloff and Wei [47] the corrosion fatigue crack growth rates for API - 2H steel in 3% NaCl at various frequencies were found to be equivalent to that measured for long cracks.

2.4.3 Mechanisms of Corrosion Fatigue Short Crack Growth

Numerous experiments have been performed to investigate the mechanisms of corrosion fatigue in metals. The possible mechanisms for the interactions between corrosive environments and fatigue cracks suggested by these investigations have generally incorporated one of the following processes; (1) adsorption of an active species, *eg* Cl^-, (2) anodic dissolution, (3) film rupture, and (4) hydrogen embrittlement.

The range of influence of adsorption is only one or two atomic planes from the surface of the metal and hence adsorption can only influence the tensile strength and shear stress of the interatomic bonds in close proximately to the crack tips. Adsorption could however promote crack growth by facilitating either tensile-decohesion or dislocation nucleation at crack tips. Inhibiting the nucleation of dislocations by adsorption could also possibly lead to embrittlement by favouring crack growth by tensile-decohesion rather than slip but would probably not produce sub-critical crack growth [54].

Several possible corrosion fatigue mechanisms related to anodic dissolution have been suggested. These include; (1) pitting induced crack initiation and short crack growth, (2) anodic dissolution interacting with active slip bands at the crack tip,

and (3) grain boundary oxidation-induced intergranular corrosion crack initiation and propagation.

In the case of a low stress level and a low loading frequency pits may play a major role in short fatigue crack initiation and propagation. Akid [51] observed short fatigue crack initiation at the corner of pits. When pit-depth together with the initiated short crack depth exceeded a critical length, short fatigue cracks propagated at increasing crack growth rates.

The mechanism of film-rupture is generally accepted as a factor in stress corrosion. For corrosion fatigue, this mechanism depends upon the applied stress/strain level and may only be applicable where loading frequency are exceptionally low and where any surface films formed act to limit corrosion at the crack tip by providing a barrier between metal and environment. It suggests that during cyclic loading an oxide film, formed on the specimen surface, is damaged mechanically by slip steps emerging from beneath the surface causing dissolution of the more anodically-active bare metal exposed to the corrosion environment. This may result in rapid dissolution and/or the development of a stress concentration leading to crack nucleation and propagation at the point of rupture. Two different attempts have been made to rationalize crack growth in terms of this mechanism [55][56][57]:

1. A fresh surface is created every fatigue cycle, without further influence by the remaining crack strain in the cycle, or
2. A fresh surface may be created many times during one cycle.

The latter assumption is based on the fact that the amount of crack tip strain, accompanying the rising-load half-cycle, is many times the fracture strain of any

solid reaction product such as an oxide. This amounts to a high-strain rate form of stress-corrosion cracking during each rising-load cycle. Ford and Hudak [58] proposed a film rupture/slip dissolution model for ductile alloy/aqueous environment systems. However in this model, a basic uncertainty still remains concerning the definition of the crack tip strain rate.

Hydrogen embrittlement plays a major role in cathodic reaction-related corrosion fatigue. There are several possible mechanisms put forward to explain hydrogen effects including: (1) a critical hydrogen concentration which induces decohesion, (2) hydrogen enhanced crack tip plasticity and (3) hydrogen trapping induced intergranular short crack initiation and growth [59].

The general idea of hydrogen induced decohesion was considered by Troiano [60] and Oriani [61] as being inherent to ductile fracture. This emerged as a valid quantitative model, particularly when it was used for the interpretation of metalloids effects. It was suggested that second phase particle decohesion, crack nucleation and crack propagation at low hydrogen fugacity, all involve fracture of atom bonds at the crack tip. The basic assumption for a decohesion mechanism is of a brittle crack tip. Oriani and Josephic [62] suggested that kinetic laws favour an irreversible, rather than a reversible process, but local flow processes can be so complex that a sufficiently accurate kinetic model is not yet available to decide this issue.

It has been suggested that the mechanism of hydrogen enhanced crack tip plasticity may be applicable in ductile materials. Beachem [63], on the basis of observations made after applying various degrees of deformation to a material degraded by hydrogen (particularly on the lowering of the torsional flow stress in a 1020 steel), proposed a hydrogen assisted cracking theory in which the role of hydrogen

was one of augmenting dislocation motion. Enhanced dislocation motion by hydrogen is now definitely established, with the extent of material softening being dictated by enhanced screw dislocation mobility, enhanced dislocation injection at surfaces and the promotion of shear instabilities.

Hydrogen attack on grain boundaries is another major effect in corrosion fatigue. Several published papers show that hydrogen induced-grain boundary decohesion is associated with impurity-hydrogen interaction and dislocation trapping of hydrogen in grain boundaries. Many of the elements which are found segregated at a grain boundary (*i.e.* the metalloid elements), act as catalytic poisons for the hydrogen evolution reaction in electrolytes hence they stimulate hydrogen adsorption. The significance of recombination poisons was pointed out by Latanision and Opperhanser [64] in a study of the intergranular embrittlement of nickel by cathodically produced hydrogen.

The permeation of hydrogen into crystalline materials may occur in part by lattice diffusion, by grain boundary, or other short circuit diffusion or, as is the case in specimens undergoing plastic deformation, by dislocation transport. In the latter instance, the transport of hydrogen occurred in the form of Cottrell atmospheres dragged by mobile dislocations[65][66].

The influence of crack coalescence during fatigue has been observed both in air and in corrosive environments [14][42][45][67]. Kitagawa *et al* [45] investigated a rail steel and a high strength steel in aqueous environments on unnotched specimens, observing that, even for corrosion fatigue in a mildly aggressive environment such as distilled water, cracks of surprisingly high density (> 400 cracks/cm^2) were initiated and that the fracture process could be characterized by the interaction and connection of these small distributed cracks. Very recent

experiments on various pH solution conditions [15] indicate that the corrosion fatigue process of BS4360 50B steel involved initiation and propagation of short cracks and crack coalescence events, especially for low pH solution conditions. A computer simulation model [43] which incorporates continued crack nucleation and propagation with increasing number of cycles and a crack coalescence criterion was established for this material-environment system.

A summary of possible mechanisms involved in an environment-assisted-cracking system is presented schematically in Figure 2.7 [68]. Some evidence has shown that several mechanisms may occur simultaneously in one system.

2.4.4 Environment-Assisted Crack Growth Models

Several attempts have been made to develop crack growth models within aqueous corrosive environments which incorporate the various mechanisms of environment-material interaction.

Wei and Landes [69] first proposed a superposition model which summed the stress corrosion component of crack growth with that of air fatigue crack growth. This model can be expressed as

$$(da/dN)_{cf} = (da/dN)_r + \int da/dt K(t) dt \qquad (2.16)$$

where $(da/dN)_{cf}$ is the rate of fatigue crack growth in an aggressive environment, $(da/dN)_r$ is the rate of fatigue crack growth in an inert environment and integral term is the environmental contribution obtained from sustained load crack growth observed in the same environment. This model takes no account of synergistic interactions between corrosion and fatigue, nevertheless good agreement

was obtained between the experimental and predicted lifetime. Furthermore the effects of frequency, stress ratio and wave-shape were also satisfactorily predicted using this model [69] [70].

A model known as 'The Process Competition Model' was suggested by Austen and Walker [71]. The basis of this model is that the processes of the stress corrosion and fatigue (or true corrosion fatigue) are mutually competitive and not additive as postulated in the Wei and Landes model [69]. Here it is assumed that the crack will propagate by the fastest available mechanism pertinent to the prevailing stress intensity. The model may be presented as;

$$(da/dN)_{cf} = max[(da/dN)_r,\ (da/dt)1/f] \tag{2.17}$$

where $(da/dN)_{cf}$ and $(da/dN)_r$ represent fatigue crack growth in aggressive and inert environments respectively and the final term accounts for the stress corrosion contribution. The influences of high frequencies on the stress corrosion plateau crack growth rate are predicted better than those of low frequencies in this model. To ensure compatibility in terms of crack growth rate per cycle rather than per second, the main idea is that the plateau velocity must be adjusted to the appropriate frequency and stress ratio [72][57]

Other models [72][73][74] have modified the above assumptions by adding further parameters. These prediction models generally provide higher crack growth rates when compared to experimentally observed growth rates. Microscopic crack branching or secondary cracking or alternating ion concentration at the crack tip may complicate the situation.

Mechanistically based models [57][75] regards the environmental effect as arising from the superposition of a strain-rate-sensitive stress corrosion process on an

inert environment fatigue crack growth process given by the familiar Paris equation. The environmental component is related to the breaking of a protective oxide film at the crack tip, by the dynamic strain, when the oxide rupture strain $\dot{\varepsilon}_f$ is exceeded. The environmental crack growth rate da/dt is a function of the crack tip strain rate $\dot{\varepsilon}$:

$$(da/dt)_{cf} = C\dot{\varepsilon}^n \tag{2.18}$$

where C and n are constants. The disadvantage of this quantitative analysis is the need to calculate the crack tip strain rate.

A dissolution based model for microstructurally short and physically small crack growth was introduced by Akid and Miller [76]. It was proposed that for torsional loading anodic dissolution at the crack tip was the major electrochemical reaction contributing to crack advance. The most significant effect observed was that of an elimination of the in-air fatigue limit. An explanation given for this was that an additional chemical driving force was available for crack growth at sub-fatigue limit stresses and that dissolution allowed growth beyond crack arresting features associated with the microstructure.

Raj and Varadan [77] proposed a hydrogen assisted crack growth model for high strength steels. In their model the crack propagates by the initiation of a secondary crack ahead of the crack-tip, and by the interaction between it and the primary crack. The initiation of the secondary crack is stress and time dependent because; (i) a threshold stress condition is required to break the Fe-H-Fe bonds in the grain boundary, and (ii) an incubation period is required to form a two-dimensional cluster of H atoms in the grain boundary which is large enough so that the Griffith criterion for fracture can be satisfied locally.

Sun [78] performed long life corrosion fatigue tests of Al-Li alloy in neutral 0.6M NaCl solution. His results suggested that hydrogen embrittlement resulting from hydrogen diffusion was the main cause of a large reduction in short crack growth resistance. He proposed a crack growth model which assumes that hydrogen diffuses to the PSB where it lowers the friction stress. A reasonable agreement between experimental and predicted fatigue lifetime was observed.

It has been suggested that the effects of hydrogen diffusion [79], hydrogen trapping [80] and dislocation sweeping of hydrogen from the crack tip into the metal [81] on crack growth behaviour should be considered in developing a crack growth model.

2.5 References

[1] Williams M.L. (1957) J. Appl. Mech. (Trans. ASME E), Vol.24, p109.

[2] Paris P.C. and Erdogan F. (1963) A critical analysis of crack propagation laws. Trans. ASME, J. Basic Eng., Vol.85, pp528 - 534.

[3] Smith R.A. (Ed.) (1986) Fatigue Crack Growth - 30 years of progress. Proceedings of a Conference on Fatigue Crack Growth, Cambridge, UK, Pergamon Press.

[4] Lindley T.C., Richards C.E. and Ritchie, R.O. (1976) Metall. Metal Forming, 43, p268.

[5] Rice J.R. (1967) in Fatigue Crack Propagation, ASTM STP 415, Philadelphia, Pa., p247.

[6] Hutchinson J.W. (1968) J. Mech. Phys. Solids, 16, p13.

[7] Rice J.R. (1968) A path independent integral and the approximate analysis of strain concentrations by notches and cracks. J. Appl. Mech., 35, pp379 - 386.

[8] Dowling N.E. and Begley J.A. (1976) Fatigue crack growth during gross plasticity and the J - integral. ASTM STP 590, pp82 - 103.

[9] Dugdale D.S. (1960) Yielding of steel sheets containing slits. J. Mech. Phys. Solids, 8, 100 - 104.

[10] Lankford J. (1976) Inclusion - matrix debonding and fatigue crack initiation in low alloy steels. Int. J. Fracture, 12, 155 - 157

[11] Kunio J., Shimizu M., Yamada K., Sakura K. and Yamamoto J. (1981) The early stage of fatigue crack growth in martensitic steel, Int. J. Fracture, 17, 111 - 119

[12] Morris W.L., James M.R. and Buck O. (1980) Computer simulation of fatigue crack initiation. Engng. Fracture Mech., 13, 213 - 221

[13] Miller K.J. (1985) Initiation and growth rates of short fatigue cracks. IUITAM Eshelby memorical Symposium, Fundamentals of Deformation and Fracture(Eds. Bilby,B.A., Miller,K.J. and Willis,J.R.) 477-500, Cambridge University Press.

[14] Wu X.J. (1991) Behaviour of short fatigue cracks in a medium carbon steel subjected to bending. Fatigue Fract. Engng Mater. Struct. 14, 369 - 372

[15] Akid R. and Miller K.J. (1990) The effect of solution pH on the initiation and growth of short fatigue cracks. In Fracture behaviour and design of materials and structures, Proceedings of ECF8, Torino, 1753 - 1758

[16] Pearson S.(1975) Initiation of fatigue cracks in commercial aluminium alloys and subsequent propagation of very short cracks. Engng Fract. Mech., 7, 235 - 247.

[17] Tanaka K., Hojo M. and Nakai Y. (1983) Fatigue crack initiation and early propagation in 3% silicon iron. Fatigue Mechanisms: Advances in Quantitative Measurement of Fatigue Damage, (Eds. Lankford *et al.*) STP 811, pp207 - 232, Philadelphia, Pa, American Society for Testing and Materials.

[18] Morris W.L. (1980) The noncontinuum crack tip deformation behaviour of surface microcracks. Metall. Trans. 11A, 1117 - 1123

[19] Hudak S.J. (1981) Small crack behaviour and the prediction of fatigue life. J. Engng Mater. Technol., 103, 26 - 35

[20] Lankford J. (1982) The growth of small fatigue cracks in 7075 - T6 aluminium alloy. Fatigue Eng. Mater. Struct., 5, 233 - 248

[21] Miller K.J. (1987) The behaviour of short fatigue cracks and their initiation part I - a review of two recent books. Fatigue Fract. Engng Mater. Struct., 10, 75 - 91.

[22] Miller K.J. (1987) The behaviour of short fatigue cracks and their initiation. Part II - A general summary. Fatigue Fract. Engng. Mater. Struct., 10, 93 - 113.

[23] Miller K.J. (1991) Metal fatigue - past, current and future. Proc. Instn. Mech. Engrs., 205, 1 - 14.

[24] Morris W.L. (1979) Microcrack closure phenomena for Al 2219 - T851. Metall. Trans., 10A, 5 - 11

[25] Tanaka K., Nakai Y and Yamashita M. (1981) Fatigue growth threshold of small cracks. Int. J. Frac., 17, 519 - 533

[26] El Haddad M.H.EL, Topper T.H. and Mukherjee B. (1981) Review of new developments in crack propagation studies. J. Test. Eval., 9, 61 - 81

[27] El Haddad M.H., Smith K.N. and Topper T.H. (1979) Fatigue crack propagation of short cracks. J. Eng. Mater. Technol. (Trans. ASME H), 101, 42 - 46.

[28] Morris W.L., James M.R. and Buck O. (1981) Growth rate models for short surface cracks in Al2219-T851. Metall. Trans., 12A, 57 - 64.

[29] Skelton R.P. (1982) The growth of short cracks during high strain fatigue and thermal cycling. Low Cycle Fatigue and Life Prediction, ASTM STP 770, 337 - 381.

[30] Wells A.A. (1961) Unstable crack propagation in metals: cleavage and fast fracture. Symp. Crack Propagation. College of Aeronautics, Cranfield, 210 - 230.

[31] Bilby B.A., Cottrell A.H. and Swinden K.H. (1963) The spread of plastic yield from a notch. Proc. R. Soc., Lond. A., 272, 304 - 314

[32] Hobson P.D., Brown M.W. and de los Rios E.R. (1986) Two Phases of short crack growth in a medium carbon steel, in The behaviour of short fatigue cracks, European Group on Fracture Publication, 1, 441-459

[33] Yates J.R. and Grabowski L. (1990) Fatigue life assessment using a short crack growth model. In: Fatigue '90, Fourth International Conference on Fatigue and Fatigue Thresholds, Hawaii, MCEP, 13, 2369 - 2376.

[34] Zhang W. (1991) Short fatigue crack behaviour under different loading systems. PhD thesis, University of Sheffield.

[35] Navarro A. and de los Rios E.R.(1987) A model for short fatigue crack propagation with an interpretation of the short-long crack transition. Fatigue Fract. Engng Mater. Struct., 10, 169 - 186

[36] Navarro A. and de los Rios E.R. (1988) An alternative model of the blocking of dislocations at grain boundaries. Phil. Mag. A, 57, 37-42

[37] Sun Z., de los Rios E.R. and Miler K.J. (1991) Modelling small fatigue cracks interacting with grain boundaries. Fatigue Fract. Engng Mater. Struct. 14, 277 - 291

[38] Xin X.J., de los Rios E.R. and Navarro A. (1991) Modelling of strain hardening for short cracks Short fatigue cracks, an EGF/ESIS publication. To be published.

[39] Cox B.N. and Morris W.L. (1987) A probabilistic model of short fatigue crack growth. Fatigue Fract. Engng Mater. Struct., 10, 419 - 428

[40] Cox B.N. and Morris W.L. (1987) Model- based statistical analysis of short fatigue crack growth in Ti 6Al-2Sn-4Zr-6Mo. Fatigue Fract. Engng Mater. Struct., 10, 429 - 446

[41] Wang S.Z., Miller K.J., Brown M.W. and de los Rios E.R. (1991) A statistical analysis of short fatigue crack growth. Fatigue Fract. Engng Mater. Struct., 14, 351 - 368

[42] Nakasone Y. Shimazaki T., Iida M. and Kitagawa H. (1987) Fatigue life prediction and material evaluation based on a statistics - of - extremes analysis of the maximum length distributions of multiple small cracks. Statistical Research on Fatigue and Fracture, Elsevier Applied Science Publishers, 91 - 104.

[43] Akid R. and Wu X.J. (1995) The influence of short crack coalescence on the prediction of corrosion fatigue life. In preparation.

[44] Lindborg U. (1969) A statistical model for the linking of microcracks. ACTA Metallurgica, 17, 521 - 526

[45] Kitagawa H., Fujita T. and Miyazawa K.(1978) Small randomly distributed cracks in corrosion fatigue. Corrosion - Fatigue Technology, ASTM STP 642 (Eds. Craig H.L., Crooker T.W. and Hoeppner D.W.), pp98 - 114. American Society for testing and Materials.

[46] Cox B.N. and Morris W.L. (1988) Monte carlo simulations of the growth of small fatigue cracks. Engng. Fract. Mechanics, 31, 591 - 691.

[47] Gangloff R.P. and Wei R.P. (1986) Small crack-environment interaction: the hydrogen embrittlement perspective. Proceedings of the Second Engineering Foundation International Conference, Small Fatigue Cracks, 239 - 264

[48] Gangloff R.P. (1981) The criticality of crack size in aqueous corrosion fatigue. Res. Mechanica Lett., 1, 299 - 306

[49] Tanaka K. and Wei R.P. (1985) Growth of short fatigue cracks in HY130 steel in 3.5% NaCl solution. Engng. Fract. Mechanics, 21, 293 - 305.

[50] Bardal J.M., Sondenfor J.M. and Gartland P.O. (1978) Slow corrosion fatigue growth in a structural steel in artificial seawater at different potentials, crack depths and loading frequencies. Proc. of Conf. European Offshore Steels Research, 415 - 438

[51] Akid R. (1986) Ph. D. Thesis, University of Sheffield. UK.

[52] Holroyd N.J.H. and Hardie D. (1984) Corrosion fatigue of 7000 series aluminium alloys. Environment - Sensitive Fracture: Evaluation and Comparison of Test methods. ASTM STP 821. (Eds. Dean S.W., Pugh E.N. and Ugianshy G. M.) American Society for Testing and Materials, Philadelphia, 534 - 547.

[53] Pao P.S. Wei, W. and Wei R.P. (1977) Effect of frequency on fatigue crack growth response of AISI4340 steel in water vapor. Environment - sensitive fracture of engineering materials (Eds Z.A. Foroulis), 565 - 580

[54] Lynch, S.P. (1977) Environmentally assisted cracking-fractographic and mechanistic aspects. Environment - sensitive fracture of engineering materials (Eds Z.A. Foroulis), 265 - 364

[55] Turnbull A. and Newman R.C. (1986) The influence of crack depth on crack electrochemistry and fatigue crack growth. Proceedings of the Second En-

gineering Foundation International Conference, Small Fatigue Cracks, 269 - 288

[56] Hudak S.J., Davidson D.L. and Page R.A. (1984) The role of crack tip deformation in corrosion fatigue growth. Embrittlement by the Localized Crack Environment, (Ed. R.P.Gangloff), AIME, New York, 173 - 198

[57] Ford F.P. and Emigh P.W. (1985) The prediction of the maximum corrosion fatigue crack propagation rate in the low alloy steel-de- oxygenated water system at 228^0C , Corrosion Science, 25, 673 - 692

[58] Ford F.P. and Jr Hudak S.J. (1986) Potential role of the film rupture mechanism on environmentally assisted short crack growth. proceedings of the Second Engineering Foundation International Conference, Small Fatigue Cracks, 289 - 308

[59] Hirth J.P. (1980) Effects of hydrogen on the properties of iron and steel. Met. Trans. A, 11A, 861-890

[60] Troiano A.R. (1960) The role of hydrogen and other interstitials in the mechanical behaviour of metals. Trans.ASM. 52, 54-80

[61] Oriani R.A. and Josephic P.H. (1974) Equilibrium aspects of hydrogen-induced cracking of steels. Acta Met., 22, 1065-1074

[62] Oriani R.A. and Jisephic P.H. (1979) Hydrogen-enhanced load relaxation in a deformed medium-carbon steel. Acta Met., 27, 997 - 1005

[63] Beachem C.D. (1972) A new model for hydrogen-assisted cracking (Hydrogen embrittlement). Met. Trans., 3, 437-451

[64] Latanision R.M. and Jr. Opperhauser H. (1974) The intergranular embrittlement of nickel by hydrogen:The effect of grain boundary segregation. Met. Trans.A, 5, 483 - 492

[65] Tien J.K., Richards R.J., Buck O. and Marcus H.L. (1975) Model of dislocation sweep-in of hydrogen during fatigue crack growth. Scripta Met., 9, 1097-1101

[66] Johnson H.H. and Hirth J.P. (1976) Internal hydrogen supersaturation produced by dislocation transport. Met. Trans., 7A, 1543-1548

[67] Hoshide T., Migahara M. and Inoue T. (1987) Life prediction based on analysis of crack coalescence in low cycle fatigue. Engineering Fracture Mechanics, 27, 91 - 101

[68] Brown B.F. (1981) Stress corrosion cracking control measures, Published by National Association of Corrosion Engineers, p3.

[69] Wei R.P. and Landes J.D. (1969) Correlation between sustained - load and fatigue crack growth in high strength steels. Mater. Res. Std., 9, 25-27.

[70] Miller G.A., Hudak S.J. and Wei R.P. (1973) The influence of loading variables on environment enhanced fatigue crack growth in high strength steels. J. of Test. and Eval., 1, 524-531.

[71] Austen I.M., Walker E.F. (1977) Quantitative understanding of effects of mechanical and environmental variable on corrosion fatigue crack behaviour. The influence of environment on fatigue. I Mech. E. Conference Publications, 1-10.

[72] Vosikovsky O. (1980) Effects of mechanical and environmental variables on fatigue crack growth rates in steel, a summary of work done at Canmet. Can. Metall. Q., 19, 87- 97

[73] Nakasa K. Takei H.and Itoh H. (1983) Mechanism of corrosion fatigue crack-propagation in high strength steels. Eng. Fract. Mech., 17, 449 - 459

[74] Wei P.R. and Simmons G.W. (1981) Recent progress in understanding environmental assisted fatigue crack growth. Int. J. Fract., 17, 235 - 247

[75] Scott P.M. (1985) A review of environment - sensitive fracture in water - reactor materials. Corrosion Science, 25, 583 - 606

[76] Akid R. and Miller K.J. (1990) The initiation and growth of short fatigue cracks in an aqueous saline environment. In Environment assisted fatigue, EGF publication 7 (Eds P. Scott and R.A. Cottis), 415 - 434 (Mechanical Engineering Publications, London)

[77] Raj R. and Varadan V.K. (1977) The kinetics of hydrogen assisted crack growth. Proc. of inter. conf. of Mechanisms of Environment Sensitive Cracking of Materials, Surrey, UK, 426-436.

[78] Sun Z.Y. (1991) Long life corrosion fatigue in an aluminium-lithium alloy. Ph.D. Thesis, University of Sheffield.

[79] Johnson H.H. and Lin R.W. (1980) Hydrogen and deuterium trapping in iron. in Proceedings of the third International Conference on Effect of Hydrogen on Behaviour of Materials, 3-25

[80] Oriani R.A. (1970) The diffusion and trapping of hydrogen in steel. Acta Met., 18, 147-157

[81] Tien J.K., Nair S.V. and Jensen R.R. (1980) Trap theory of hydrogen embrittlement: Experimental investigation. in Proceedings of the third International Conference on Effect of Hydrogen on Behaviour of Materials, 27-36

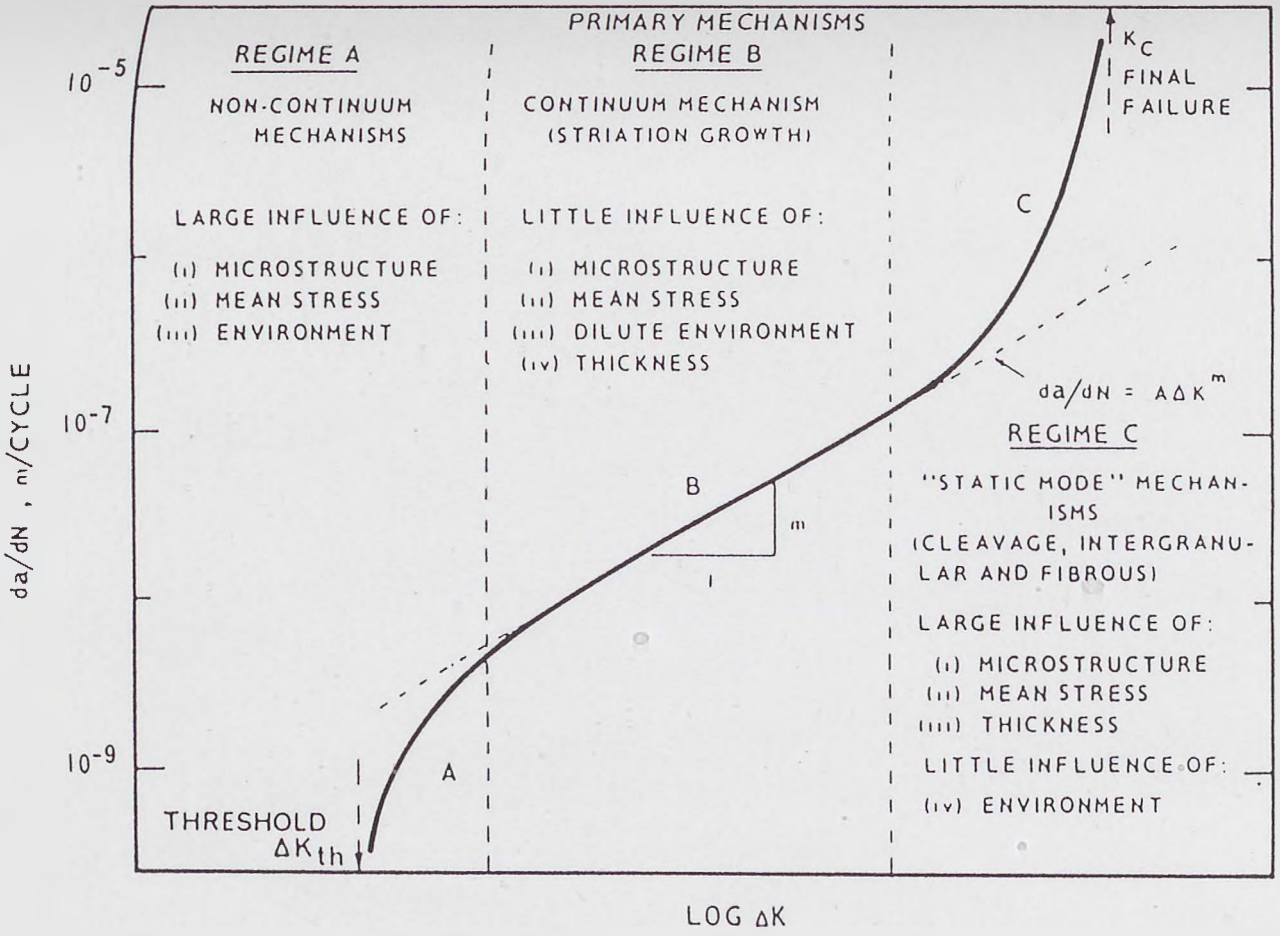

Fig.2.1 Schematic diagram indicating the three regimes of LEFM fatigue crack growth [4].

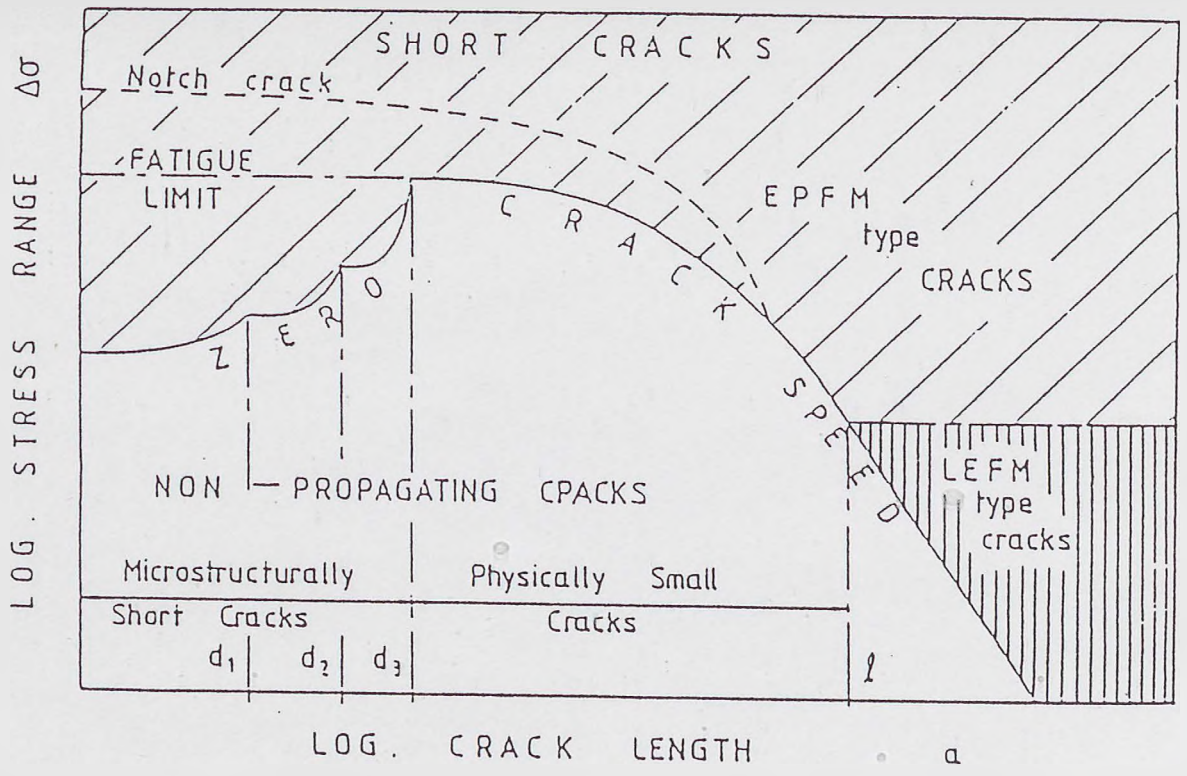

Fig.2.2 Three regimes of short crack behaviour [22].

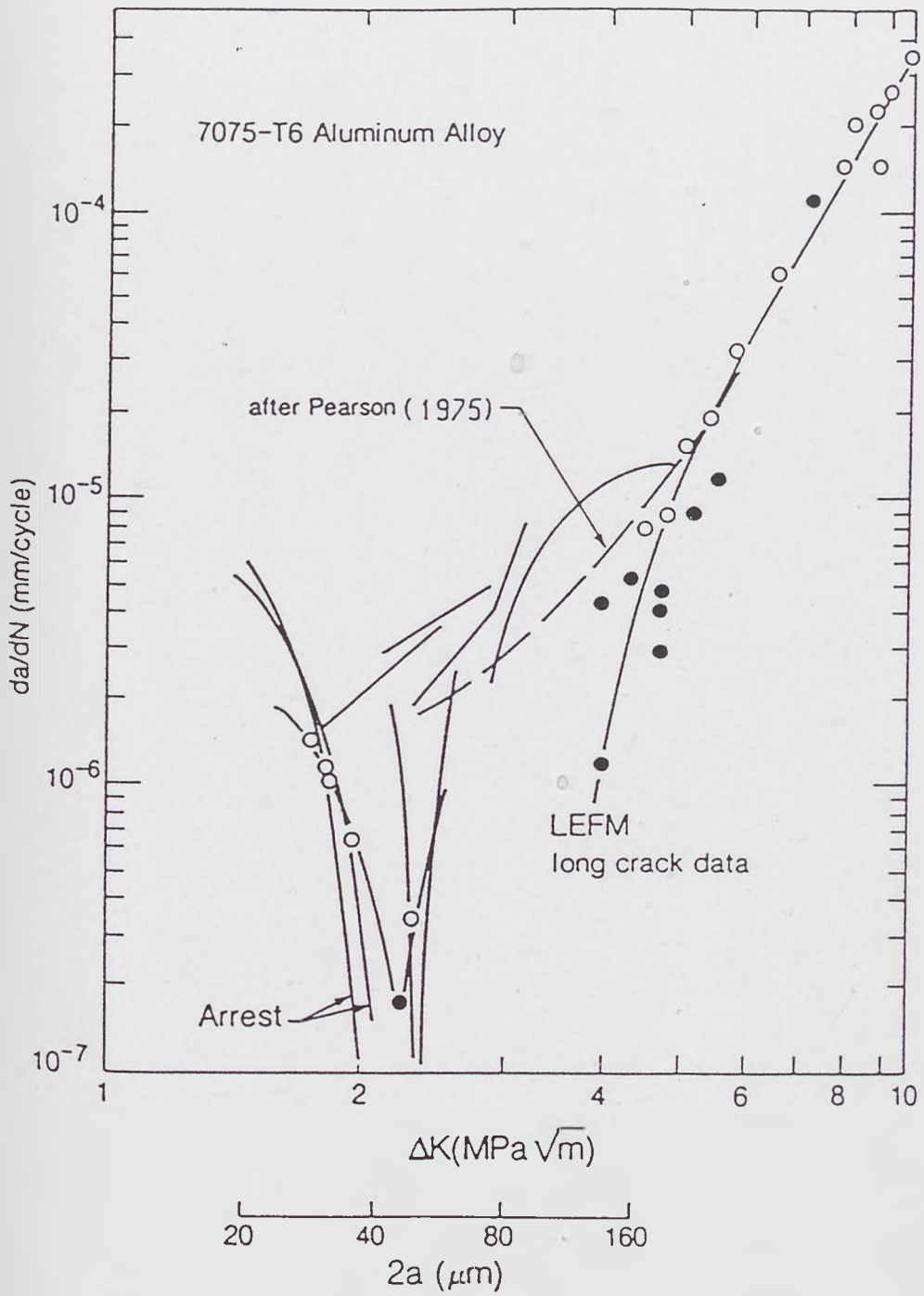

Fig.2.3 Comparison of growth of short and long cracks in aluminium alloys [20].

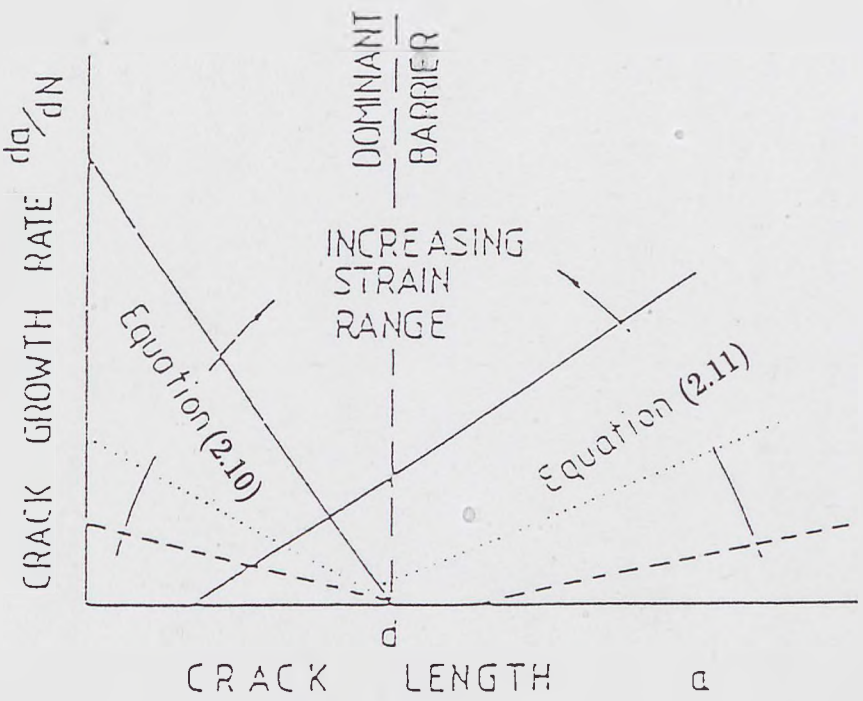

Fig.2.4 Schematic plot of a short crack growth model [22].

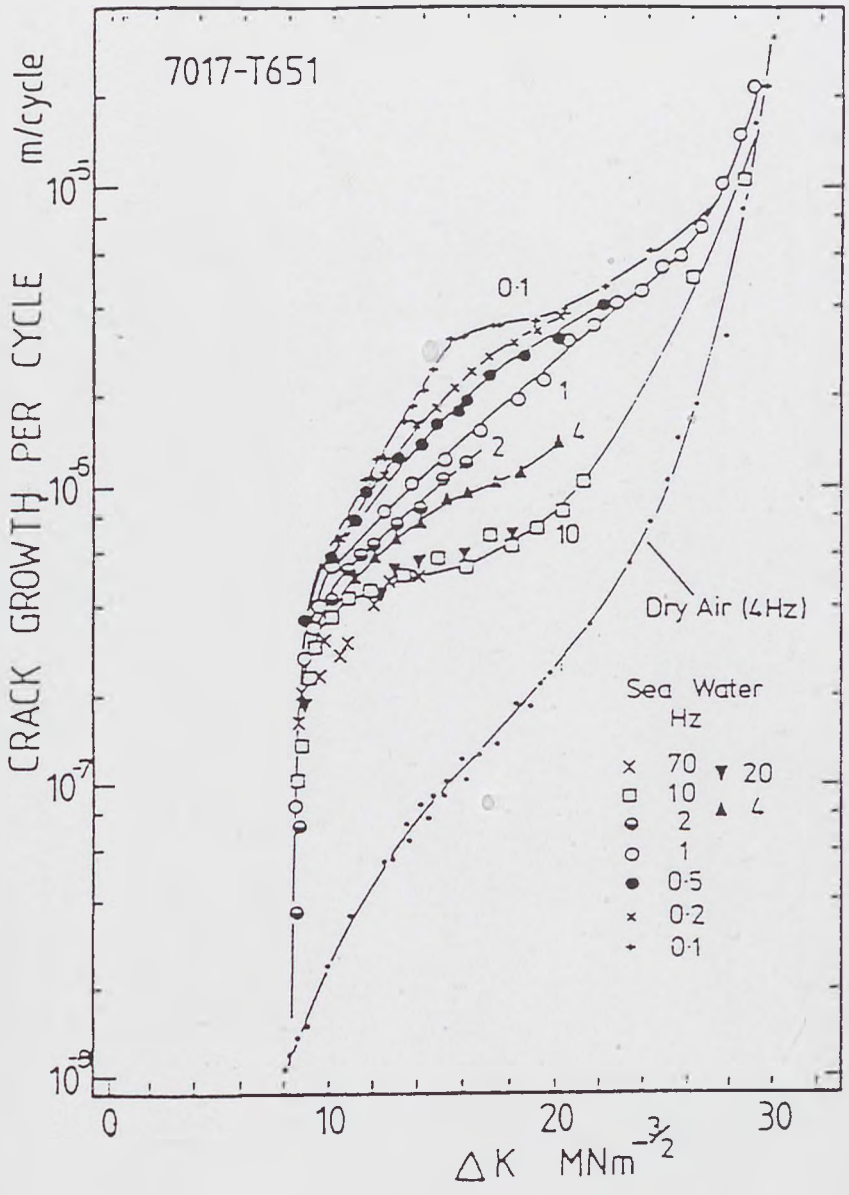

Fig.2.5 Crack growth rates during fatigue of 7017-T651 in dry air and seawater at frequencies from 0.1 to 70 Hz [52].

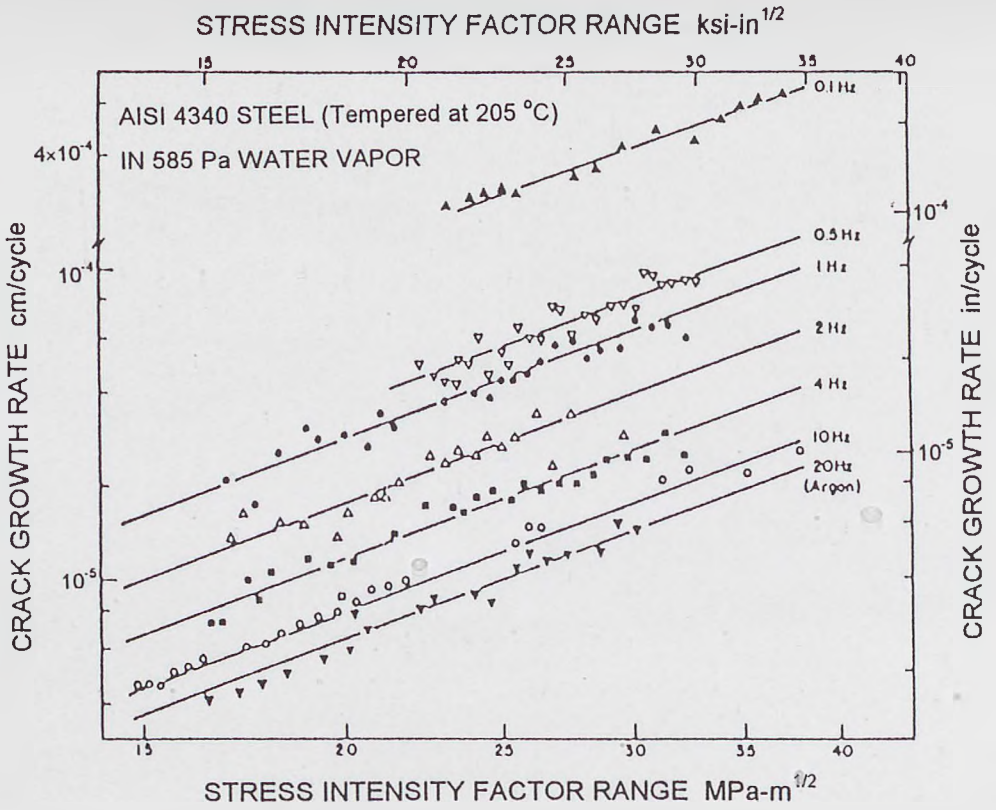

Fig.2.6 Fatigue crack growth kinetics of AISI4340 steel in dehumidified argon and in water vapour [53].

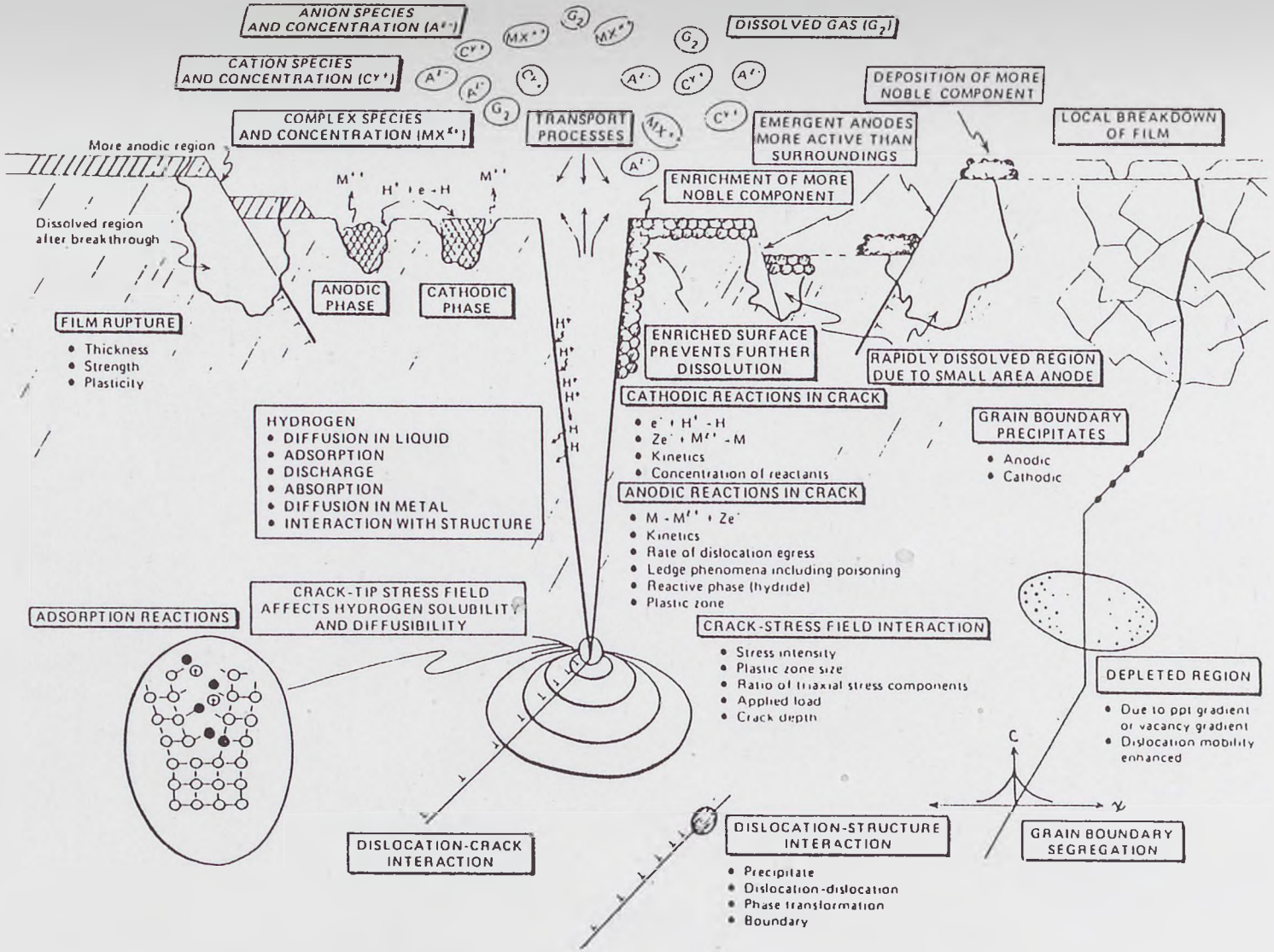

Fig.2.7 Schematic summary of the microfeatures and microprocesses contributing to environment-assisted cracking [68].

Chapter 3

Material and Test Facilities

3.1 Material

The material used in this study is that of Q2N, a quenched and tempered structural steel. The nominal chemical composition, in weight %, is given in Table 3.1 [1]. The material was tested in the 'as received' condition ; austenitise at 900 ^{o}C; water quench, temper at 650 - 680 ^{o}C; air cool.

C	Si	Mn	P	S	Cr	Mo	Ni
0.09-0.15	0.15-0.35	0.30-0.50	0.01max	0.01max	1.30-1.70	0.40-0.50	3.15-3.65
Al	As	Cu	N	Sn	V	Pb	Sb
0.015min	0.03 max	0.02max	0.01max	0.02max	0.05-0.10	0.005max	0.01 max

Table 3.1: Chemical composition of test material

The mechanical properties of this material were obtained by conducting tensile

tests on a MAYES testing machine according to ASTM-E8M [2]. The average results of two tensile tests are listed in Table 3.2.

The engineering stress - strain curve together with the specimen geometry used for the tensile testing are shown in Figure 3.1.

UTS (MPa)	0.2% Proof stress (MPa)	Elongation (%)	Reduction of area (%)	Young's modulus (GPa)
863	793	20	71 min	206.8

Table 3.2: Mechanical properties of test material

3.2 Microstructure

Metallographic specimens were polished using a standard procedure with specimens receiving a final surface polish of $1\mu m$. In order to reveal the microstructure some samples were etched in 2% Nital solution. Typically the microstructure of this material, as shown in Figure 3.2, is that of tempered lath martensite. Much effort was put into revealing the details of the prior austenite grain boundaries of the material, which are shown in Figure 3.3. This microstructure was revealed by using $FeCl_3$ solution etchant. Measurement of 85 grains by the standard mean linear intercept method produced a mean grain diameter value of $9.86\mu m$. A histogram showing the grain size distribution is given in Figure 3.4.

3.3 Fatigue Specimens

To determine the long fatigue crack growth behaviour of this material a pre-cracked fatigue specimen was designed and machined. The specimen was machined and ground finished from 50 mm thick plate in the T - L orientation having a configuration as shown in Figure 3.5. In order to create sharp crack-like conditions, the specimen was pre-cracked by fatigue prior to testing [3]. The importance of the precracking is to ensure that

- The effect of the machined notch is removed from the specimen.
- The effects on subsequent crack growth rate results caused by the changing crack front shape or pre-crack load history are eliminated.

In accordance with standard procedures [3] the final K_{max} during precracking shall not exceed the initial K_{max} for which the test data is to be obtained. A load corresponding to a given K_{max} was used to initiate cracking at the machined notch. A load range was then incrementally stepped-down to meet the above requirement. Furthermore, the reduction in P_{max} for any of these steps was no greater than 20% of the previous load level and measurable crack extension should be observed before proceeding to the next step as suggested in [3].

The fatigue specimens used for all short crack growth test were also machined from 50 mm thick plate in the T - L orientation. Dimensions of the three point bend specimen are shown in Figure 3.6. The working area of the specimen had a rectangular cross section with nominal dimensions of 15 $\times$ 30 mm. The gauge area was carefully polished with a succession of finer grade emery papers followed by diamond paste. The preparation of the specimen surface was finished by

electropolishing at room temperature in an electrolyte of 6% perchloric acid and 94% of acetic acid. The specimen to be polished was made the anode and a cell potential of 10 V was applied for 7 minutes.

3.4 Fatigue Test Facilities

A Schenck 250 kN servohydraulic testing machine was used to perform the three-point-bend fatigue tests. This machine is a universal servo hydraulic testing instrument for static and dynamic materials testing. Static, ramp, impulse, periodic and randomly varying loads can be generated. The controlled parameter can be force and actuator piston displacement, using standard built-in transducers, or specimen strain or acceleration, using appropriate transducers.

The test force is measured by a load cell and and its associated signal conditioner. Alternative variables, measured with other transducers, can be used as control parameters. In the servo controller the feedback signal, *i.e.* the actual measured value of the selected parameter, is continuously compared with the command signal, which is produced by a function generator. The power amplifier converts the resulting difference or error signal into the control signal for the servo valve.

The command signal conditioner is used to set the mean level and to superimpose dynamic signals from any two desired sources to form a combined signal command for the machine. The function generator produces sine, triangular or square wave forms.

Typical technical data for this machine is listed below:

- Rated force (F_n): 250 kN .
- Dynamic force rating: $\pm 0.8 F_n$.
- Frequency range: 0 - 200 Hz.
- Max. piston travel: 100 mm.

A schematic of the specimen and loading pins arrangement is shown in Figure 3.6. Stress on specimen surface, σ, was calculated for each specimen using Equation 3.1.

$$\sigma = \frac{3PS}{TW^2} \tag{3.1}$$

where P is applied load and S, T and W are length of moment, thickness and width of specimen respectively

3.5 Crack Growth Monitoring

3.5.1 Plastic Replication Technique

A plastic replication technique has been used in the present study to obtain information on short crack development and growth.

The technique consists of preparation of cellulose acetate material, replication and replica fixture. A sheet of cellulose acetate material is cut into small pieces. At the time of replication the specific area of specimen is sprayed with acetone and immediately a piece of acetate sheet is placed on the specimen's surface with

the help of a pair of tweezers. After 3-5 minutes, when the replica is dry, it can be removed from the specimen's surface with the aid of a pair of tweezers. Finally the replica was fixed onto a microscope glass slide for subsequent microscopical examination. The number of replicas taken in a test depends upon the expected fatigue lifetime of that specimen. Ideally replicas would show the growth of cracks from the initiation sites to complete failure.

This technique, which has been used in this and previous studies, has the following advantages:

- it is an efficient method of detecting cracks of a few microns length.
- the method provides information relating the influence of microstructure on crack initiation and growth.
- it provides an excellent permanent record of each test from start to end.
- it allows an estimate of crack density.
- it is economic.

3.5.2 Image Analysis System

Replicas made during a fatigue test were examined using an Image Analysis System. This system consists of a high-resolution metallurgical microscope, an image capturing monitor, a camera for relaying an image from the replica to an image capturing board incorporated within a personal computer. The system software offers a number of measuring options which include crack length, area and volume fraction. The results of measurements carried out are displayed on the PC monitor and can be permanently stored on a hard or floppy disc. The

microscope provides a facility for automatic-exposure photography by replacing the video camera by a standard 35mm photographic camera.

3.6 Environment Control

A corrosion cell was designed with an overall size of $120 \times 70 \times 43mm$ and an inner chamber size of $72 \times 34 \times 28mm$ thus avoiding any interaction between the loading grips, pins and the cell whilst at the same time providing sufficient specimen/solution contact area. The cell body and all fittings were made of perspex or PTFE. The cell was designed with a removable lid for the purpose of monitoring short crack growth using the replication technique. Silicon rubber was used to seal the clearance between the cell body and specimen. The inlet and outlet fittings allowed a continuous flow of the seawater through the cell. An additional fitting was assembled on the bottom lid for emptying the cell before opening the cell to take replicas. Figure 3.7 shows a schematic of the installation of a specimen for testing, together with the assembly of the test cell.

A recirculation system was designed and built for pumping the solution to the corrosion cell and controlling the solution volume flow rate. The recirculation loop is essentially a 5 litre tank, linked to a circulation pump, flow meter and a solution filter. Figure 3.8 shows the main components of this recirculation system. The volume flow rate can be easily adjusted using the flow meter on the inlet side. The solution filter added on the bypass is to minimize blockage of the loop and is also helpful in reducing the time spent in clearing solution from the specimen at each replication interval.

3.7 References

[1] Galsworthy J.C. (1990) Low frequency corrosion fatigue behaviour of Q2N steel. Admiralty Research Establishment, Holton health, Poole, Dorset, Report No ARE TM(UMM) 90419.

[2] Annual Book of ASTM standards, E8M, 1985.

[3] Annual Book of ASTM standards, E647, 1991.

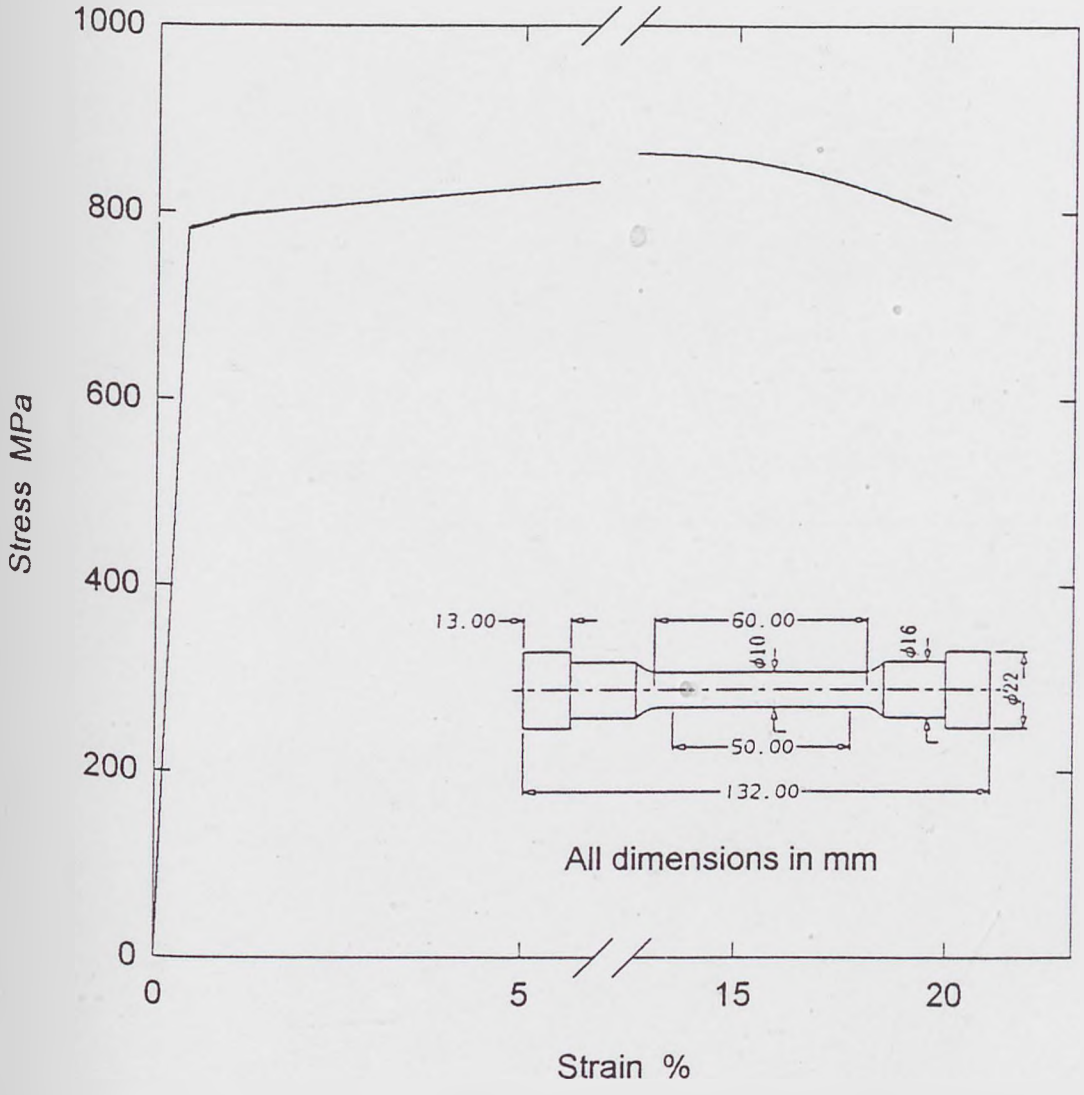

Fig.3.1 Monotonic tension stress-strain curve.

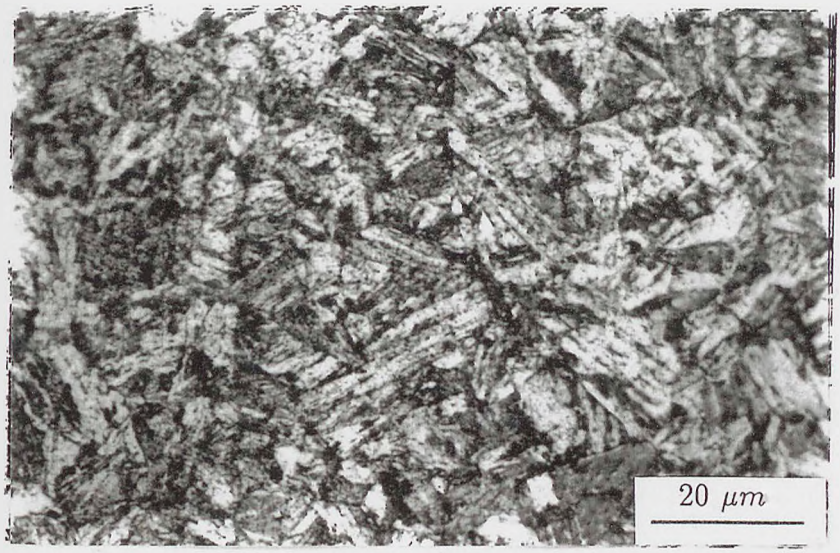

Fig.3.2 Microstructure of Q2N steel etched in 2% Nital.

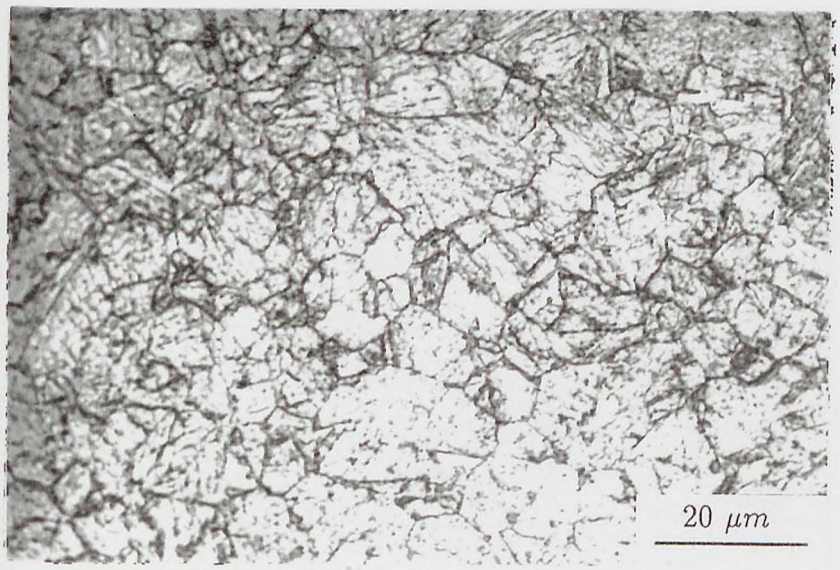

Fig.3.3 Microstructure of Q2N steel revealing the prior austenite grain boundaries.

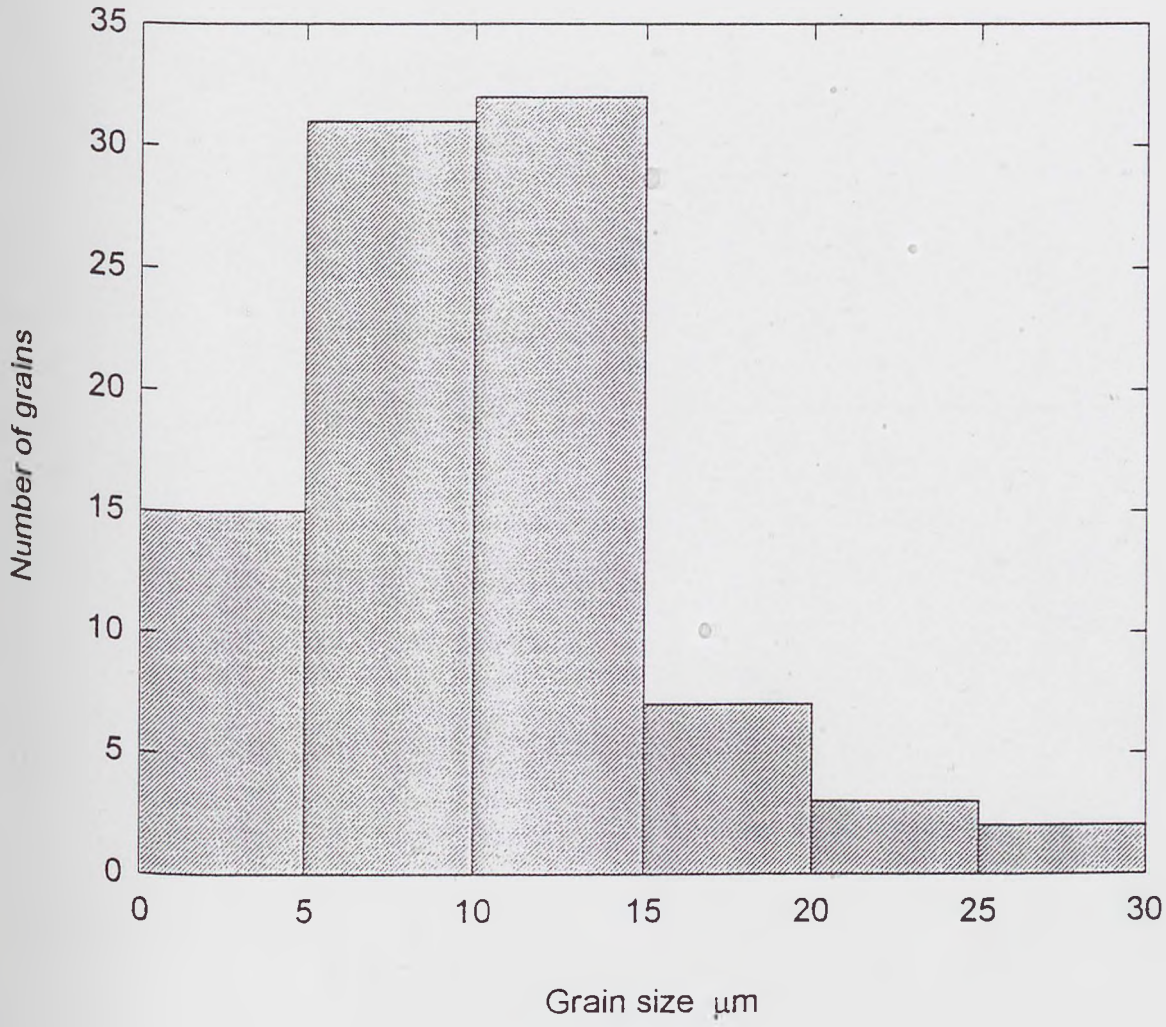

Fig.3.4 Prior austenite grain size distribution.

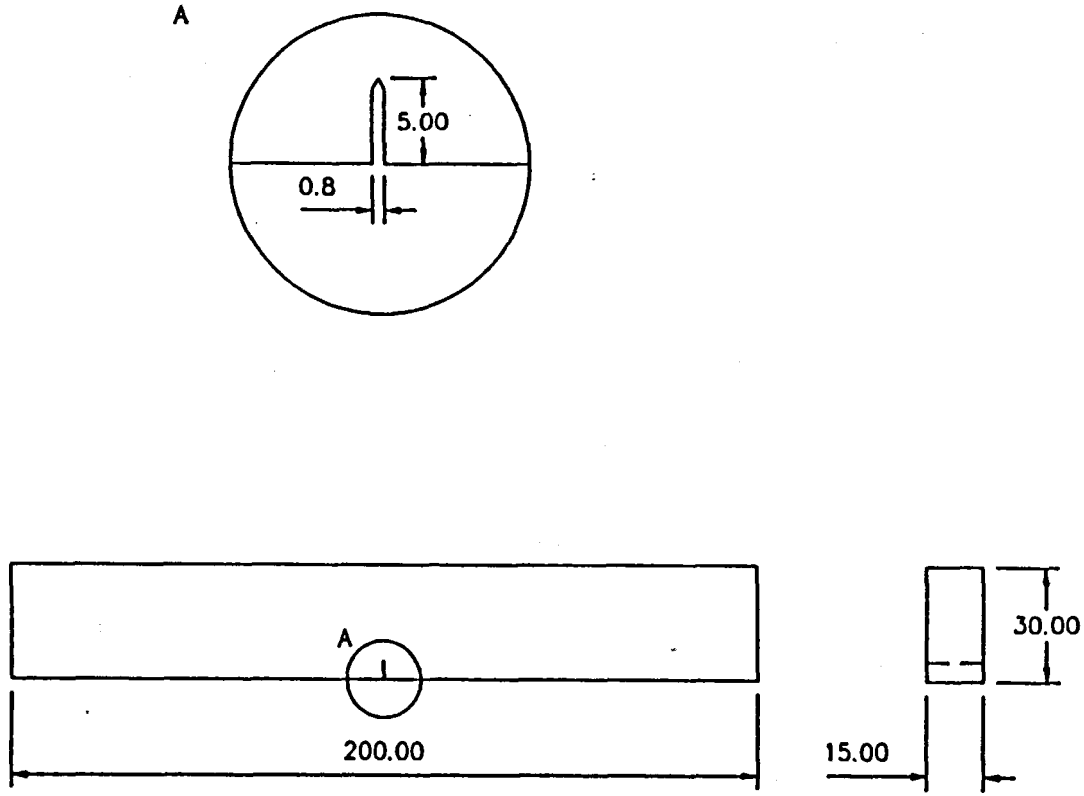

Fig.3.5 Configuration of pre-cracked specimen (all dimensions in mm).

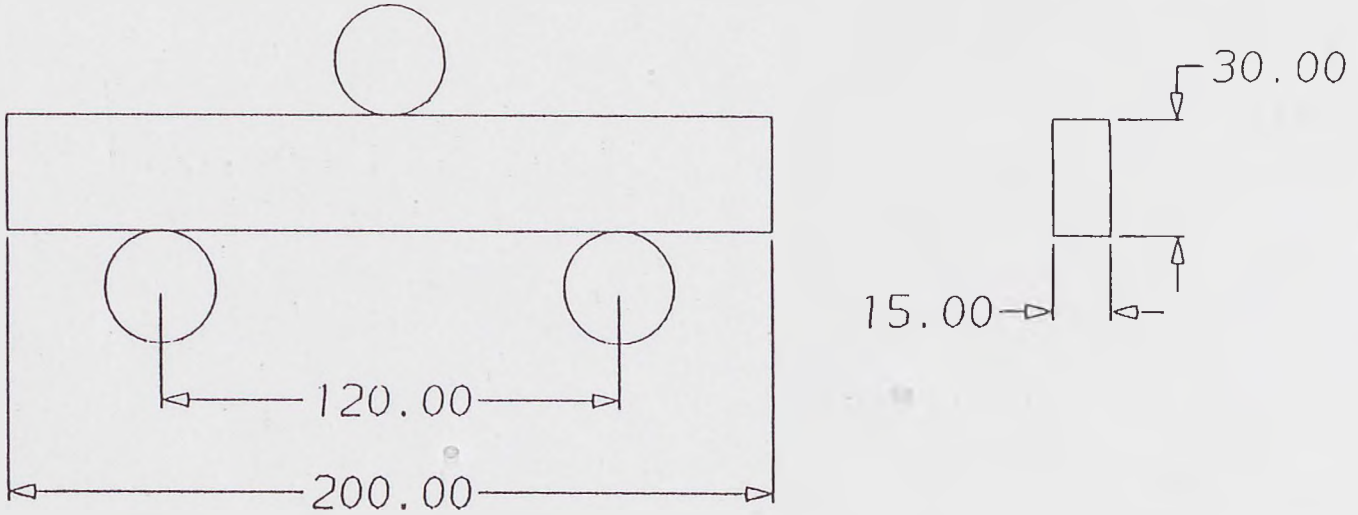

Fig.3.6 Arrangement showing three-point bend specimen and loading pin configuration (all dimensions in mm).

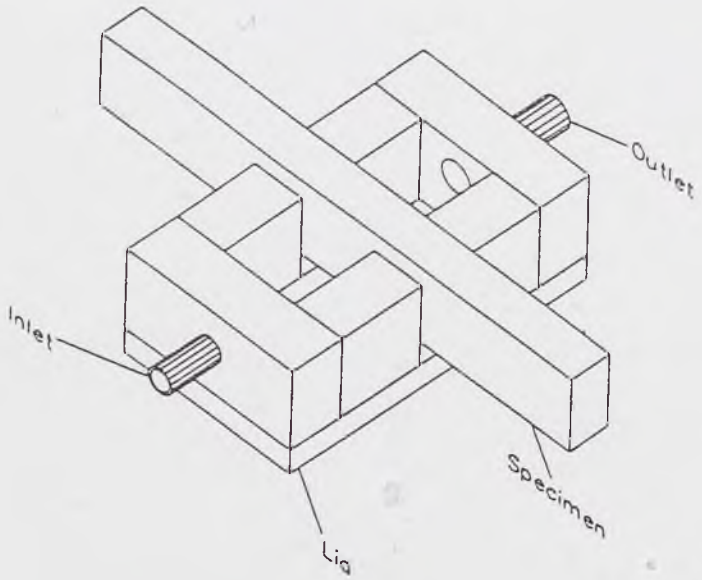

Fig.3.7 Schematic of corrosion cell and fatigue specimen assembly.

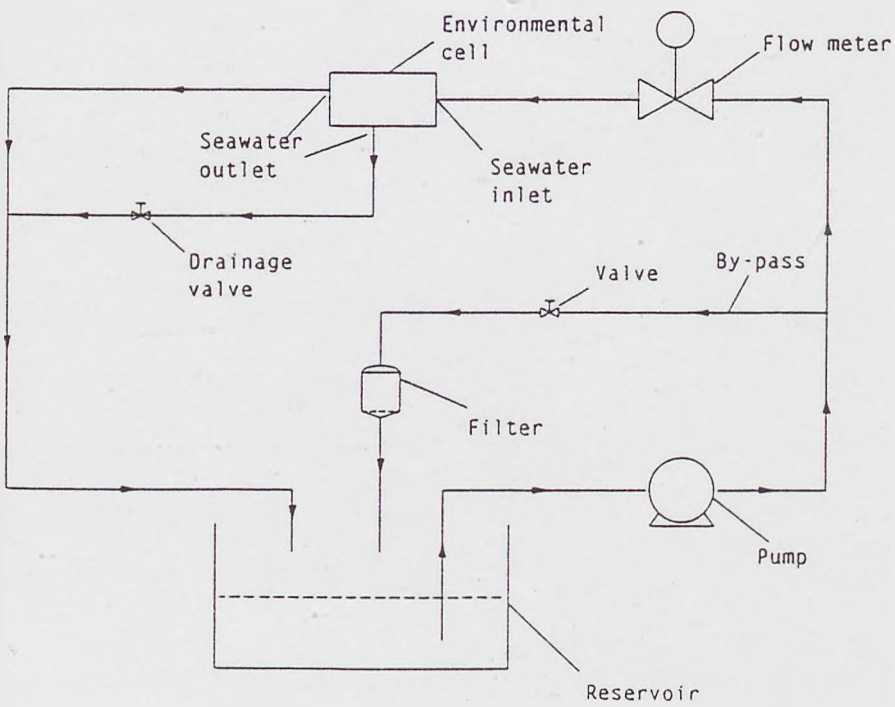

Fig.3.8 Schematic diagram of recirculation loop system for environment control.

Chapter 4

Short Fatigue Crack Growth Behaviour in Air

4.1 Introduction

The work described in this chapter relates to the fatigue crack growth behaviour of Q2N steel in air.

Three - point - bend fatigue tests have been performed at various stress levels in laboratory air conditions. Short crack development was monitored by adopting an acetate surface replication technique. LEFM long fatigue crack growth tests using pre-cracked specimens were also conducted so that a comparison between short and long crack growth could be made.

The characteristics of short crack propagation, such as fast initial MSC growth, crack growth rate retardation and interaction between short cracks and mi-

crostructure were studied. Fracture surfaces were examined using a scanning electron microscope to enhance the understanding of the metallurgical process involved.

A short fatigue crack growth model has been developed based on the experimental results obtained and the application of a microstructural fracture mechanics analysis. This model was then used to predict the in-air fatigue lifetime.

4.2 Experimental Procedure

4.2.1 Long Crack Growth Tests Using a Pre-cracked Specimen

Long fatigue crack growth threshold and crack growth rates were obtained by testing pre-cracked specimens using a Schenck 250 kN servo-hydraulic testing machine employing an on site optical microscope for crack length measurement. The specimen configuration is shown in Figure 3.5. In order to create a sharp crack at the notch, prior to testing, the specimen was fatigue pre-cracked as recommended by ASTM standard E647-91[1].

In order to determine the fatigue crack growth threshold, ΔK_{th}, a K - decreasing test procedure was applied [1].

Long crack growth rate was obtained by conducting crack growth tests using the K - deceasing test procedure (for crack growth rates $< 10^{-2}$ $\mu m/cycle$) and constant - loading - amplitude test procedure (for crack growth rates $> 10^{-2}$ $\mu m/cycle$) respectively [1].

The K - decreasing procedure was started by cycling at a ΔK and K_{max} level equal to or greater than the terminal pre-cracking values. Subsequently, loads were decreased as the crack grew, and test data was recorded until the lowest ΔK or crack growth rate of interest was achieved.

A constant - load - amplitude test procedure was applied to produce crack growth data for $da/dN > 10^{-2}\ \mu m/cycle$. The specimen used was tested at a constant load and a fixed set of loading variables namely, stress ratio R= 0.1 and test frequency f=25 Hz.

4.2.2 Fatigue Lifetime and Short Crack Growth Testing

The same test machine, as used for determining long crack growth, was used to perform the three-point-bend fatigue tests on smooth specimens. The working area of the specimen had a rectangular cross section with nominal dimensions of $15 \times 30\ mm$. The gauge area was carefully polished with a succession of finer grade emery papers and diamond paste after which electropolishing was carried out. A schematic of the specimen and loading fixture arrangement is shown in Figure 3.6. Load controlled fatigue tests were conducted to obtain fatigue lifetime results and to study the behaviour of short cracks. All tests were carried out at a stress ratio close to zero, that is R= 0.02, and a test frequency, f of 10 Hz.

Acetate replicas were taken of the polished specimen surface, at frequent intervals during tests, to monitor the growth of short cracks. The frequency at which replicas were taken depended on the estimated duration of the test. Ideally replicas would show the growth of cracks from the initiation sites to complete failure. Short crack lengths were measured from plastic replicas using an optical micro-

scope having a video camera attachment and dedicated image analysis system.

4.2.3 Method of Analysis

The growth rate of long fatigue crack was determined from the crack length versus elapsed cycles data (a versus N). A secant method was applied to calculate da/dN for the K - decreasing tests and an incremental polynomial method (fitting a second - order polynomial to sets of 7 successive data points) was applied to determine da/dN data for the constant, ΔP, test.

The stress - intensity factor range corresponding to a given crack growth rate was calculated from following expression [2]:

$$\Delta K = \frac{3S\Delta P}{2TW^2}\sqrt{a}F_I(\alpha) \tag{4.1}$$

where α is given by

$$\alpha = \frac{a}{W} \tag{4.2}$$

The geometry factor $F_I(\alpha)$ is given in 4.3

$$F_I(\alpha) = \frac{1.99 - \alpha(1-\alpha)(2.15 - 3.93\alpha + 2.7\alpha^2)}{(1+2\alpha)(1-\alpha)^{3/2}} \tag{4.3}$$

The short crack growth rates, da/dN, were estimated using a secant method as shown in 4.4

$$\frac{da}{dN} = \frac{a_{i+1} - a_i}{N_{i+1} - N_i} \tag{4.4}$$

where a_i and a_{i+1} are two consecutive half surface crack lengths at N_i and N_{i+1} number of cycles respectively. Since the crack growth rate represents the growth of a crack at the mid point of two consecutive crack lengths, the corresponding average crack length $\overline{a} = \frac{1}{2}(a_{i+1} + a_i)$.

In order to compare the results of short crack growth with the long crack data a normalization procedure was adopted applying the stress intensity factor, ΔK.

The method for calibrating nominal stress intensity factors for semi-elliptic surface cracks formed during bend tests given in reference [3] is applied here. Assuming the cracks have an average aspect ratio of 0.8 for bending tests [4] and are small compared to the thickness of the specimen then the calibrations for surface small cracks simplify to

$$\Delta K = 0.673 \Delta\sigma\sqrt{\pi a} \tag{4.5}$$

4.3 Experimental Results

4.3.1 Long Fatigue Crack Results

According to ASTM standard E647 in order to determine the fatigue crack growth threshold, ΔK_{th}, five da/dN, ΔK data sets, for growth rates between $10^{-3}\mu m/cycle$ and $10^{-4}\mu m/cycle$, are required from the K - decreasing test. The data points obtained from such a test are listed in Table 4.1 and plotted in Figure 4.1.

ΔK $(MNm^{-2/3})$	da/dN $(\mu m/cycle)$
7.00	1.0×10^{-3}
6.39	5.0×10^{-4}
6.36	8.8×10^{-4}
6.20	4.0×10^{-4}
6.00	2.0×10^{-4}

Table 4.1: $da/dN - \Delta K$ data for determining crack growth threshold

The best - fit straight line of the five data points obtained from a linear regression of $\log(da/dN)$ versus $\log(\Delta K)$ is

$$\frac{da}{dN} = 1.175 \times 10^{-11}(\Delta K)^{9.493} \tag{4.6}$$

The fatigue crack growth threshold determined by calculating the ΔK - value which corresponds to a growth rate of $10^{-4}\mu m/cycle$ is 5.4 $MNm^{-3/2}$.

The data for long crack growth rates obtained from both K - decreasing test and constant ΔP tests is presented in Figure 4.1. The shape of the crack growth rate curve exhibits a linear relationship on this $log - log$ plot when $\Delta K > 10$ $MNm^{-2/3}$. The crack growth behaviour at this region can be described by the Paris and Erdogan relation

$$\frac{da}{dN} = 9.77 \times 10^{-5}(\Delta K)^{2.123} \tag{4.7}$$

4.3.2 $S-N$ Curve

Twelve smooth specimens were tested using three-point bend loading. The fatigue life results are given in Table 4.2. Here the fatigue lifetime is considered as the number of cycles required to form a crack which spans the width of the specimen.

Specimen	Stress range (MPa)	Lifetime (cycles)
AF-1*	1400	2.35×10^4
AF-2*	1300	3.6×10^4
AF-3*	1200	5.6×10^4
AF-4	1200	5.4×10^4
AF-5	1176	4.6×10^4
AF-6	1097	6.8×10^4
AF-7*	1050	1.25×10^5
AF-8	1000	1.4×10^5
AF-9*	850	3.1×10^5
AF-10	840	1.6×10^6
AF-11	750	9.57×10^6
AF-12	650	$> 10^7$

Table 4.2: Fatigue lifetime results at different stress ranges

* — specimen with replicas.

The $S-N$ curve for the above data is plotted in Figure 4.2. The relationship between stress range and fatigue life time obtained through a regression analysis for data where $N_f \leq 3 \times 10^5$ is given in the following equation,

$$\Delta\sigma^{5.225} N_f = 6.310 \times 10^{20} \tag{4.8}$$

From Figure 4.2 a fatigue limit can be estimated to be $\approx 740\ MPa$.

4.3.3 Short Fatigue Crack Growth Results

Characteristics of Short Crack Growth

Five stress levels, *i.e.* $\Delta\sigma = 1400$, 1300, 1200, 1050 and 850 MPa, were chosen to monitor short crack growth behaviour. Observation of the crack growth behaviour was achieved by examination of surface replicas using an image analysis system.

Figure 4.3(a) presents a typical example of crack growth behaviour showing crack development at the site of a small non-metallic inclusion. This crack initiation mechanism was noted at all stress ranges tested. Similar results have also been observed in other materials [5][6]. Following this initial crack development stage cracks then grow along preferentially oriented crystallographic planes as shown in Figure 4.3(a). It can be seen from this figure that the crack deflects at points A and B to follow the slip band directions until it reaches point C; up to this point the crack may be referred to as a microstructurally short crack (MSC)[7]. At the point C a change in direction occurs and the crack moves on to a plane perpendicular to the tensile stress axis. At this stage the crack tip stress intensity is sufficiently high such that any microstructural aspects which normally affect short crack growth progressively diminish. The crack at this stage may be referred to as a physically small crack (PSC) [7]. Figure 4.3(b) shows the same crack as that in Figure 4.3(a) but taken after a further 2000 load cycles (about 10 percent of fatigue lifetime). It can be seen from a comparison of Figures 4.3(a) and

4.3(b) that there is little change in crack length. The maximum retardation in crack growth, which occurs at this point, is a result of the transition from a microstructurally short crack to a physically small crack.

It should be noted that the behaviour of MSC growth is also influenced by the material texture. This influence causes a large scatter in crack growth data in the MSC regime when compared to crack growth rates in the physically small crack growth regime.

Figures 4.4 and 4.5 present typical examples of the short crack growth behaviour. As previously mentioned a large scatter in growth rates occurs within the MSC regime. This is clearly seen from Figures 4.5(a - e). This is consistent with crack growth mechanisms previously presented by other researchers [8] [9], notably that resulting from the interaction between a crack and material texture. Additional features are also evident from Figures 4.4 and 4.5, these included; (a) short cracks do not achieve very high propagation rates on emerging from the small inclusion sites which appears to differ from observations made for cracking in other materials [10][11][12] where high growth rates are observed on initial crack development, (b) the average crack length corresponding to the minimum crack growth rate is about 48 μm which does not correspond with the value of the mean grain diameter of 9.9 μm. In fact the majority of cracks show maximum crack growth deceleration at surface lengths between 30 μm and 60 μm. These values are generally above the size of the largest grains measured for this material. Based on these observations it is apparent that for this material the maximum retardation in crack growth occurs during the transition from a MSC to a PSC rather than the first grain boundary encountered.

A comparison of the short crack growth rates obtained at various stress levels with

that of long cracks is given in Figures 4.6(a)-4.6(e). It is apparent, from these figures, that at all stress levels, for an equivalent stress intensity value, initial short crack growth rates are much faster than that of a long crack. Furthermore short cracks can grow at a value of stress intensity range well below the threshold value for the long crack. The da/dN data for short cracks gradually approach the da/dN values for long crack as ΔK increases. Clearly the ΔK based LEFM analysis is not valid in the short crack regime.

Fractography

Fracture surfaces of the specimens obtained from the present tests were examined by a scanning electron microscope. The initial stage of crack propagation is characterized by crystallographic cracking, as shown in Figure 4.7(a). At a later stage in growth fatigue striations were observed, see Figure 4.7(b). The final macroscopic fracture of this steel is characterized by dimple features, as shown in Figure 4.7(c).

4.4 Modelling of Short Fatigue Cracks

4.4.1 Short Crack Regimes and the Crack-Tip Plastic Zone

Based on the above experimental results it is possible to describe the two regimes of short crack growth, *i.e.*, microstructurally short crack (MSC) and physically small (PSC) regimes in schematic form as shown in Figure 4.8(a). During the initial MSC stage cracks grow mainly along crystallographic planes appearing to

face less resistance compared to PSC-type cracks which have to cut across the martensite laths. If assuming different uniform resistances to crack growth for the MSC and PSC regimes respectively, *ie*, different friction stresses, σ_I and σ_{II}, it is clear that the friction stress for MSC-type crack should be less than the friction stress for PSC-type crack. Based on this assumption the plastic zone emanating from the tip of a crack at different crack lengths can be modelled as shown schematically in Figure 4.8(b). The following conditions are therefore used to describe the growth of a short crack.

(A) MSC equilibrium plastic zone. ($c \leq d$)

(B) Transition regime plastic zone. ($a < d, c \geq d$)

(C) PSC equilibrium plastic zone. ($a \geq d$)

The plastic zone size at the crack tip can be determined using microstructural fracture mechanics analysis, *i.e.*, by solving the equilibrium equations of all the internal and external forces acting on the continuously distributed dislocation system. This method was proposed by Bilby *et al* [13], Tanaka *et al* [14], and Navarro *et al* [15]. Taking into consideration the different friction stresses for the MSC and PSC regimes the plastic zone size for each case may be calculated as follows:

(1) Case (A): MSC equilibrium plastic zone. The size of the plastic zone is determined by solving an equilibrium equation which expresses the requirement that the resultant stress on any dislocation is zero[13]:

$$A \int_{-c}^{c} \frac{D(s)ds}{x-s} + \sigma^0 = 0 \tag{4.9}$$

where A is material constant, $D(s)$ is dislocation density at a given location s on the axial coordinate of x and σ^0 is the stress applied to dislocations:

$$\sigma^0 = \begin{cases} \sigma & |x| < a \\ \sigma - \sigma_I & a < |x| < c \end{cases} \tag{4.10}$$

At $x = \pm c$, the dislocation density $D(s)$ must vanish, i.e. $D(s) = 0$. The conditions for the solution of Equation 4.9 to exist reduce to the expression

$$\int_{-c}^{c} \frac{\sigma^0 ds}{(c^2 - s^2)^{1/2}} = 0 \tag{4.11}$$

which in turn leads to the relation

$$r_p = c - a = a\left(sec\left(\frac{\pi\sigma}{2\sigma_I}\right) - 1\right) \tag{4.12}$$

(2) Case (B): Transition regime plastic zone. In this regime the equilibrium equation is the same as that of Equation 4.9. However the resultant external stress, σ^0, becomes

$$\sigma^0 = \begin{cases} \sigma & |x| < a \\ \sigma - \sigma_I & a < |x| < d \\ \sigma - \sigma_{II} & d < |x| < c \end{cases} \tag{4.13}$$

Similar to case (A) σ^0 in Equation 4.13 leads to the relation

$$cos^{-1}(a/c) + (\frac{\sigma_{II}}{\sigma_I} - 1)cos^{-1}(d/c) = \frac{\pi\sigma}{2\sigma_I} \tag{4.14}$$

and

$$r_p = c - a \tag{4.15}$$

(3) Case (C): PSC equilibrium plastic zone. The plastic zone size may be obtained in a similar way to Case (A) with the exception that a different friction stress, σ_{II}, is used as in this case the crack length is greater than d.

$$r_p = a\left(sec\left(\frac{\pi\sigma}{2\sigma_{II}}\right) - 1\right) \tag{4.16}$$

For cyclic loading, the cyclic plastic zone size may be derived by taking the stresses at maximum load as an initial or prestressed condition, and superimposing a compressive unloading stress of $\Delta\sigma$ [20]. The change in all the equations for the cyclic loading condition is achieved through the following transposition:

$$\sigma \longrightarrow \Delta\sigma$$

$$\sigma_I \longrightarrow 2\sigma_I, \quad \sigma_{II} \longrightarrow 2\sigma_{II},$$

$$r_p \longrightarrow \Delta r_p$$

4.4.2 Crack Closure Effect

It is widely accepted that a propagating mode I crack (physically small crack in this case) can close up even at a positive stress intensity factor and therefore only the portion of the applied stress intensity range ΔK_{eff}, for which the crack is open, is effective for crack growth [17] [18]. For convenience of application ΔK_{eff} for a mode I crack can be approximately estimated as follows [19]:

$$\Delta K_{eff} = \Delta K - \Delta K_{th} \tag{4.17}$$

On the other hand there is little or no crack closure effect on the growth of a crystallographic shear crack (microstructurally short crack in this case) and therefore a factor, f_c, should be introduced in order to consider the variation of the effect of closure on the short crack growth at different stages, *i.e.*,

$$\Delta K_{eff} = \Delta K - f_c \cdot \Delta K_{th} \tag{4.18}$$

It is assumed that crack closure begins to effect crack growth at the beginning of the transition from MSC growth to PSC growth. At this point $f_c = 0$ and increases in a simple linear manner to $f_c = 1$ for a physically small crack (PSC). Based on these assumptions *i.e.*, $f_c = 0$ for case(A) cracks, $f_c = \frac{a-a_c}{d-a_c}$ for case (B) cracks, where a_c is the limit crack length for a microstructurally short crack, and $f_c = 1$ for case (C) cracks.

Equation 4.18 can then be rewritten as:

$$Y\Delta\sigma_{eff}\sqrt{\pi a} = Y\Delta\sigma\sqrt{\pi a} - f_c\Delta K_{th} \tag{4.19}$$

so the effective stress can be expressed as:

$$\Delta\sigma_{eff} = \Delta\sigma - f_c\frac{\Delta K_{th}}{Y\sqrt{\pi a}} \tag{4.20}$$

4.4.3 Short Crack Growth Rate

In the present model the damage which leads to crack propagation is assumed to be controlled by the plastic zone at the crack tip. The crack growth rates for MSC and PSC type cracks can therefore be estimated using the following two expressions respectively:

$$\frac{da}{dN} = C_I(\Delta r_p)^{m_I} \qquad MSC\ type\ cracks \tag{4.21}$$

$$\frac{da}{dN} = C_{II}(\Delta r_p)^{m_{II}} \qquad PSC\ type\ cracks \tag{4.22}$$

where C_I, m_I, C_{II} and m_{II} are stress level independent material constants. Figure 4.8(c) shows schematically the corresponding crack growth rate determined by Equations 4.9 - 4.22. Similar assumptions have been made previously by several investigators and are discussed elsewhere [16] [21].

In Equations 4.12, 4.14 and 4.16 the friction stress for a PSC type crack, σ_{II} is generally taken as the yield stress of the material. However the flow stress at a crack tip will be higher than the yield stress owing to strain hardening [16] [20] it is more sensible to choose tensile strength for the friction stress σ_{II} than the yield stress. An MSC-type crack experiences less growth resistance than a PSC-type crack as the friction stress on a favourable crystallographic orientation is smaller. Assuming the resistance to growth of the plastic zone for a MSC-type crack is equivalent to the fatigue limit, σ_I can be equaled to the fatigue limit σ_{fl}.

The values of the material constants of C_I, m_I, C_{II} and m_{II} are obtained by performing a best fit regression analysis of the data set, $(da/dN, \Delta r_p)$ for MSC and PSC type cracks respectively are given as; $C_I = 2.948 \times 10^4$, $m_I = 0.472$, $C_{II} = 7.112 \times 10^4$ and $m_{II} = 0.852$. Crack growth rates predicted at different stress levels using Equations 4.9 - 4.22 are shown in Figures 4.5(a)-4.5(e). Satisfactory agreement between predicted crack growth rates and experimental data can be found at all stress levels.

4.4.4 Fatigue Lifetime Estimation

Fatigue lifetime can be calculated by adding together individual lifetimes spent within each crack growth regime. Individual lifetimes can be obtained by integrating Equation 4.21 and equation 4.22 in appropriate ranges respectively, *i.e.*,

$$N_f = \int_{a_0}^{a_c} \frac{da}{C_I(\Delta r_p)^{m_I}} + \int_{a_c}^{d} \frac{da}{C_I(\Delta r_p)^{m_I}} + \int_{d}^{a_f} \frac{da}{C_{II}(\Delta r_p)^{m_{II}}} \tag{4.23}$$

Where a_0 is an assumed value of the surface roughness for polished specimen, *i.e.* 1 μm, a_c is the crack length at $c = d$ and a_f is the average crack length at which fatigue tests were terminated *i.e.* 10 mm. The plastic zone size within each regime in Equation 4.23 is determined by Equations 4.12, 4.15 and 4.16 for $a_0 < a < a_c$, $a_c < a < d$ and $d < a < a_f$ respectively. In practice Δr_p in Equation 4.21 cannot be expressed as a simple integrated function of crack length, a, therefore numerical analyses were applied to calculate the fatigue lifetimes with the aid of a proprietry mathematics package.

Figure 4.9 presents a comparison of experimental and predicted fatigue lifetimes within the stress range at which short crack behaviour was studied.

4.5 Discussion

The anomalous behaviour of short cracks observed previously [7] and from tests conducted in this study has been rationalized as the result of the influence of microstructural texture, particularly grain boundaries, on crack growth [22] [23][8]. In some of these cases the dominant deceleration length may be estimated as the length from the crack initiation site to the first grain boundary encountered.

A recent study [4] conducted using Waspaloy showed that cracks are most likely to initiate in the largest grains. Statistical analyses based on the distribution of grain sizes, with and without initial cracks, show that the size of a grain having an initial crack is taken as the upper bound of the average grain size, *i.e.* the mean grain size plus one standard deviation. Crack initiation in large grains has also been observed in an aluminum alloy, Al2219-T851[24].

For the material used in this study the average grain size was found to be 9.9 μm having a standard deviation of 5.1 μm and a maximum grain size below 30 μm. Observation of crack growth behaviour at various stress levels revealed that the range of crack lengths at which minimum crack speeds were observed was found to be in the range of 30 – 60 μm. The crack lengths associated with these minima are above the size of the largest prior austenite grains measured. In addition it should be noted that all of the main cracks causing failure were associated with cracks initiated at the site of non-metallic inclusions and are therefore not necessarily associated with the largest grains. It appears therefore that the maximum retardation in crack growth for this material is a result of the transition from a microstructurally short crack to a physically small crack rather than being associated with the first grain boundary encountered by the crack. In this study individual deceleration lengths were determined by experiment. It

is acknowledged however that further work is required to develop an analytical method in order to predict the occurrence of a deceleration minima for this type of complex material microstructure.

In the current modelling of crack growth behaviour it has been assumed that the values of the friction stresses, σ_I and σ_{II}, acting over the MSC and PSC regimes respectively, remain constant throughout crack extension within each regime. As previously mentioned these friction stresses will vary as the crack length increases and as the crack tip approaches microstructural barriers such as second phases, inclusions, grain boundaries and cyclically induced micro- and macro anisotropy. The assumption of applying constant friction stresses for the MSC and PSC regimes respectively is considered based on the main characterisation of the material's resistance to crack growth, *i.e.* the transition from the MSC regime to the PSC regime.

It should be noted that the exact value of σ_I is not known and no reasons have previously been given for the friction stress σ_I to be equal to the fatigue limit σ_{fl} as suggested in this study. However the following points should be taken into account when considering a value for the friction stress σ_I. Firstly, as indicted in Figure 4.8(a), a crack can grow along preferentially oriented crystallographic planes in the MSC regime. As a result of this growth mechanism the friction stress during this regime will be somewhat below the gross yield stress which may represent a macroscopic definition of the propagation of plastic slip. Secondly it has been recognized that microplastic strain is still present below the fatigue limit, although on a restricted scale[25]. This indicates that the resistance to the movement of a single dislocation on a slip plane under cyclic loading is small compared with the fatigue limit. Since the friction stress σ_I is the average stress over the whole of MSC regime, which necessarily incorporates material texture

effects, its value will be larger than the resistance on a single slip plane. The fatigue limit σ_{fl} is a material constant which satisfies the above requirements and it therefore appears not unreasonable to choose σ_{fl} as the value of the friction stress σ_I within the MSC regime.

As mentioned earlier the transition crack length was determined directly from the experimental data however individual transition crack lengths exhibited a large variation and the standard deviation determined from the current test results was found to be 25 μm. In order to investigate the influence of the transition crack length on the predicted crack growth rate three transition crack lengths were chosen, *i.e.*, $d - 20\%d$, d and $d + 20\%d$. Crack growth rates were recalculated at a stress range, $\Delta\sigma = 1200$ MPa. The crack growth results obtained using the transition crack lengths given above are shown in Figure 4.10. It can be seen from this figure that there is no significant effect on crack growth rates as d is increased from $d - 20\%d$ to $d + 20\%d$. The predicted crack growth rate at the transition regime and the minimum crack growth rate increase slightly with an increase in the value of d. All the values of d taken give a reasonable prediction to the experimental results and it can therefore be concluded that slight differences of the value of d, resulting from different experiments, does not cause significant variation in predicting fatigue crack growth rates.

4.6 Summary of Air Fatigue Results

1. All cracks observed initiate at non-metallic inclusions. This is followed by crack growth along crystallographic planes.

2. At longer crack lengths it becomes more difficult for a crack to deflect away from a path perpendicular to the tensile stress axis and consequently it is

necessary for the crack to cut across the martensite laths.

3. The initial growth rates of short cracks are faster than those of long cracks at all stress levels. Short cracks are seen to grow at a stress intensity factor range well below the threshold value for a long crack.

4. The plastic zone emanating from the tip of a crack is modelled for three cases reflecting the development of the plastic zone within the microstructurally short crack (MSC) and physically small crack (PSC) regimes.

5. Cyclic plastic zone size Δr_p appears to be a suitable parameter for predicting short crack growth. The following short crack growth model has been proposed for Q2N steel,

$$\frac{da}{dN} = 2.948 \times 10^{-4}(\Delta r_p)^{0.472} \qquad MSC\ growth$$

and

$$\frac{da}{dN} = 7.112 \times 10^{-4}(\Delta r_p)^{0.852} \qquad PSC\ growth$$

6. Good agreement exists, over a wide range of stress levels, between the crack growth rates obtained using the present model and the observed experimental data.

4.7 References

[1] Annual Book of ASTM standards (1991), E647.

[2] Srawley J.E. (1987) In: Stress intensity factors handbook, Editor Y.Murakami, Pergamon Press, Oxford, 13 - 14.

[3] Newman J.C. and Raju I.S. (1987) In: Stress intensity factors handbook, Editor Y.Murakami, Pergamon Press, Oxford, 723 - 724.

[4] Zhang W. (1991) Short fatigue crack behaviour under different loading systems, Ph.D thesis, University of Sheffield.

[5] Akid R. and Murtaza G. (1992) Environment assisted short crack growth behaviour of a high strength steel. Short Fatigue Cracks, ESIS 13, Edited by K.J. Miller and E.R. de los Rios, 193-207, (Mechanical Engineering Publications, London).

[6] Boukerrou A. and Cottis R.A. (1992) The influence of corrosion on the growth of short fatigue cracks in structural steels. Short Fatigue Cracks, ESIS 13, Edited by K.J. Miller and E.R. de los Rios, 209-216, (Mechanical Engineering Publications, London).

[7] Miller K.J. (1987) The behaviour of short fatigue cracks and their initiation part I - a review of two recent books. Fatigue Fract. Engng Mater. Struct., 10, 75 - 91.

[8] Hobson P.D. (1985) The growth of short fatigue cracks in a medium carbon steel. Ph.D Thesis, University of Sheffield, U.K.

[9] Petit J., Mendez J., Berata W., Legendre L. and Muller C. (1992) The influence of environment on the propagation of short fatigue cracks in a titanium alloy. Short Fatigue Cracks, ESIS 13, Edited by K.J. Miller and E.R. de los Rios, pp235-250 (Mechanical Engineering Publications, London)

[10] Lankford J. (1983) The effect of environment on the growth of small fatigue cracks. Fatigue Eng. Mater. Struct., 6, 15 - 31.

[11] Hobson P.D., Brown M.W. and de los Rios E.R. (1986) Two phases of short crack growth in a medium carbon steel, in The behaviour of short fatigue cracks, European Group on Fracture Publication, 1, 441-459

[12] Brown C.W.and Hicks M.A.(1983) A study of short fatigue crack growth behaviour in Titanium alloy IMI 685. Fatigue Engng. Mater. Struct., 6, 67-76

[13] Bilby B.A., Cottrell A.H. and Swinden K.H. (1963) The spread of plastic yield from a notch. Proc. Roy. Soc., London, A., 272, 304 - 314

[14] Tanaka K. and Akiniwa Y. (1985) A model of the propagation small fatigue cracks interacting with grain boundary. J. Soc. Mat. Sci., Japan 34, 1310-1316.

[15] Navarro A. and de los Rios E.R.(1987) A model for short fatigue crack propagation with an interpretation of the short-long crack transition. Fatigue Fract. Engng Mater. Struct., 10, 169 - 186

[16] Brown M.W. (1988) Aspects of fatigue crack growth. Proc. Instn. Mech. Engrs., 202, C1, 19 - 29, IMechE.

[17] Morris W.L., James M.R. and Buck O. (1983) A simple model of stress intensity range threshold and crack closure stress. Engng Frac. Mech., 18, 871-877.

[18] Nakai Y., Tanaka K., and Yamashita M. (1983) Analysis of closure behavior of small fatigue cracks. J. Soc. Mat. Sci., Japan 32, 19-25.

[19] Allen R.J., Booth G.S. and Jutla T.(1986) Fatigue crack growth methodology and application - a review of principles and data generation. The Welding Institute, Contract report 3918/2/86.

[20] Brown M.W., de los Rios E.R. and Miller K.J. (1988) A critical comparison of proposed parameters for high-strain fatigue crack growth. Basic Questions in Fatigue: Volume I, *ASTM STP* 924, Editors J.T. Fong and R.J. Fields, American Society for Testing and Materials, Philadelphia, 233 - 259.

[21] Tanaka K. and Mura K. (1984) Fatigue crack growth along planar slip bands. Acta Met., 33, 1731-1740.

[22] Morris W.L. (1979) Microcrack closure phenomena for Al 2219 - T851. Metall. Trans., 10A, 5 - 11.

[23] Tanaka K., Nakai Y. and Yamashita M. (1981) Fatigue growth threshold of small cracks. Int. J. Frac., 17, 519 - 533.

[24] James M.R. and Morris W.L. (1983) The role of microplastic deformation in fatigue crack initiation. Fatigue Mechanisms: Advances in Quantitative Measurement of Physical Damage, (Edited by J. Lankford *et al*), ASTM STP 811, pp46-70.

[25] Tomkins B. (1968) Fatigue crack propagation - An analysis. Phil. Mag., Vol.18, pp1041 - 1065.

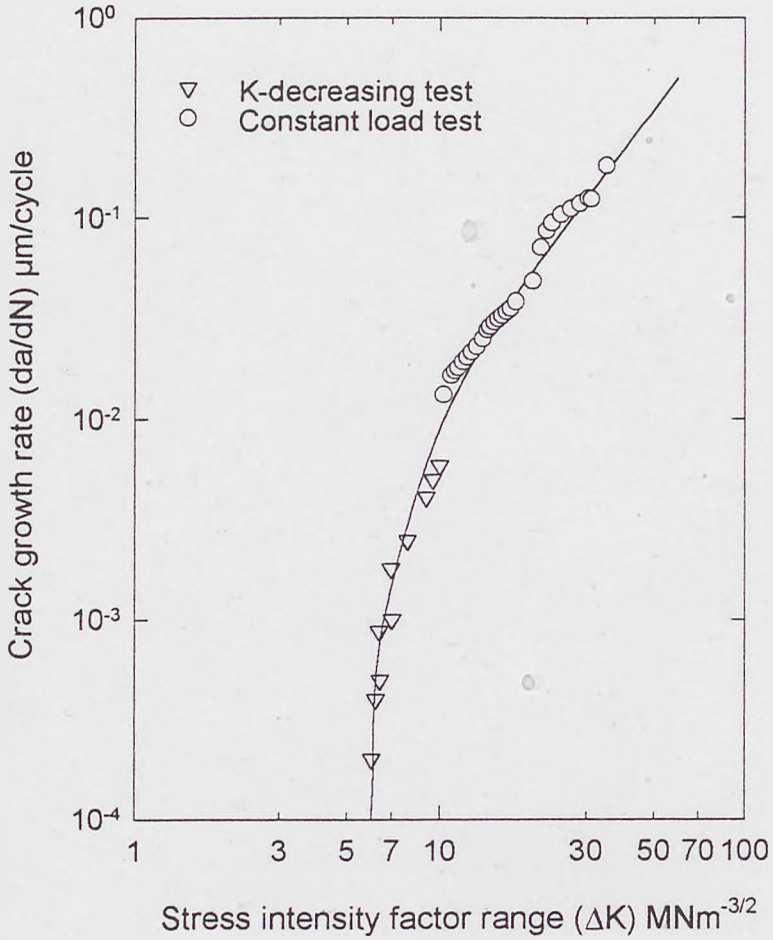

Fig.4.1 LEFM long crack growth behaviour of Q2N steel.

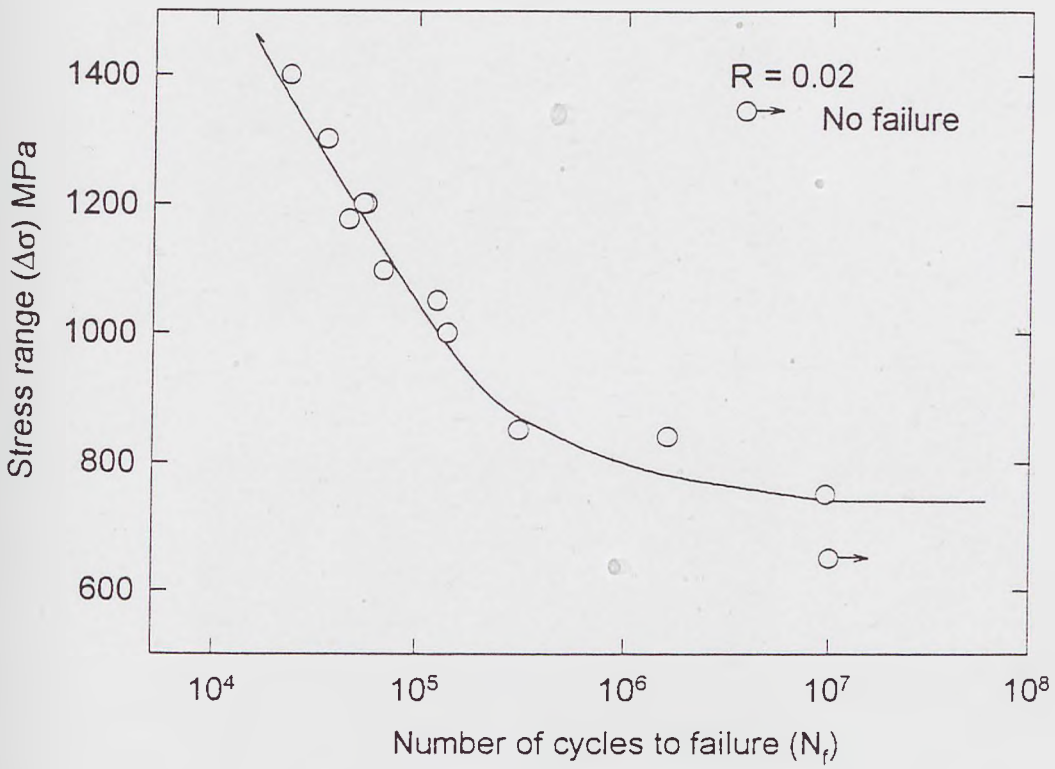

Fig.4.2 $S-N$ air fatigue endurance curve for Q2N steel.

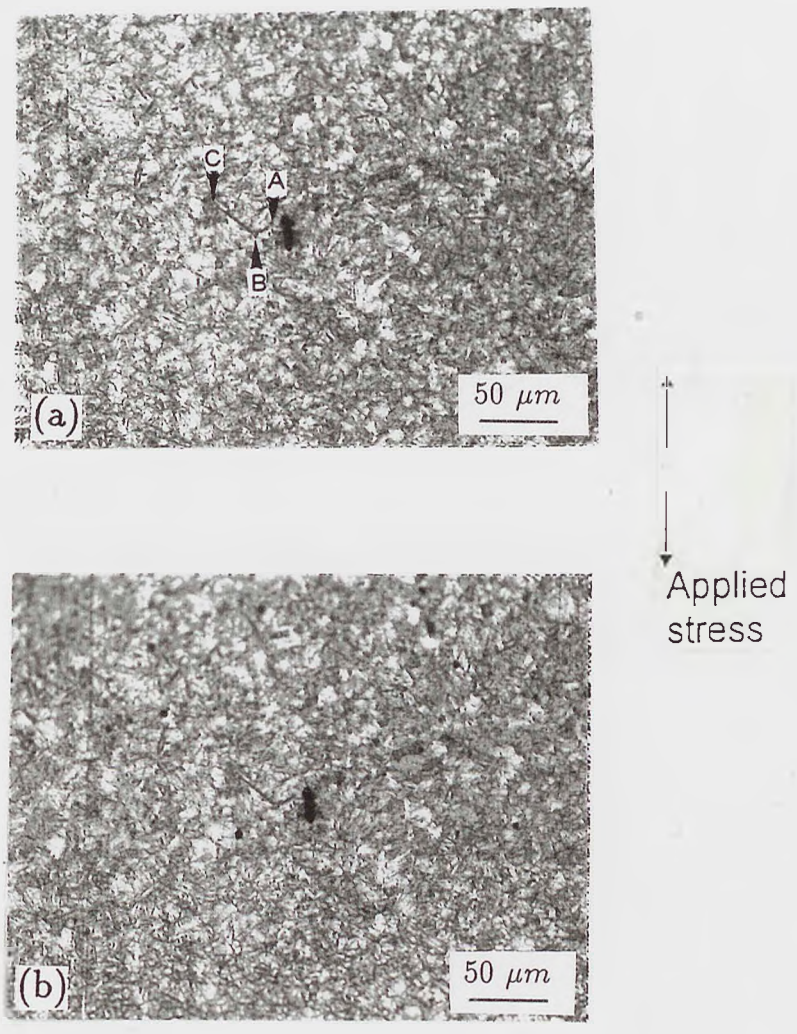

Fig.4.3 Deceleration of crack growth during the transition of an MSC to a PSC $N_f = 2.35 \times 10^4$ (a) $N/N_f = 0.46$, (b) $N/N_f = 0.55$.

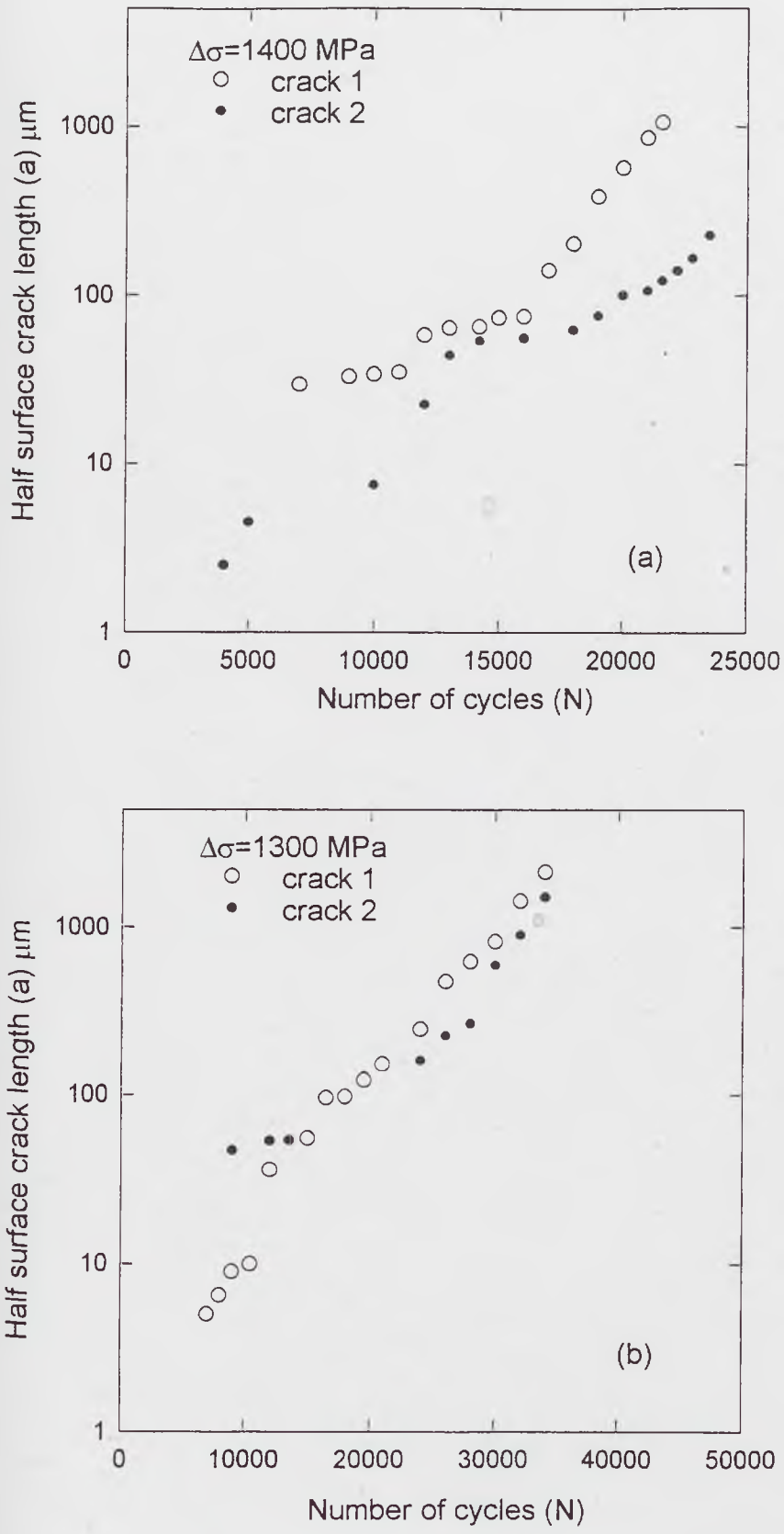

Fig.4.4 Short fatigue crack growth results (crack length versus number of cycles).

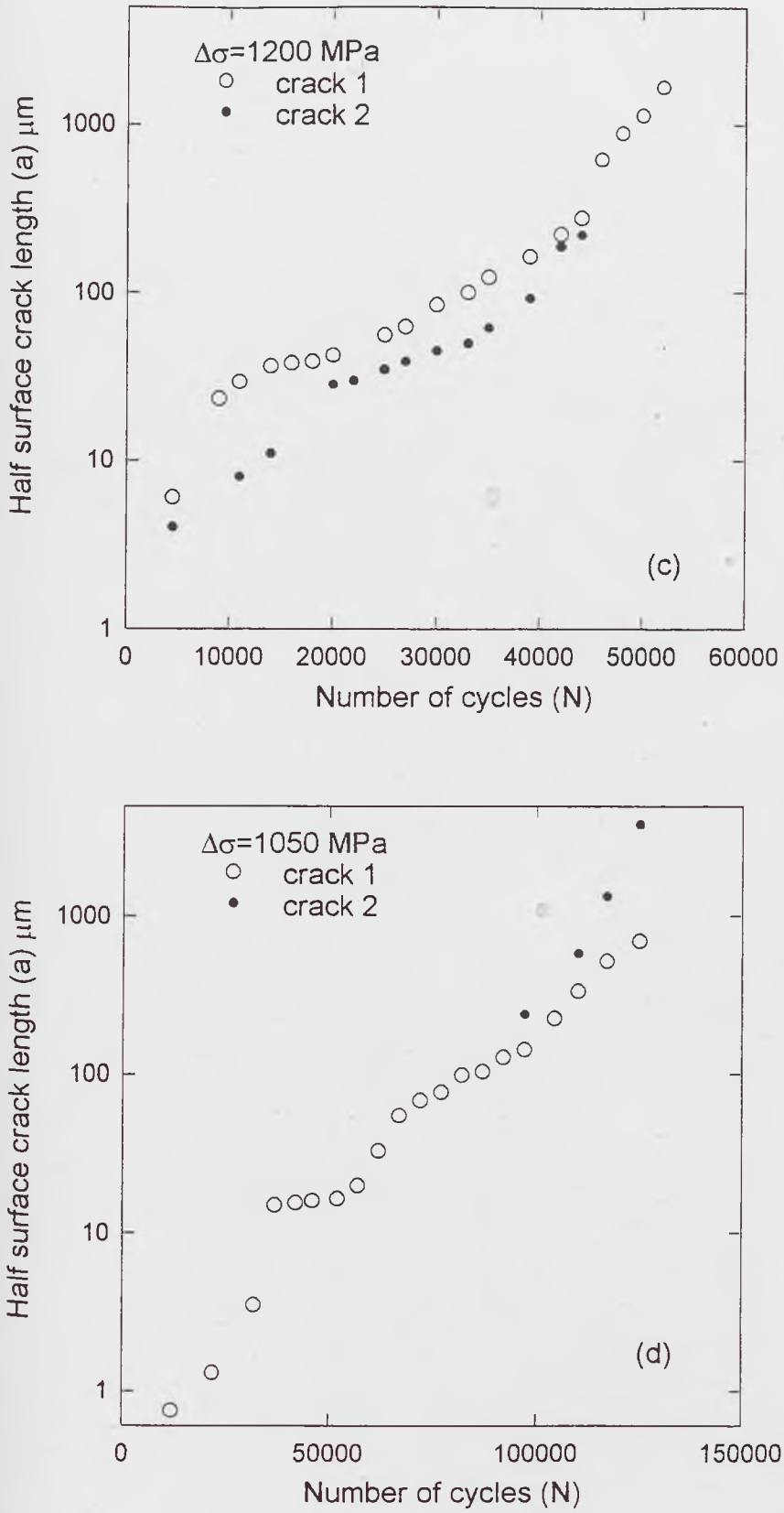

Fig.4.4 Short fatigue crack growth results (crack length versus number of cycles).

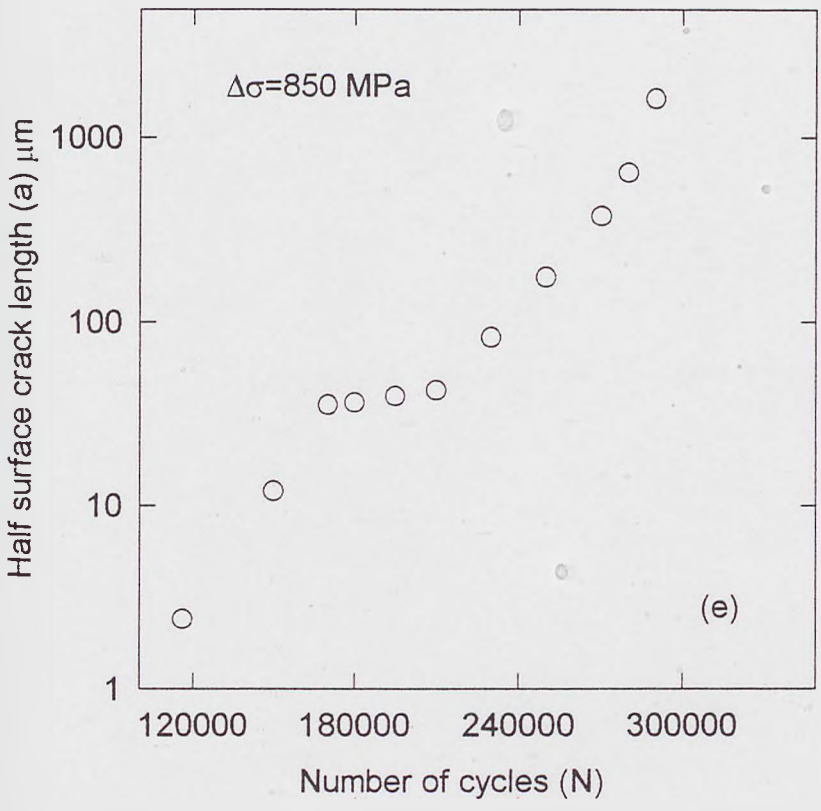

Fig.4.4 Short fatigue crack growth results (crack length versus number of cycles).

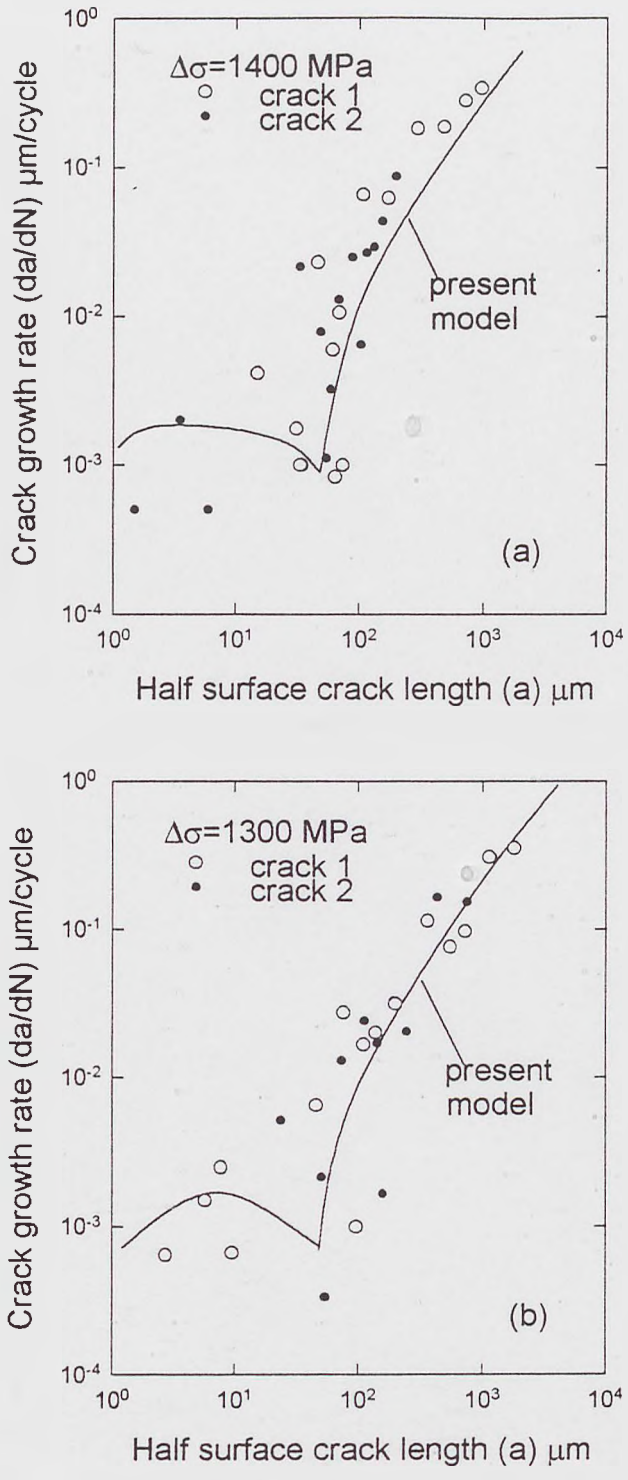

Fig.4.5 Comparison of the present crack growth model with experimental crack growth data.

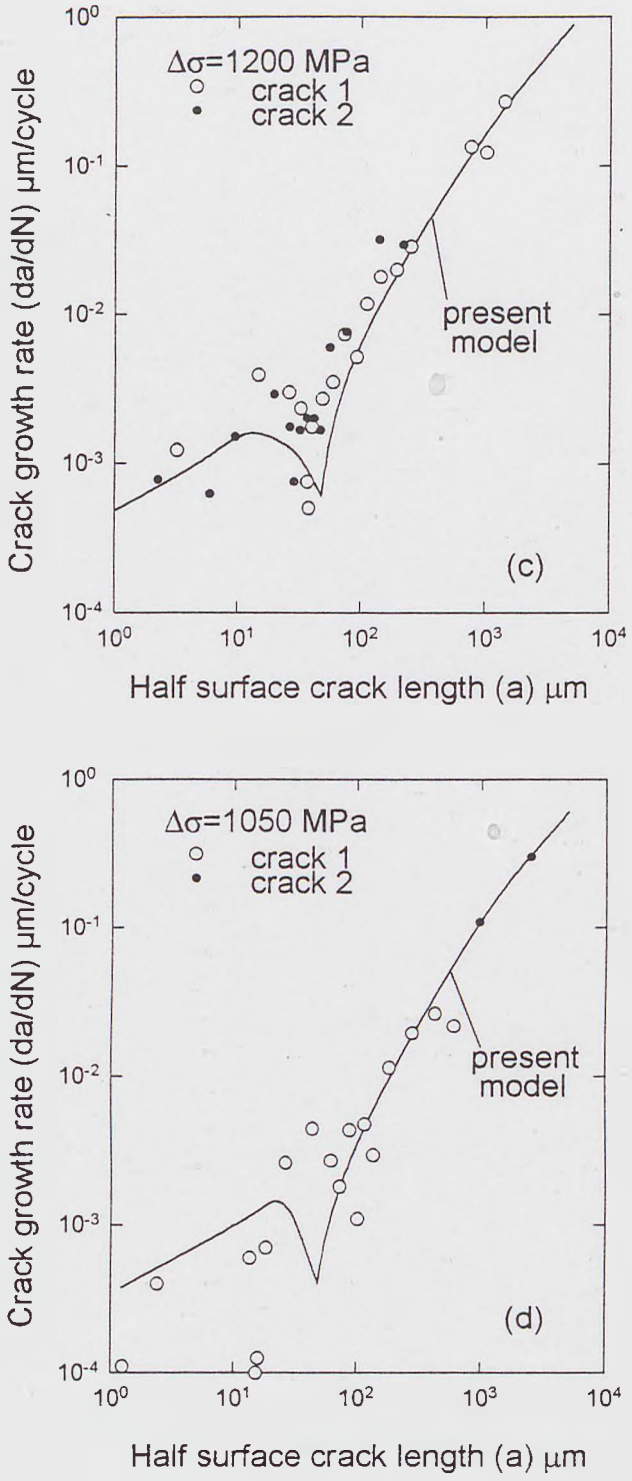

Fig.4.5 Comparison of the present crack growth model with experimental crack growth data.

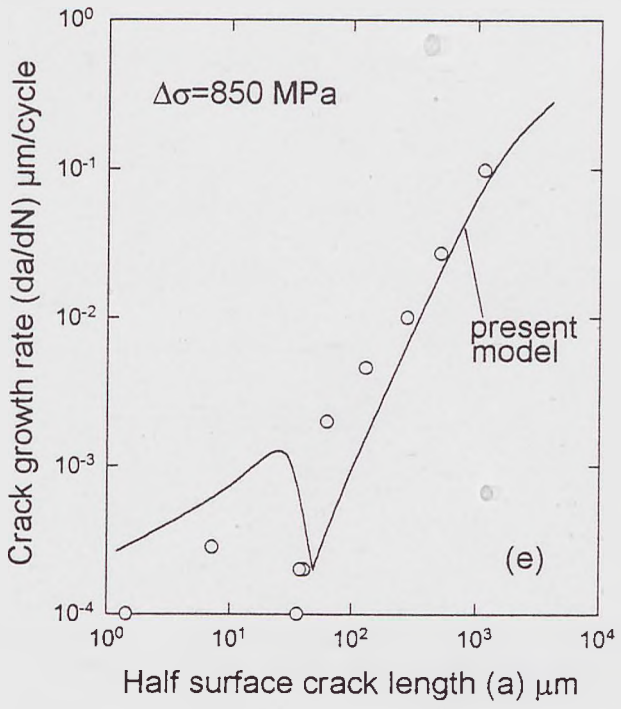

Fig.4.5 Comparison of the present crack growth model with experimental crack growth data.

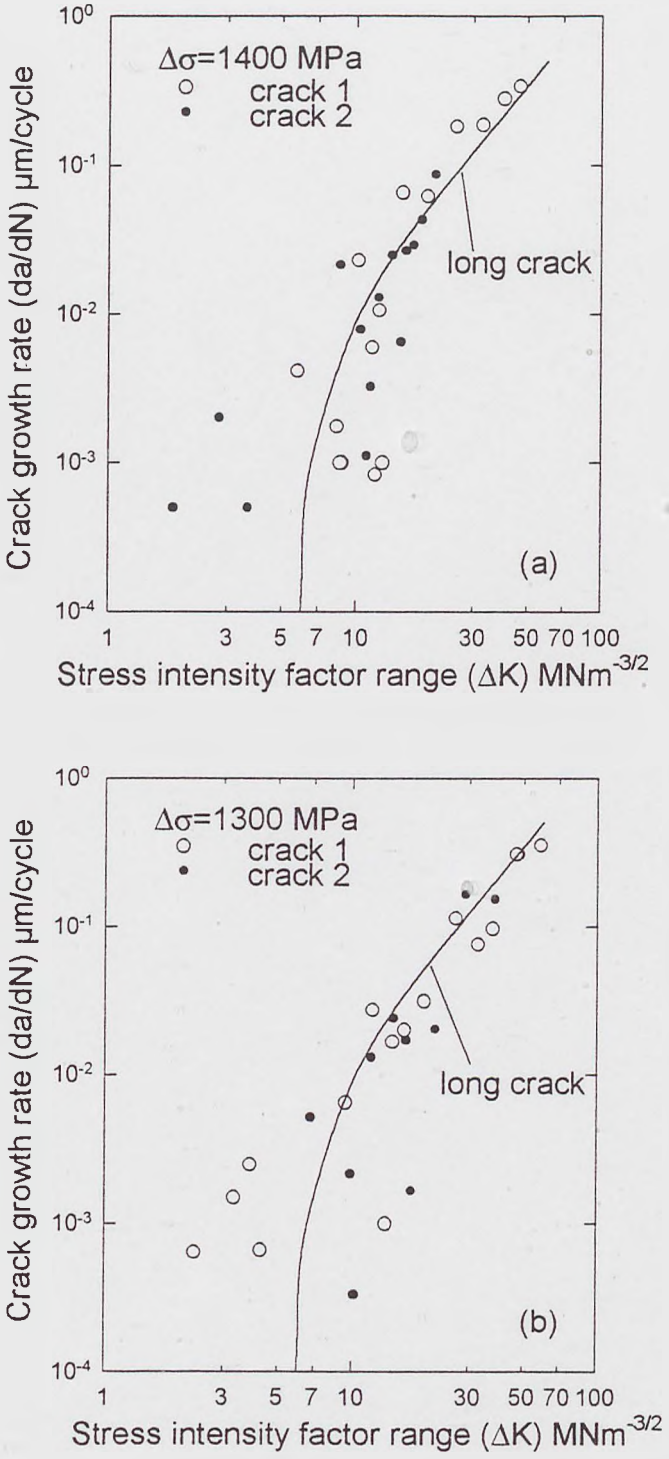

Fig.4.6 Comparison of short and long crack growth rates.

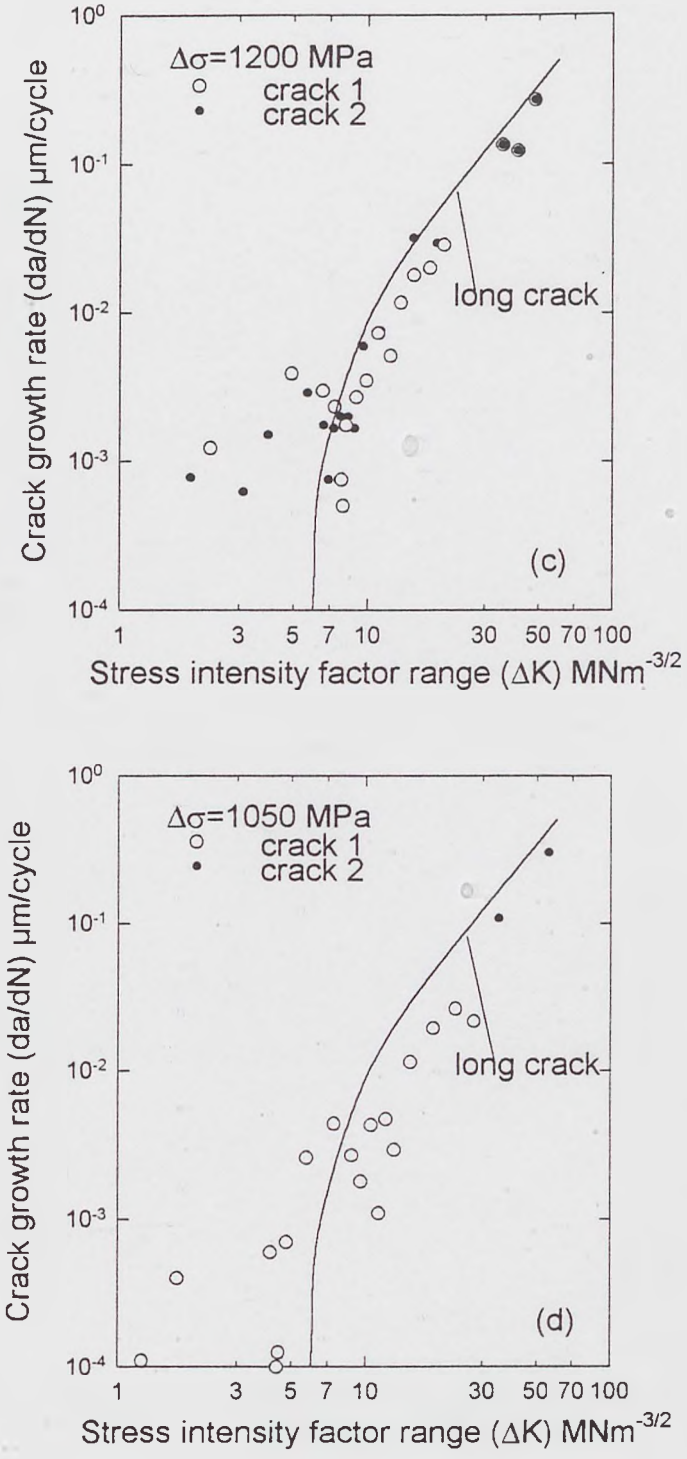

Fig.4.6 Comparison of short and long crack growth rates.

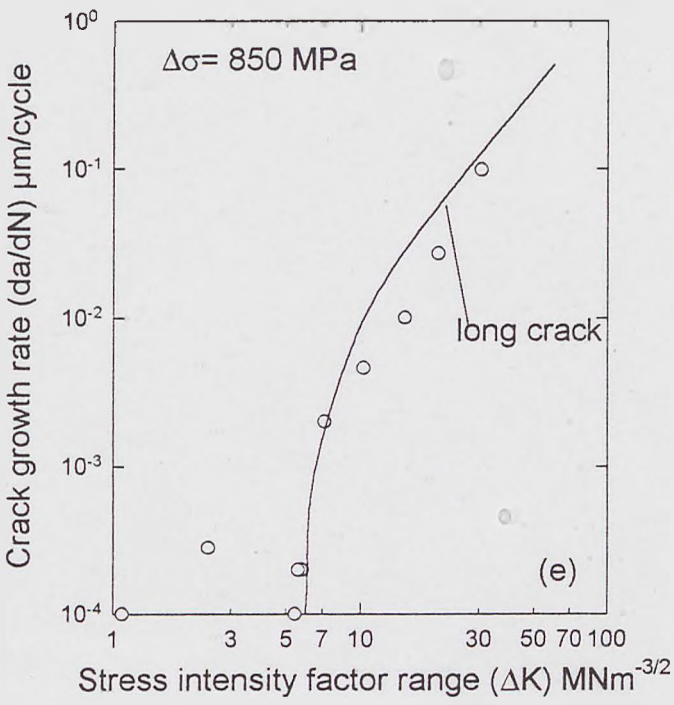

Fig.4.6 Comparison of short and long crack growth rates.

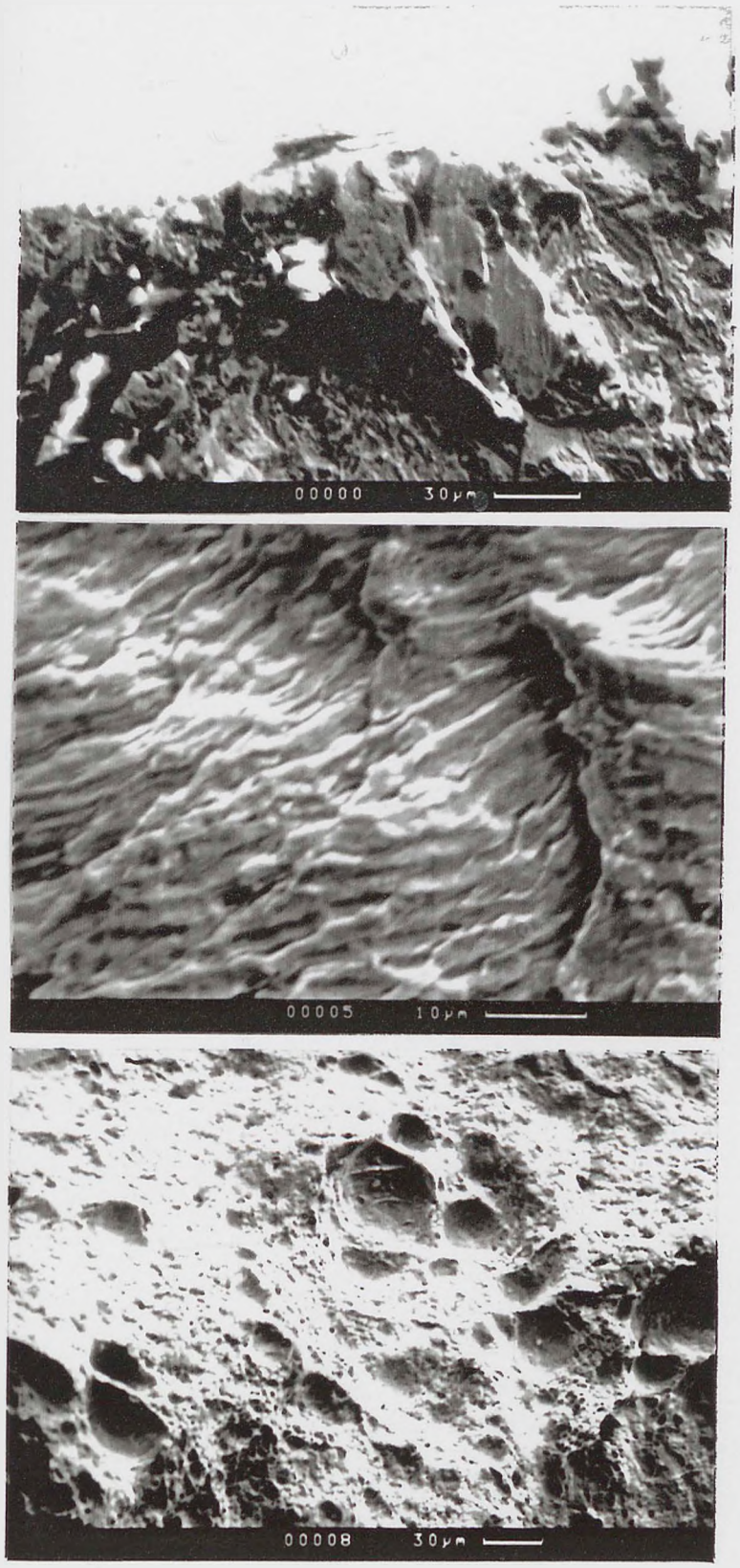

Fig.4.7 Characteristics of fracture surfaces at different crack growth stages

(a) crystallographic cracking

(b) striation crack growth

(c) dimple features in final fracture surface.

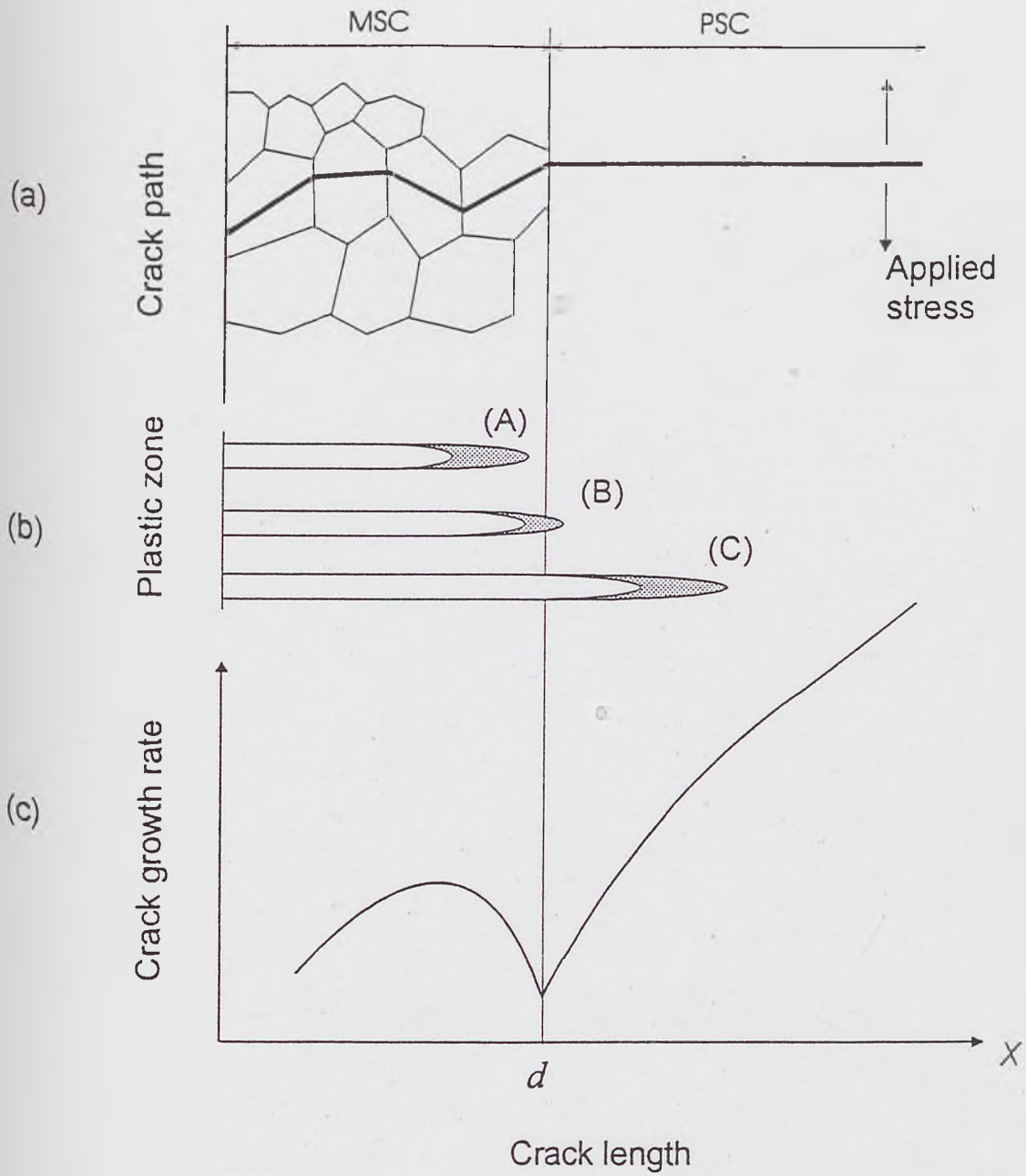

Fig.4.8 Schematic diagram indicating the short crack growth regimes and the development of the crack tip plastic zone (model).

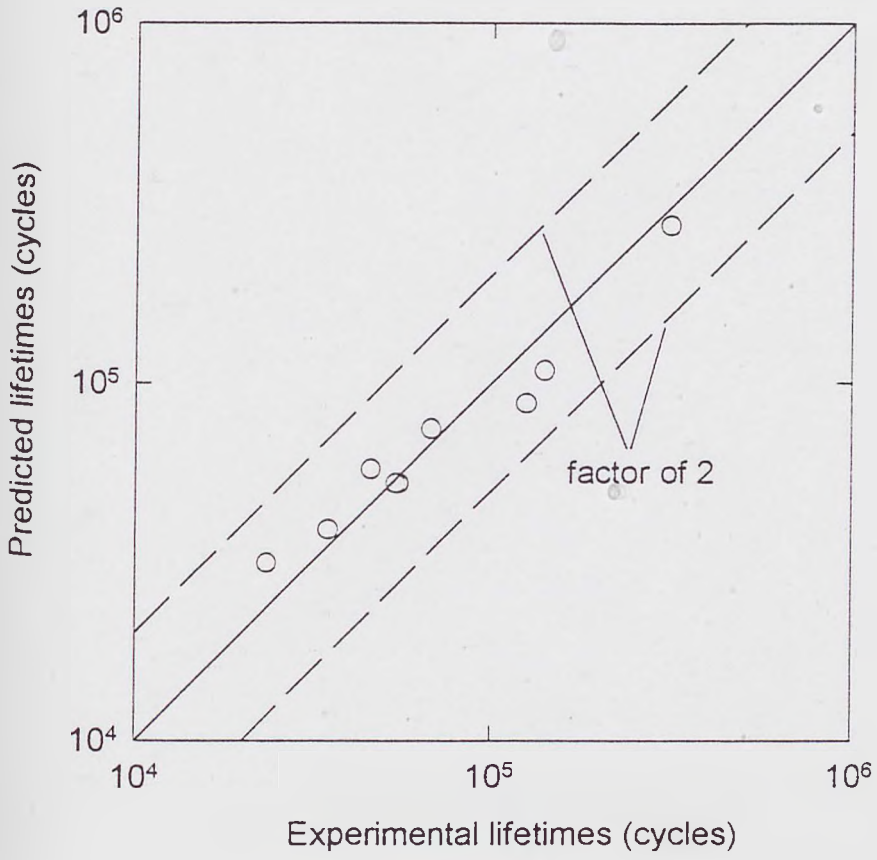

Fig.4.9 Comparison between experimental and predicted air fatigue lifetimes.

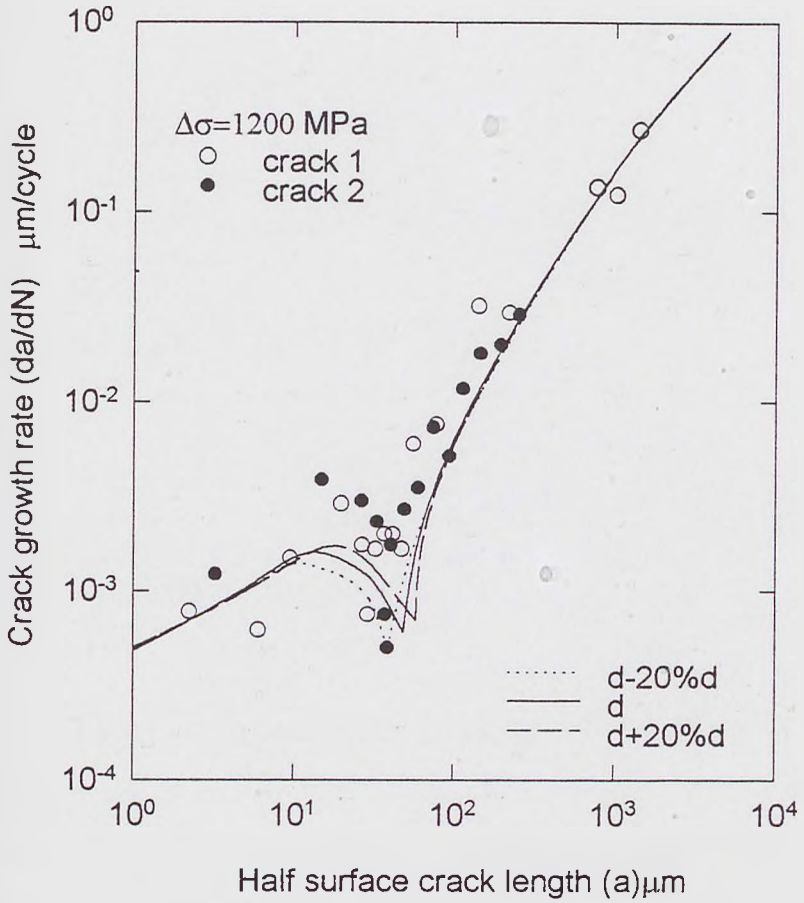

Fig.4.10 Comparison of predicted crack growth rates using different transition crack lengths d.

Chapter 5

Seawater Effects on Short Crack Growth Behaviour

5.1 Introduction

Considerable effort has been made to gain an understanding of short fatigue crack growth behaviour and in this respect several models have been proposed which estimate the fatigue lifetime in air [1][2][3][4]. In comparison however to the short fatigue crack growth data obtained from tests conducted in air, only a limited amount of data is available concerning short crack growth behaviour within corrosive environments. In this chapter details of the results from tests conducted to investigate the short fatigue crack behaviour of Q2N steel in seawater are presented.

Seven three-point-bend corrosion fatigue tests, each at different stress levels, have been conducted in seawater at a stress ratio of $R \approx 0$. Fatigue lifetimes were

recorded and acetate surface replicas of specimens were taken, at frequent intervals during the tests, in order to evaluate the initiation and propagation behaviour of short cracks.

Summarised below are the main findings from the corrosion fatigue tests conducted in this study;

1. In comparison to air fatigue lifetimes a significant decrease in fatigue lifetime is noted for tests conducted in seawater.
2. Crack initiation is preceded by the formation of corrosion pits at all stress levels used.
3. It is observed that in the presence of seawater short cracks can grow at stress levels well below the in-air fatigue limit.
4. For this material/environment system defect development is characterised by the pitting followed by crack development. Based on observations made during tests models have been derived to estimate total corrosion fatigue lifetime.

5.2 Experimental Procedure

A Schenck 250 kN servo-hydraulic testing machine, as described in Chapter 3, was used to perform all three-point-bend corrosion fatigue tests. Fatigue tests were carried out in seawater at various stress levels, under load control, to produce $S-N$ endurance and short crack growth data.

The following test conditions were used:

- Loading mode: three point bend;
- Stress ratio: $R \approx 0.02$;
- Testing frequency: $f = 0.1$ Hz;
- Environment: artificial seawater to specification BS:3900.

Specimens were tested at seven different stress levels and short fatigue cracks were monitored at six out of the seven different stress levels used. Among these was one specimen tested at a stress level well below the in-air fatigue limit stress. Acetate replicas were taken of the specimen surface at frequent intervals during tests to record detailed information concerning the development and growth of defects. Additional information on material microstructure, specimen dimensions and loading fixture arrangement are provided in Chapter 3 and references [5][6][7].

Fatigue crack growth rates, da/dN, were estimated using a secant method;

$$\frac{da}{dN} = \frac{a_{i+1} - a_i}{N_{i+1} - N_i} \tag{5.1}$$

where a_i and a_{i+1} are two consecutive half surface crack lengths at N_i and N_{i+1} cycles respectively. Since the crack growth rate represents the growth of a crack at the mid point of two consecutive crack lengths, the corresponding average crack length $\overline{a}$ is given as $\frac{1}{2}(a_{i+1} + a_i)$.

5.3 Results

5.3.1 $S-N$ Curve

Corrosion fatigue lifetime results obtained by conducting fatigue tests in seawater are given in Table 5.1. The relationship between applied stress range and fatigue lifetime is given in Equation 5.2 and plotted in Figure 5.1.

$$\Delta\sigma^{3.141} N_f = 3.890 \times 10^{13} \tag{5.2}$$

Specimen	Stress range (MPa)	Lifetime (cycles)
CF-1	1400	4.60×10^3
CF-2	1300	6.46×10^3
CF-3	1200	7.77×10^4
CF-4	1050	1.55×10^4
CF-5*	900	1.95×10^4
CF-6	850	2.99×10^4
CF-7	650	4.89×10^4

Table 5.1: Fatigue lifetime results in seawater

* — specimen without replicas.

The in-air fatigue lifetime results obtained in Chapter 4 are also plotted on this figure for the purpose of comparison.

5.3.2 Corrosion Fatigue Crack Growth Behaviour

Figures 5.2(a) - 5.2(f) give a typical example of short corrosion fatigue crack development from initial pit development to final failure. It can be seen that corrosion pits developed rapidly during the early stages of the fatigue tests (Figure 5.2(a)). However as can be seen from Figure 5.2 the shape of corrosion pits is not always typically hemispherical. The elongated pit profile suggests that a mechanism involving stress - assisted dissolution might be operative during this stage. As cycling continued a mode I, PSC type crack can be clearly seen to develop (Figure 5.2(c)). The PSC type crack continues to propagate until eventually rapid growth leads to fatigue failure (Figures 5.2(c)-5.2(f)).

Crack growth results, *i.e.*, crack length versus the corresponding number of loading cycles and crack growth rate versus crack length are presented in Figures 5.3 and 5.4 respectively. The in-air crack growth rates are also presented in Figure 5.4 for the purpose of comparison. It can be seen from Figure 5.4 that the crack growth in seawater shows higher crack growth rates than for equivalent tests conducted in air and that the any decelerations in corrosion fatigue crack growth rate are not as low as those for air fatigue. This suggests that the corrosion fatigue crack growth mechanism proposed in [8] [9], *i.e.*, conjoint action of chemical and mechanical processes to overcome the strength of the microstructural barrier, may be operative for the present system.

5.4 Modelling of Corrosion Pitting and Short Crack Growth

A short crack growth model describing air fatigue crack growth has been previously developed in Chapter 4. This model assumes that short crack growth can be divided into two regimes, *i.e.*, a microstructurally short crack (MSC) regime and a physically small crack (PSC) regime. In seawater however it appears that corrosion pit growth may be a dominant process during the early stages of the corrosion fatigue test. The pit growth is then followed by the PSC growth

To address the two - stage corrosion fatigue damage mechanism corrosion pit growth and short corrosion fatigue crack growth models have been proposed to describe corrosion fatigue defect growth.

5.4.1 Modelling of Corrosion Pit Growth

Pits which leads to the initiation of dominant cracks were measured during the corrosion fatigue test and the results are presented in Figure 5.5. It can be seen, from this figure, that the size of pits increases with increase time. Furthermore these pits grow rapidly at the initial stage then exhibit a decelerating trend.

It has been reported that the growth of corrosion pits can be expressed by an equation of the following type [12]

$$a_p = At^B \tag{5.3}$$

where A and B are material and environment system constants. In this equation the growth of corrosion pits is expressed only as a function of time. However, as

shown in Figure 5.5, the growth of corrosion pits is also affected by the magnitude of the applied cyclic stress range. This effect should therefore be taken into account in the growth law of corrosion pits developing during corrosion fatigue loading.

Changes in the size of corrosion pits versus the time ratio, t/t_f, where t_f is the time corresponding to the final fatigue failure, for different stress levels is shown in Figure 5.6. This figure shows that:

i. pits grow rapidly in the initial stage of corrosion fatigue test;

ii. pits growth rates tend to decelerate at a similar pit size.

iii. the relationship between pit size and time ratio is restricted to a relatively narrow range regardless of applied stress level.

These features of pit growth lead us to propose an equation of the form giving in 5.4

$$a_p = A(t/t_f)^B \tag{5.4}$$

for estimation the pit growth under fatigue loading.

A least squares analysis on the experimental data was carried out giving values for A and B of 96.21 and 0.6932 respectively. The estimation for pit size obtained by Equation 5.4 is also given as a solid line in Figure 5.6.

5.4.2 Modelling of Corrosion Short Fatigue Crack Growth

In Chapter 4 it is assumed that the growth of a physically small crack is controlled by the plastic zone size at the crack tip. The plastic zone size at the crack tip can be determined using microstructural fracture mechanics analysis, *i.e.*, by solving the equilibrium equations of all the internal and external forces acting on the continuously distributed dislocation system [10][11][3]. The solutions of the plastic zone size for this case, together with the transposition for cyclic loading are given in Section 4.4.

Figure 5.7 presents the relationship between Δr_p obtained by adopting the plastic zone model given in section 4.4 and corrosion fatigue crack growth rate for the PSC regimes. It can be seen that the data pairs (da/dN, Δr_p) for PSC regime agree with each other for all stress levels. This indicates that Δr_p is a acceptable parameter to control short crack growth in seawater conditions.

A least squares fit was performed on the data set of pairs (da/dN, Δr_p) giving a crack growth equation as follows:

$$\frac{da}{dN} = 1.028 \times 10^{-4} (\Delta r_p)^{1.306} \tag{5.5}$$

5.4.3 Fatigue Lifetime Estimation

As previously mentioned the corrosion fatigue process for the present material/environment system consists of corrosion pit growth and corrosion - assisted short crack growth. The total fatigue lifetime can therefore be given as the summation of the pit growth period (N_{pit}) and the PSC propagation period (N_{PSC}),

i.e.,

$$N_f = N_{pit} + N_{PSC} \tag{5.6}$$

In Section 5.4.1 pit size was modelled as a function of the time ratio, t/t_f. In considering that the number of fatigue cycles, N, may be expressed in terms of a time, t, through the test frequency, f, *i.e.*, $N = t \times f$, Equation 5.4 can be rewritten in terms of the number of cycles as the relationship of (N/N_f);

$$a_p = A(N/N_f)^B \tag{5.7}$$

Equations 5.2 and 5.7 can then be combined to give an expression to estimate the number of cycles, N_{pit}, to grow a pit to a certain length, a_p,

$$N_{pit} = 5.305 \times 10^{10} a_p^{1.442} \Delta\sigma^{-3.139} \tag{5.8}$$

The number of cycles elapsed during the PSC regime, N_{PSC}, can be obtained by integrating Equation 5.5 in the appropriate ranges, *i.e.*,

$$N_{PSC} = \int_{a_p}^{a_f} \frac{da}{1.028 \times 10^{-4} (\Delta r_p)^{1.306}} \tag{5.9}$$

The final equation to estimate fatigue lifetime can be given as

$$N_f = 5.305 \times 10^{10} a_p^{1.442} \Delta\sigma^{-3.139} + \int_{a_p}^{a_f} \frac{da}{1.028 \times 10^{-4} (\Delta r_p)^{1.306}} \tag{5.10}$$

In Equation 5.10 the average pit size, a_p, at which a PSC crack was observed is determined experimentally to be $\approx 60\mu m$ and the final crack length, a_f, at which fatigue test was terminated, is about 4 mm. Based on these values of a_p and a_f Figure 5.8 presents a comparison of actual lifetime and estimated lifetime obtained using Equation 5.10.

5.5 Discussion

Pitting was observed after a few number of cycles as shown in Figure 5.2. and it appears that corrosion pits play an important role during the early development of short cracks. Corrosion pits may accelerate the fatigue processes in a number of ways, for example pits can create defects which act as stress concentrators and/or provide sites where low pH solutions may be formed during the dissolution and hydrolysis of metal cations and sulphide inclusions. Furthermore sulphides dissolution may provide species which act to catalyse the dissolution of iron.

Figure 5.5 shows that cyclic loading has a significant effect on pit growth. The early models that expressed pit growth only as a function of time [13] not appear to be suitable under corrosion fatigue conditions and it is essential to take into account the effects of cyclic stress when modelling pit growth.

Recent research work has shown that in polycrystalline metals crack initiation may occur immediately under cyclic stress [14][15][2]. This suggests that a short crack may initiate at the bottom of a corrosion pit before it can be observed on the surface. However it is difficult to form such a conclusion from surface replicas. Furthermore it should be noted that the surface condition of a specimen can have a significant effect on subsequent pit development and initial corrosion

crack growth.

5.6 Summary

1. The fatigue strength of Q2N steel is strongly influenced in the presence of seawater. When compared to tests conducted in air there is a significant decrease in fatigue lifetime in the presence of seawater.

2. The first evidence of corrosion fatigue damage on specimens is the formation of corrosion pits. Crack initiation is then observed from the sites of these corrosion pits.

3. Short fatigue crack growth is significantly enhanced by the presence of a corrosive environment. The minimum crack growth rates observed in air tests are much lower than those observed in seawater tests suggesting a corrosion fatigue crack growth mechanism, that consists of the conjoint action of chemical and mechanical processes which operates to overcome the resistance of microstructural barriers.

4. Corrosion pit growth and corrosion fatigue crack growth have been modelled in order to quantify the defect development for this material/environment system. Corrosion pit growth under fatigue loading was modeled in terms of the time ratio of t/t_f. A least squares analysis on experimental data gives following equation for estimating the pit growth.

$$a_p = A(t/t_f)^B$$

The proceeding PSC growth behaviour was modelled in terms of the crack tip plastic zone size (Δr_p).

The use of these models provides a suitable method for estimating corrosion fatigue lifetime.

5.7 References

[1] El Haddad M.H., Smith K.N. and Topper T.H. (1986) Fatigue crack propagation of short cracks. J. Eng. Mater. Technol. (Trans. ASME H), 101, 1979, 42 - 46.

[2] Hobson P.D., Brown M.W. and de los Rios E.R., Two Phases of short crack growth in a medium carbon steel, in The behaviour of short fatigue cracks, European Group on Fracture Publication, 1, 441-459

[3] Navarro A. and de los Rios E.R. (1987) A model for short fatigue crack propagation with an interpretation of the short-long crack transition. Fatigue Fract. Engng Mater. Struct., 10, 169 - 186

[4] Navarro A. and de los Rios E.R. (1988) An alternative model of the blocking of dislocations at grain boundaries. Phil. Mag. A, 57, 37-42

[5] Wu X.J. and Akid R. (1992) An investigation of the frequency effect on the short fatigue crack behaviour of Q2N steel. SIRIUS, University of Sheffield, Report No.2-CPC12/0171.

[6] Wu X.J. and Akid R. (1992) Modelling of short fatigue crack growth of Q2N steel, SIRIUS, University of Sheffield, Report No.3-CPC12/0171.

[7] Wu X.J. and Akid R. (1993) Frequency Effect on the Short Crack Behaviour of Q2N Steel in Artificial Seawater. SIRIUS, University of Sheffield, Report No.4-CPC12/0171.

[8] Akid R. and Miller K.J. (1990) The initiation and growth of short fatigue cracks in an aqueous saline environment. In Environment assisted fatigue, EGF publication 7 (Eds P. Scott and R.A. Cottis), 415 - 434 (Mechanical Engineering Publications, London)

[9] Akid R. and Murtaza G. (1992) Environment assisted short crack growth behaviour of a high strength steel. Short Fatigue Cracks, ESIS 13 (Eds K.J. Miller and de los Rios ER), 193 - 208. (Mechanical Engineering Publications, London)

[10] Bilby B.A., Cottrell A.H. and Swinden K.H. (1963) The spread of plastic yield from a notch. Proc. R. Soc., Lond. A., 272, 304 - 314

[11] Tanaka K. and Akiniwa Y. (1985) A model of the propagation small fatigue cracks interacting with grain boundary. J. Soc. Mat. Sci., Japan 34, 1310-1316.

[12] Kawai S. and Kasai K. (1985) Considerations of allowable stress of corrosion fatigue. Fatigue Fract. Engng Mater. Struct., 8, 115 - 127.

[13] Godard H. P. (1960) The corrosion behaviour of aluminum in natural water. Can. J. Chem. Engng., 38, 167.

[14] Miller K. J. (1993) Materials science perspective of metal fatigue resistance. Materials Science and Technology, 9, 453-462.

[15] Miller K.J. (1985) Initiation and growth rates of short fatigue cracks. IUITAM Eshelby memorial Symposium, Fundamentals of Deformation and Fracture(Eds. Bilby,B.A., Miller,K.J. and Willis,J.R.), 477-500, Cambridge University Press.

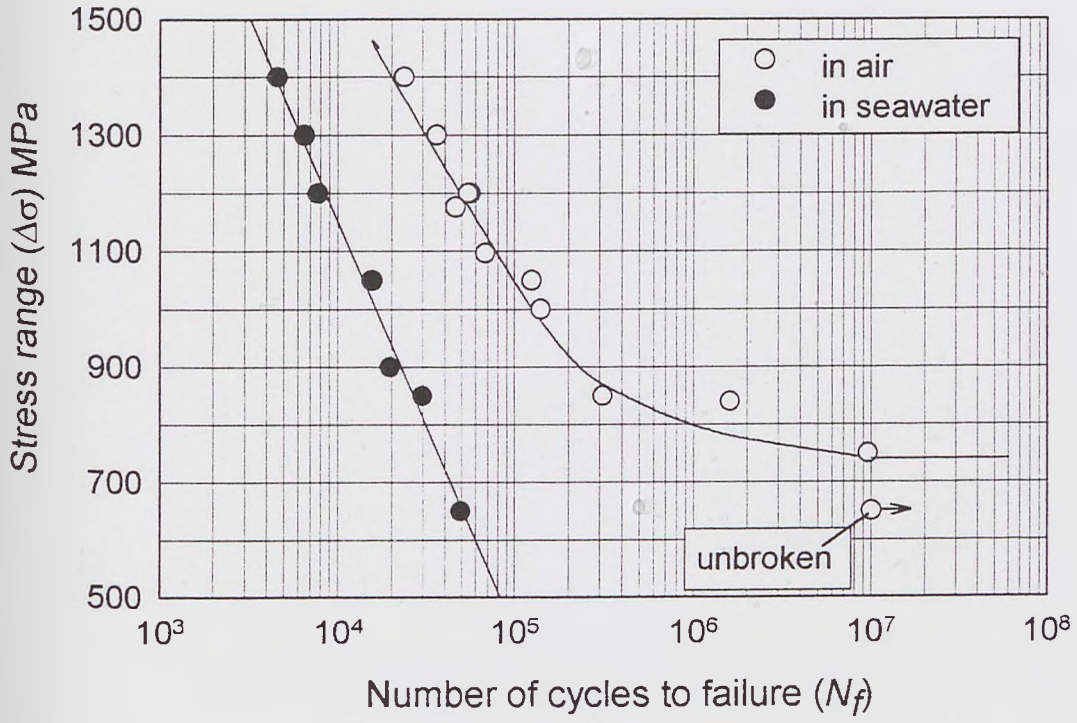

Fig.5.1 $S-N$ corrosion fatigue endurance curve for Q2N steel.

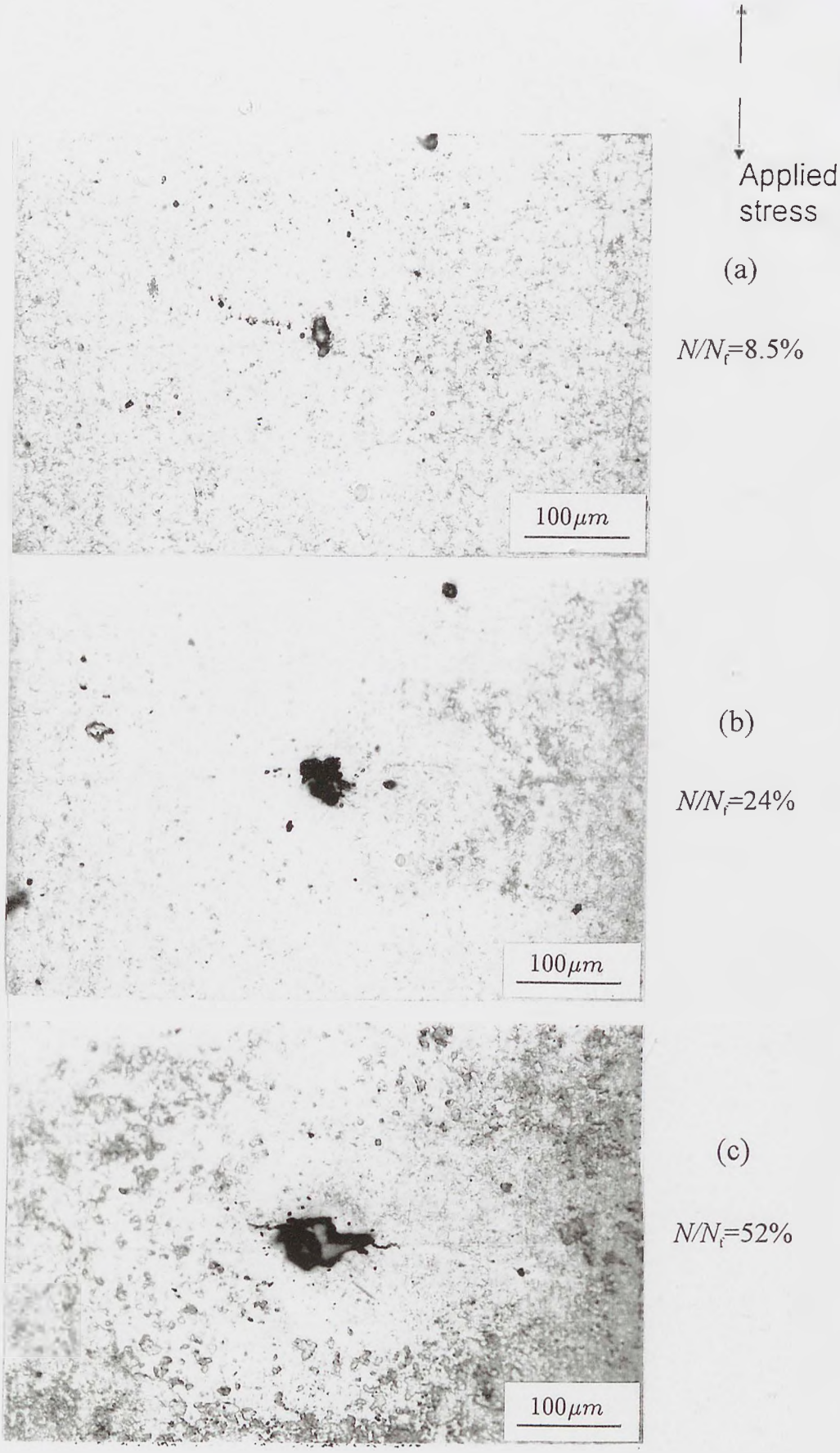

Fig.5.2 Development of a corrosion fatigue crack in seawater,

$f = 0.1\ Hz$, $\Delta\sigma = 1300 MPa$.

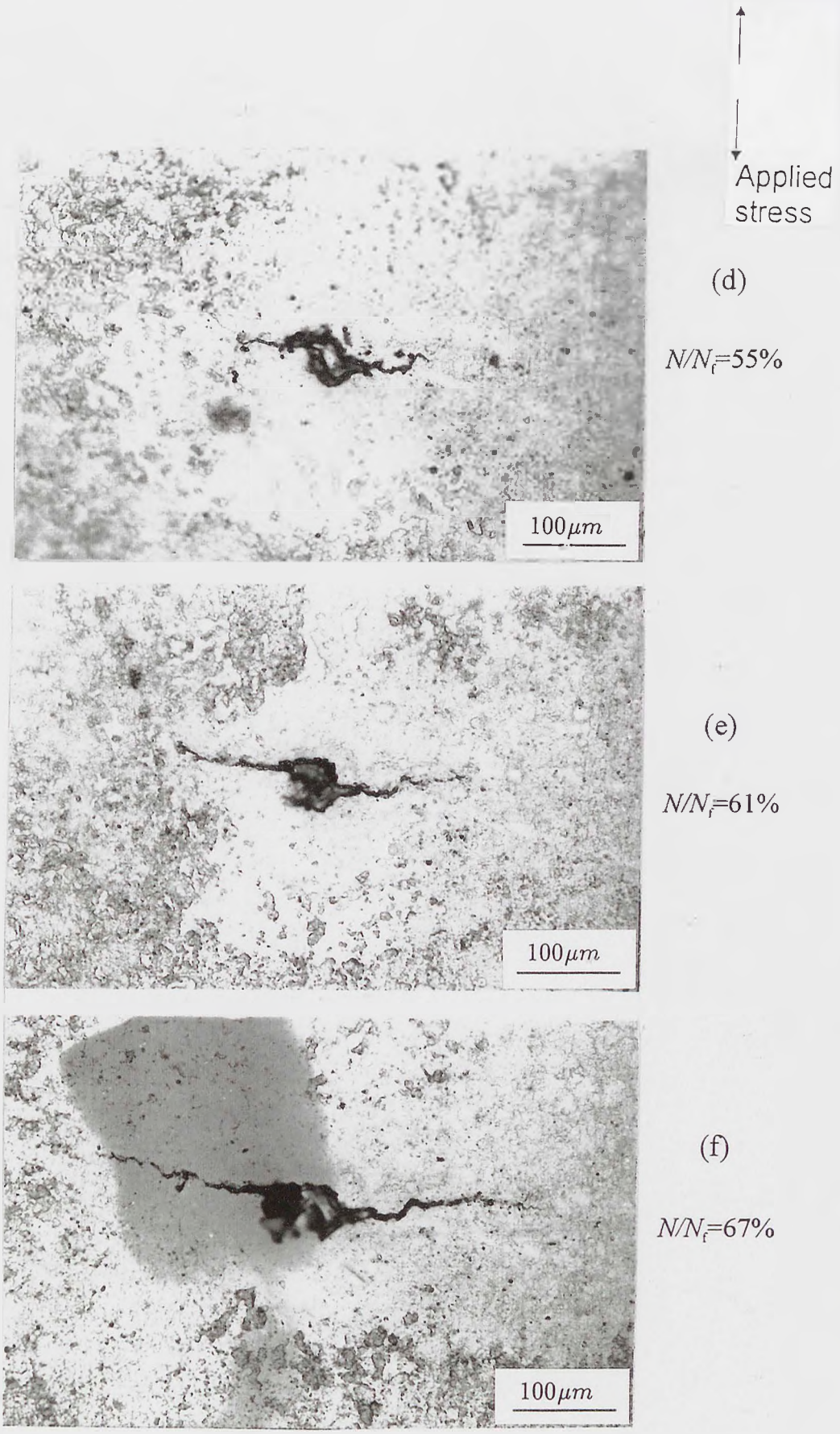

Fig.5.2 Development of a corrosion fatigue crack in seawater, $f = 0.1\ Hz$, $\Delta\sigma = 1300 MPa$.

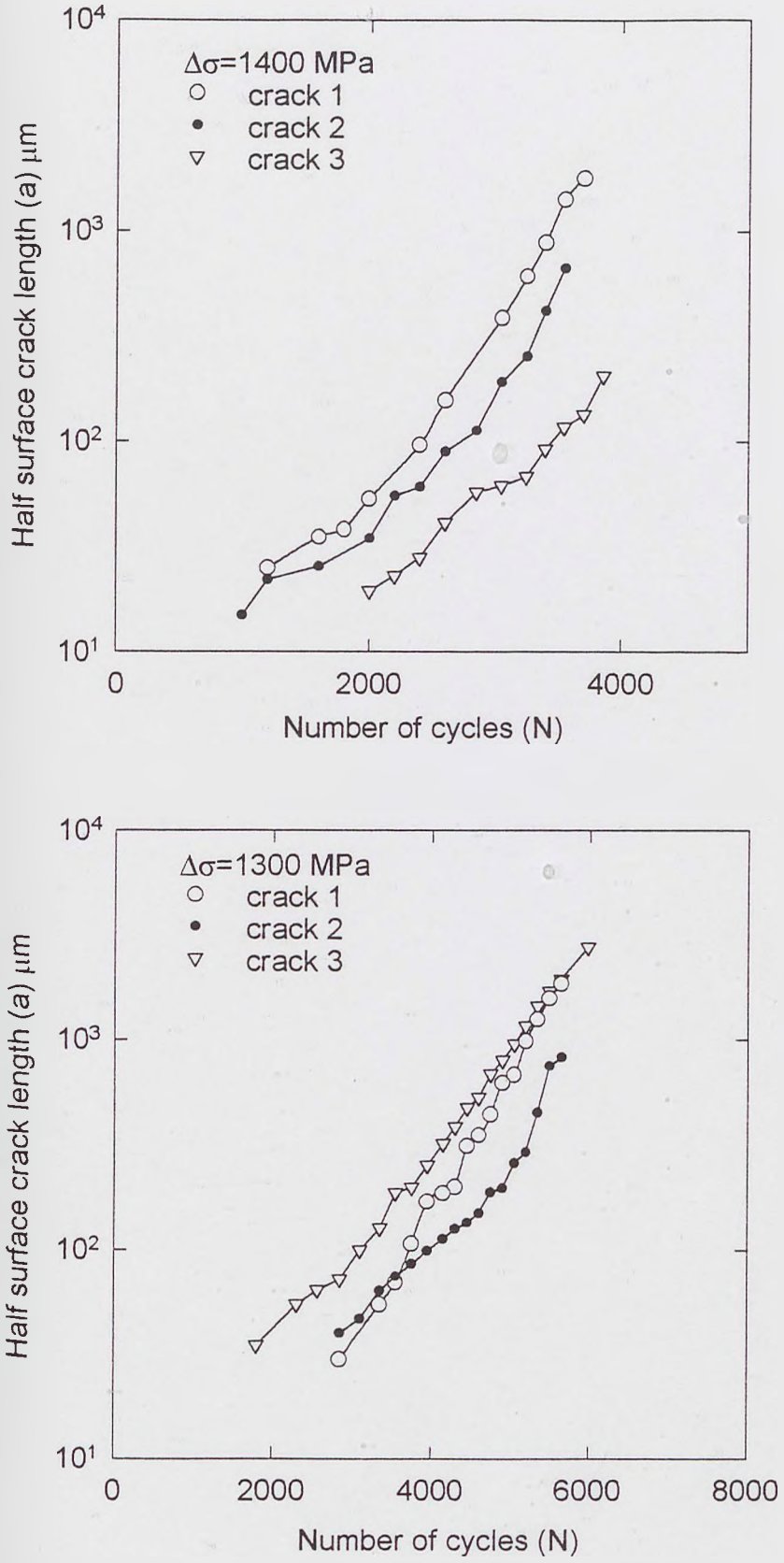

Fig.5.3 Crack length versus number of cycles for Q2N in artificial seawater at different stress levels.

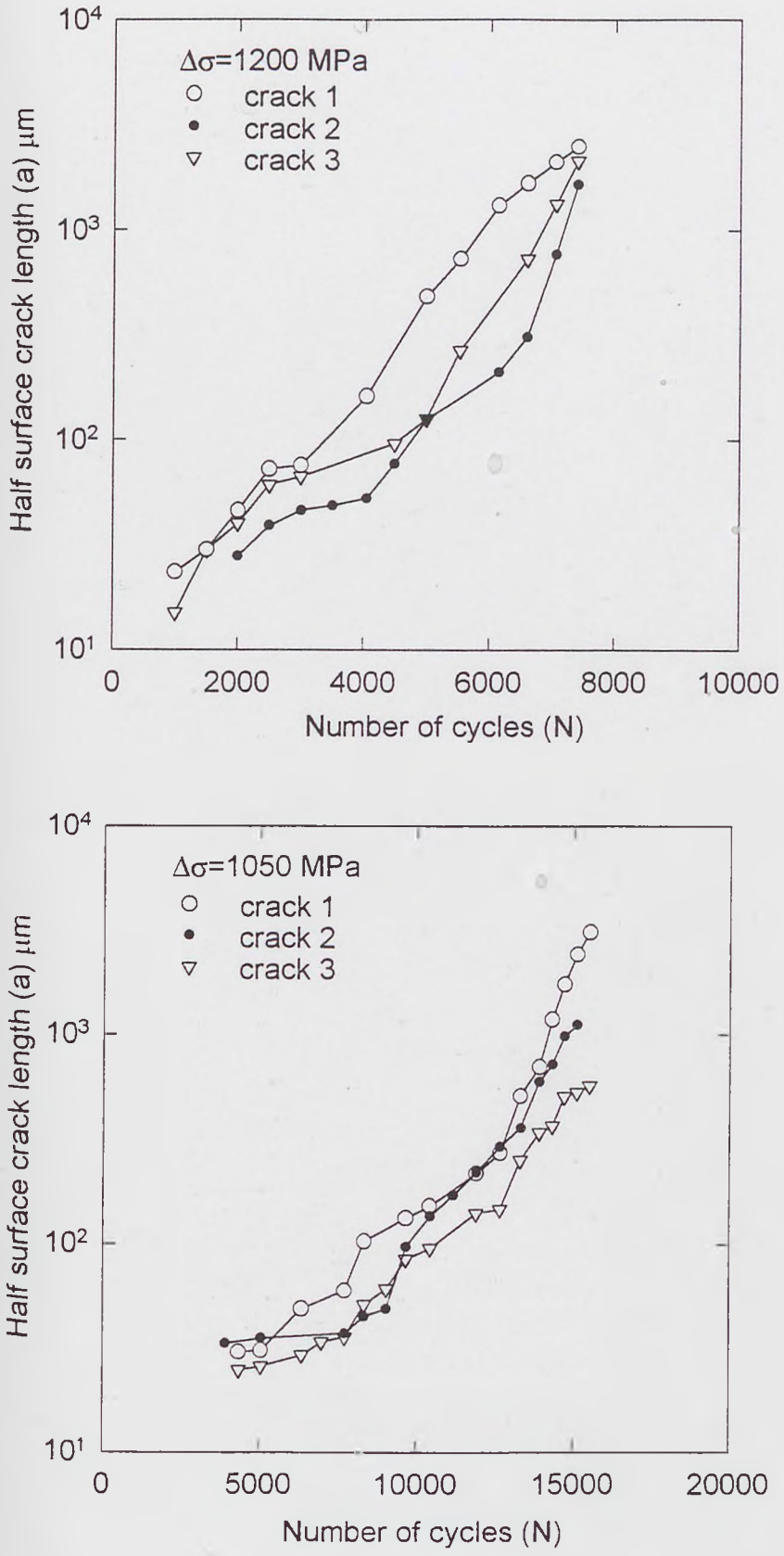

Fig.5.3 Crack length versus number of cycles for Q2N in artificial seawater at different stress levels.

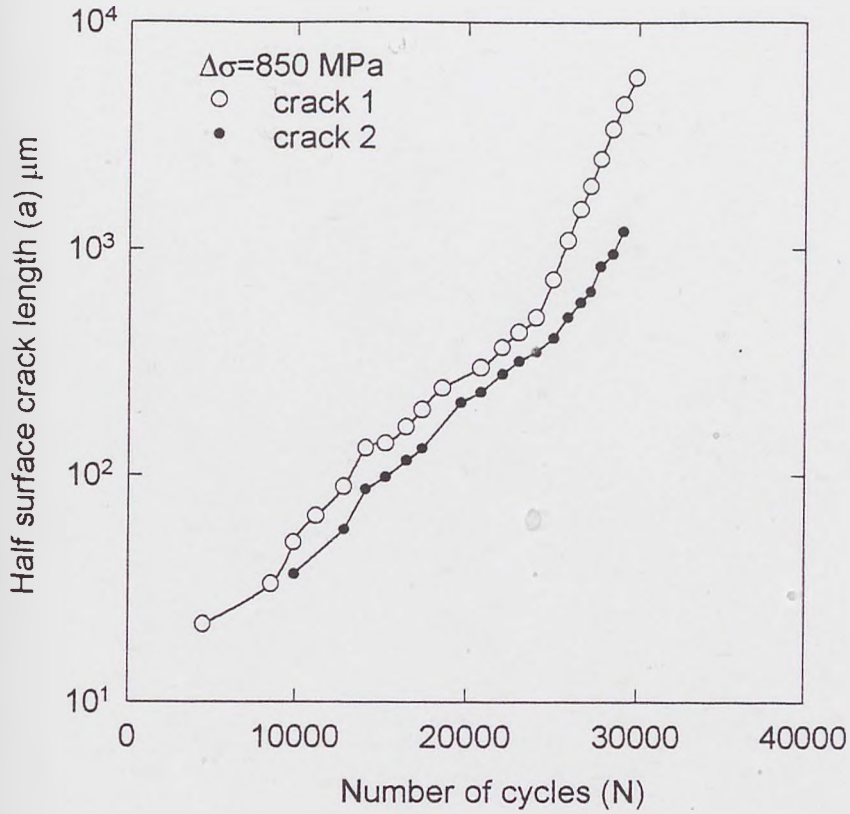

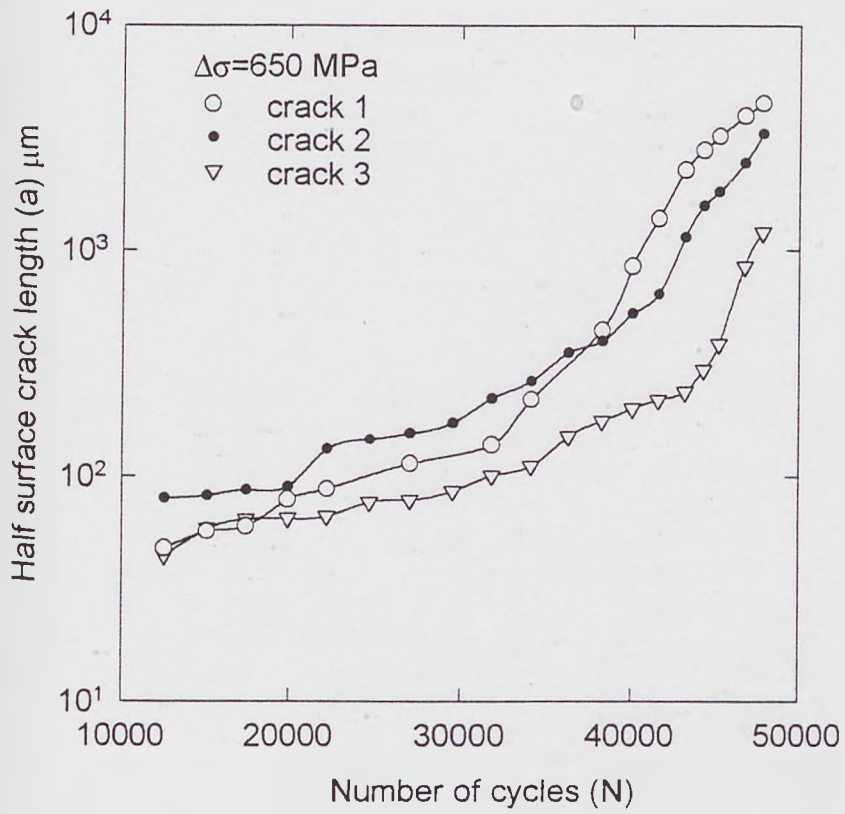

Fig.5.3 Crack length versus number of cycles for Q2N in artificial seawater at different stress levels.

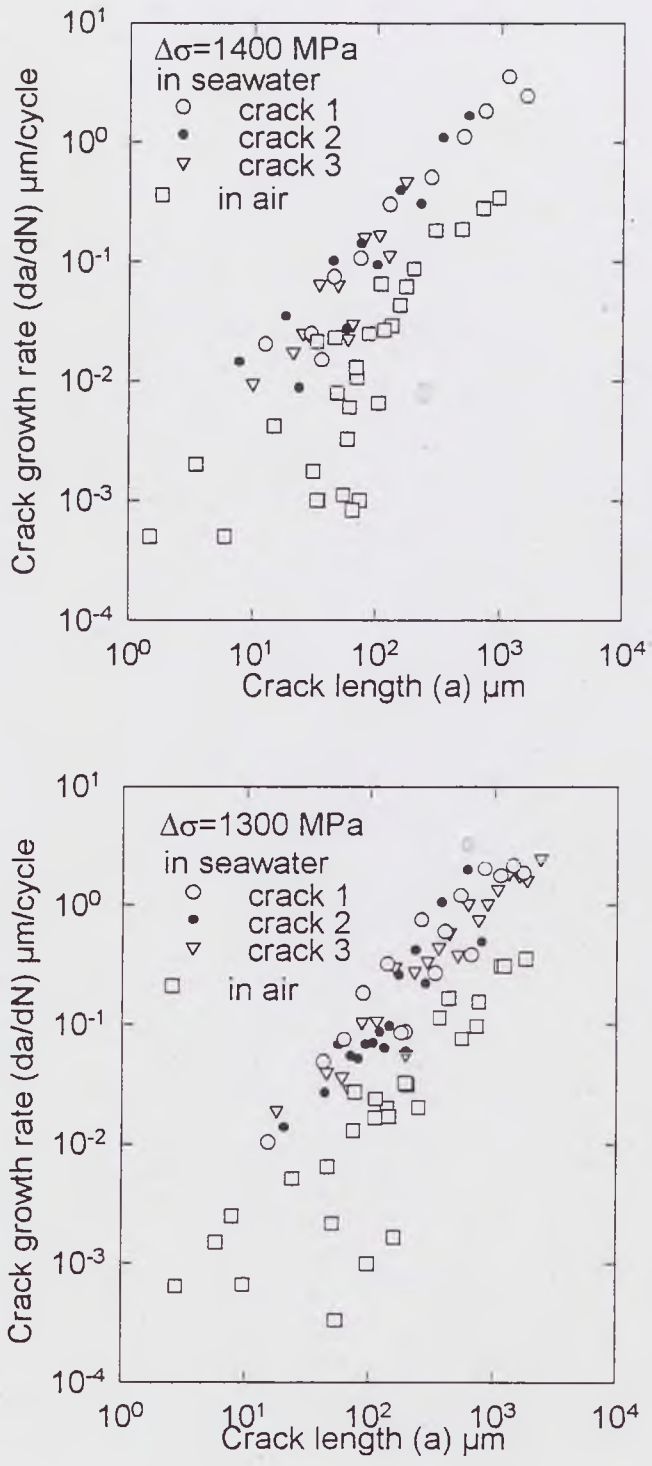

Fig.5.4 Comparison of fatigue crack growth rate in artificial seawater and in air at different stress levels.

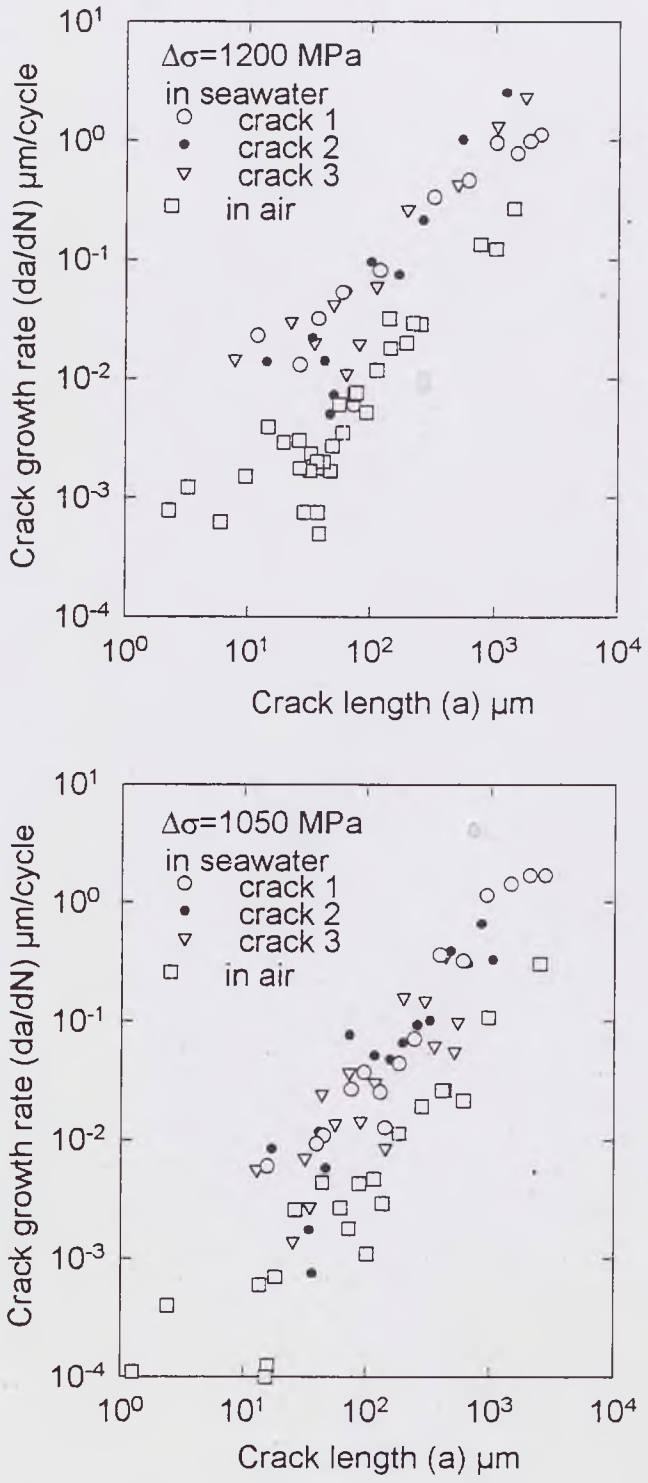

Fig.5.4 Comparison of fatigue crack growth rate in artificial seawater and in air at different stress levels.

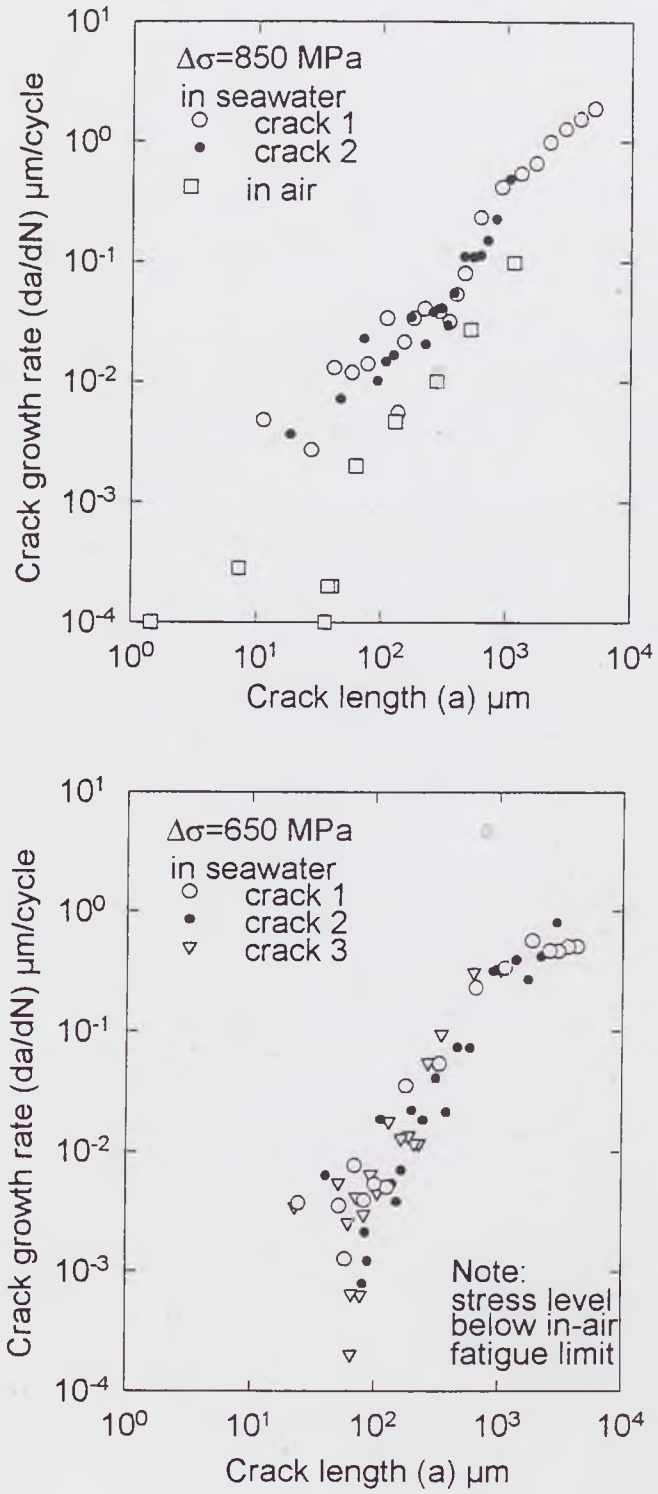

Fig.5.4 Comparison of fatigue crack growth rate in artificial seawater and in air at different stress levels.

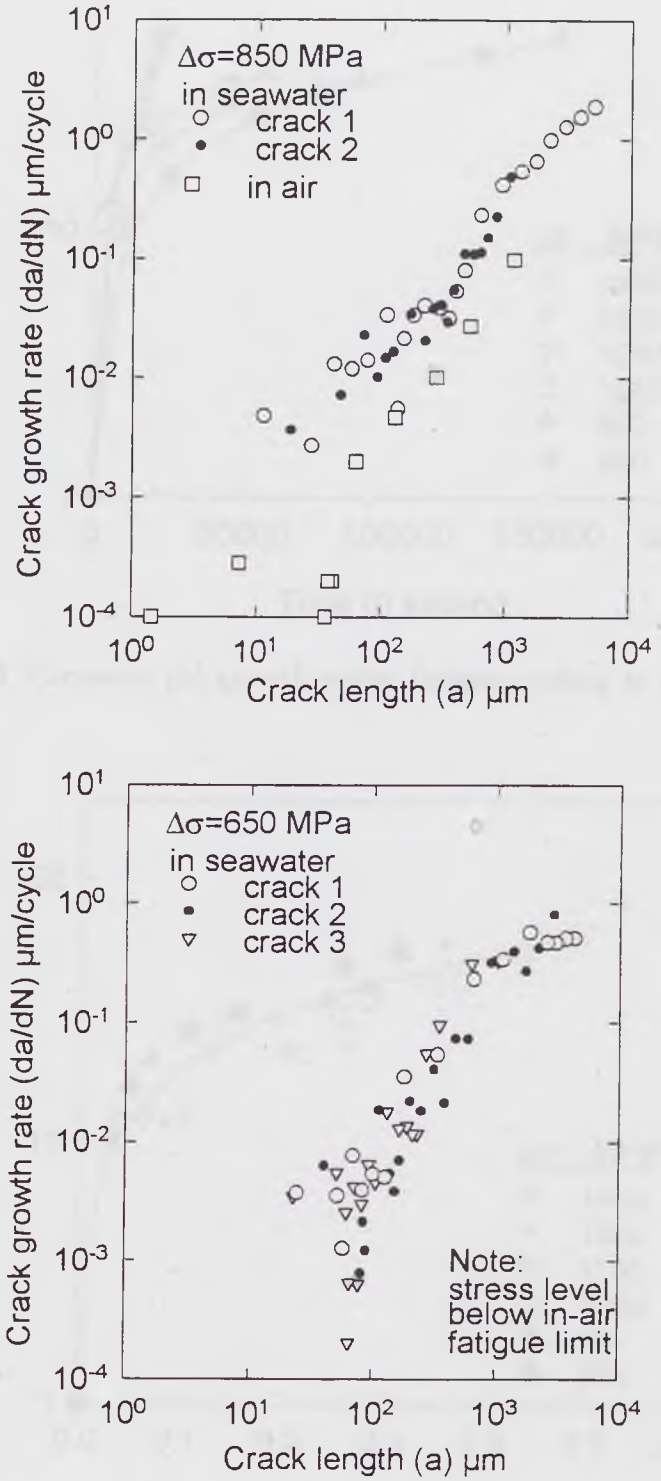

Fig.5.4 Comparison of fatigue crack growth rate in artificial seawater and in air at different stress levels.

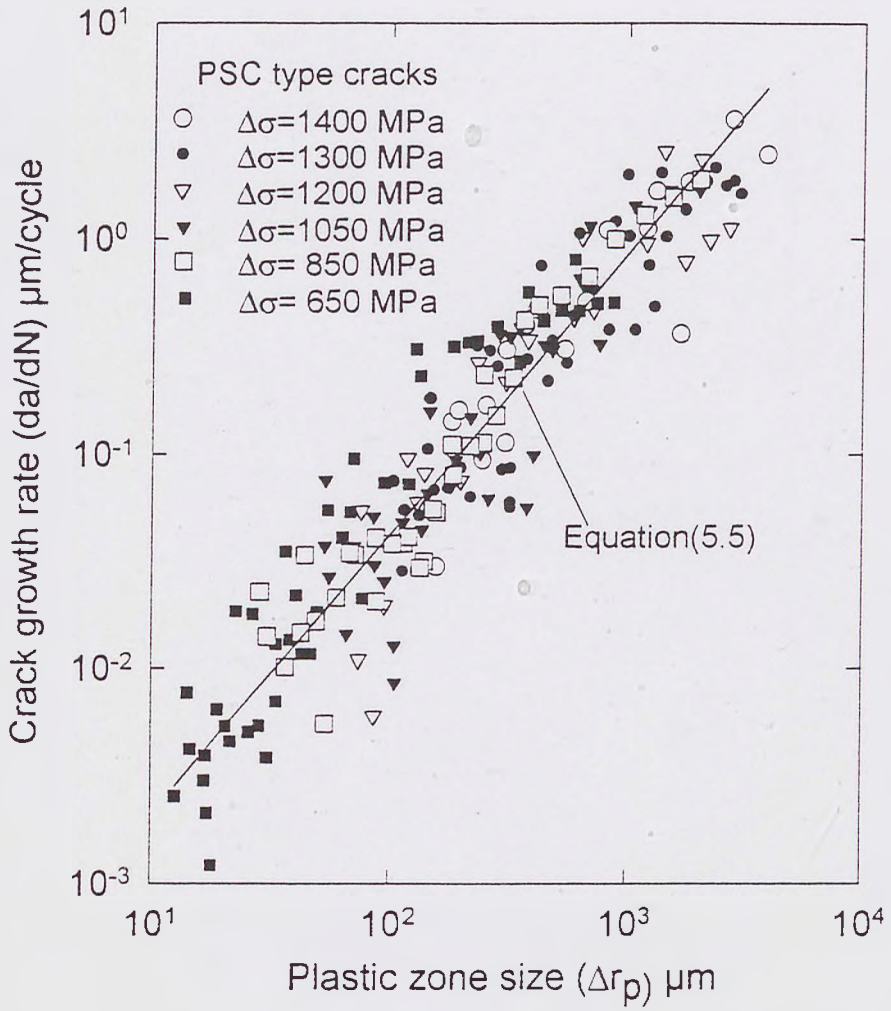

Fig.5.7 Short fatigue crack growth rate of *PSC* type cracks versus calculated plastic zone size at different stress levels.

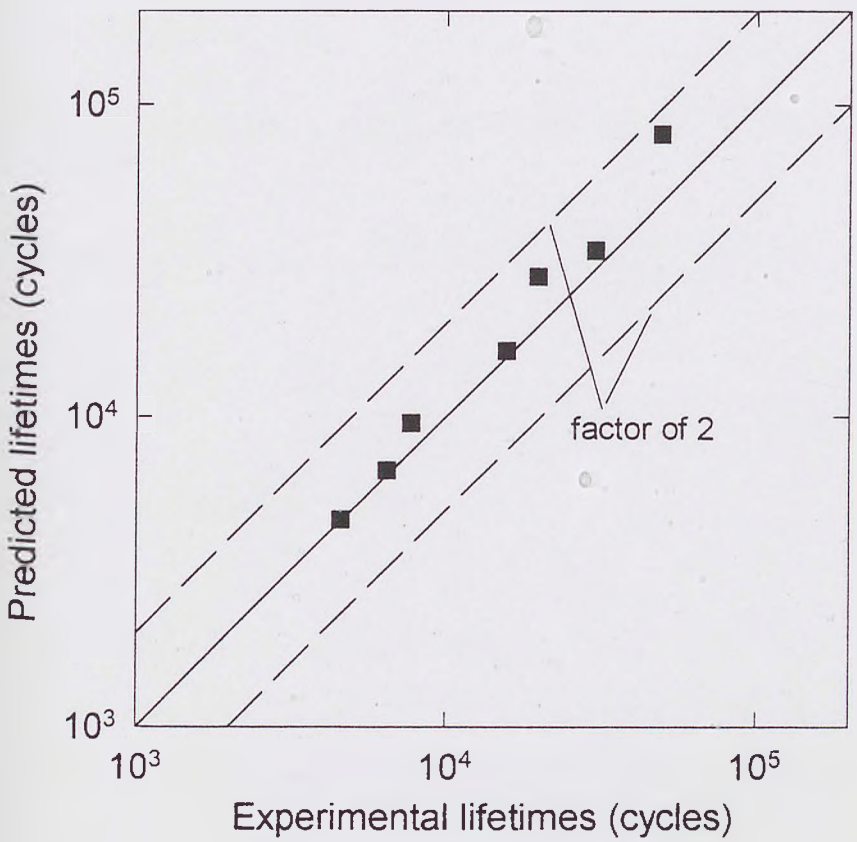

Fig.5.8 Comparison of calculated fatigue lifetime with experimental fatigue lifetime.

Chapter 6

Frequency Effects on the Growth of Short Fatigue Cracks

6.1 Introduction

The fatigue strength of most materials tested in air under normal laboratory conditions is little effected by cyclic loading frequency as suggested by some authors in earlier studies [1] [2]. Experimental results on a number of steels at frequencies up to 150,000 cycles/min (2500 Hz) obtained by Lomas *et al* [3] are shown in Figure 6.1. It can be seen from this figure that all the ferritic steels show a slight increase in fatigue strength as the frequencies increase from 7000 cycles/min (116 Hz) up to 100,000 cycles/min (1666 Hz) but which is followed by a decline for frequencies above this. The data of the 36Ni-12Cr austenitic steels however exhibited a slight different behaviour.

Fatigue crack growth data obtained at different loading frequencies for different

materials were summarised by Frost in [4] and show a similar picture as those of the fatigue lifetime tests, *i.e.*, frequency had little or no effect although there was some suggestion of a tendency for faster growth rates at very low frequency. Aluminium alloy sheet specimens 160 mm wide by 2 mm thick showed that the crack growth rates of cracks from a central slit were about 30 per cent faster at 0.33 Hz than cracks propagating in specimens tested at 33 Hz. However tests conducted using Cu-aluminium alloy sheets showed no significant difference between the crack growth rate for frequencies of 33 Hz and 3.3 Hz [4].

For corrosion fatigue loading it has been well established that fatigue lifetime is heavily time - dependent. Substantial effort has been made for many years to quantify the effects of cyclic frequency on fatigue lifetime and crack growth behaviour under corrosive environments [5] - [13]. In general it has been found that a given number of cycles results in greater damage at lower frequencies. Endo and Miyas [6] reported that for low alloy steels in fresh water a frequency of 24 Hz caused failure in 10^6 cycles, but at a frequency of 0.08 Hz failure took place after 1.1×10^5 cycles. The work for 7017-T651 aluminium alloy in seawater at frequencies from 0.1 to 70 Hz shows that corrosion fatigue crack growth rates are significantly increased with decreasing of cyclic frequency [10]. Austen and Walker [11] carried out corrosion fatigue crack growth tests at various combinations of frequencies and stress ratios. Their results show that the corrosion fatigue crack growth mechanism can change to one consistent with stress corrosion cracking as cyclic frequency decreases and stress ratio increases.

It is extremely difficult to lay down general principles in order to design a structure against corrosion fatigue or to assess the corrosion fatigue behaviour of a service structure based on the laboratory data, the data of which has usually been obtained using accelerated tests. A full understanding of the effects of cyclic fre-

quency on the corrosion fatigue lifetime for a given material - environment system is therefore needed if laboratory data is to be used with confidence.

Currently no data exists concerning the effects of cyclic frequency on the fatigue strength and short crack behaviour of Q2N steel in both air and seawater conditions. The results presented in this chapter attempt to address this short fall.

Air fatigue and corrosion fatigue tests have been conducted at a stress ratio $R \approx 0$, cyclic stress range $\Delta\sigma = 1200MPa$ and cyclic load frequencies of 10, 1, 0.1 and 0.01 Hz. Fatigue lifetimes were recorded and a surface replication technique was applied to monitor the initiation and propagation of short cracks under both environmental conditions.

The main findings of the present chapter are summarised below.

1. The effects of cyclic frequency on fatigue lifetime in both air and artificial seawater were revealed.

2. Detail experimental results have been obtained showing the effect of cyclic frequency on the development of short fatigue cracks in both air and seawater.

3. The initiation of multiple short corrosion fatigue cracks was observed on specimen surfaces in seawater tests. The number of cracks developed during a test was found to be dependent upon test frequency.

4. The coalescence of multiple randomly distributed short corrosion fatigue cracks was studied. Typical mechanisms of short crack coalescence are presented.

5. Frequency effects on the short crack growth behaviour in seawater is quan-

tified by the introduction of a time dependent parameter.

6.2 Experimental Procedure

6.2.1 Fatigue and Short Crack Growth Tests

A Schenck 250 kN servo-hydraulic testing machine was used to perform the three - point - bend fatigue tests in both air and seawater to investigate the cyclic frequency effects on fatigue strength and short crack growth behaviour.

Testing conditions are as follows:

- Loading mode: three point bend;
- Stress ratio: $R \approx 0.02$;
- Stress range: $\Delta\sigma = 1200$ MPa;
- Testing frequencies: $f = 10$, 1, 0.1 and 0.01 Hz.
- Environments: laboratory air and artificial seawater.

Acetate replicas were taken of the polished specimen surface at frequent intervals during tests. The replicas provide a permanent record of surface cracks developed during the test. The frequency at which replicas were taken depended on the estimated duration of the test. Detail information on the microstructure of this material, specimen dimensions and loading fixture arrangement are provided in Chapter 3.

The corrosive environment was artificial seawater, specified to BS 3900. The corrosion cell and recirculation system, described in Chapter 3, was adopted to conduct corrosion fatigue tests at different frequencies. During the tests the artificial seawater was circulated through the specimen chamber at the rate of about 15 litre/hour.

6.2.2 Method of Analysis

The crack growth rates, da/dN, were estimated using a secant method where

$$\frac{da}{dN} = \frac{a_{i+1} - a_i}{N_{i+1} - N_i} \tag{6.1}$$

and the corresponding average crack length is $\overline{a} = \frac{1}{2}(a_{i+1} + a_i)$.

Since multiple cracks have been observed during the fatigue tests, especially in seawater conditions, it is necessary to define a dominant length for the purpose of comparing the fatigue damage of each specimen. In the present study a dominant crack length, a_d, is defined as length of the longest crack, *i.e.*,

$$a_d = \max(a_1, a_2, \ldots, a_n) \tag{6.2}$$

where n is the number of cracks observed on the specimen.

Accordingly, dominant crack growth rates, da_d/dN, can be estimated from the dominant crack length a_d and the number of cycles N using a secant method where

$$\frac{da_d}{dN} = \frac{a_{d(i+1)} - a_{d(i)}}{N_{(i+1)} - N_{(i)}} \tag{6.3}$$

and the corresponding average crack length is $\overline{a_d} = \frac{1}{2}(a_{d(i+1)} + a_{d(i)})$.

6.3 Results

6.3.1 Fatigue Life Results

The duration of fatigue tests conducted in air and seawater at various cyclic frequencies, are given in Table 6.1 and Table 6.2 respectively.

Specimen	Frequency (Hz)	Lifetime
FA-1*	10	5.5×10^4
FA-2	10	5.4×10^4
FA-3*	1	4.1×10^4
FA-4	1	4.4×10^4
FA-5	0.1	4.6×10^4
FA-6	0.01	3.2×10^4

Table 6.1: Fatigue lifetime results in air

Specimen	Frequency (Hz)	Lifetime
FC-1	10	2.1×10^4
FC-2*	1	1.8×10^4
FC-3	1	1.4×10^4
FC-4	0.1	7.7×10^3
FC-5	0.01	6.1×10^3

Table 6.2: Fatigue lifetime results in artificial seawater

* — specimen without replicas.

The results presented in Table 6.1 and Table 6.2 are plotted in Figure 6.2. From this figure it is apparent that corrosion fatigue lifetime is strongly influenced by testing frequency, *i.e.*, the fatigue lifetime decrease with decreasing cyclic frequency. Similar dependence of corrosion fatigue lifetime on the cyclic frequency has also been observed by other researchers [5] [6]. For tests conducted in air little effect of frequency is noted except a slight decrease in fatigue lifetime at the lowest test frequency of f =0.01 Hz. A possible reason for this decrease will be discussed later. In comparing the seawater and air data it can be found that the magnitude of the reduction of fatigue lifetime, *i.e.*, different between air and seawater lifetimes is dependent upon cyclic frequency, that is, the lower the cyclic frequency the greater the difference between corrosion fatigue lifetime and air fatigue lifetime. However even at very high frequencies a large reduction in fatigue lifetime is still apparent for seawater tests.

6.3.2 Development of Short Fatigue Cracks

Short Crack Growth in Air

Figures 6.3(a) - (i) present a typical example of short crack initiation and growth in air at a test frequency of 1 Hz. From these figures it can be clearly seen that the dominant crack initiates from a small inclusion. Subsequent crack growth then occurs along crystallographic facets. After reaching a certain length crack growth shows less dependence upon the microstructure

Crack development at a test frequency of 0.01 Hz exhibits different characteristics when compared to crack development obtained at the higher test frequencies, (see Figure 6.4). In this case the final failure crack, as shown in Figure 6.4(i)

was formed through the coalescence of several short cracks. A number of these coalescence events are indicated in Figures 6.4(e) and 6.4(g).

Short crack growth results at different test frequencies, presented in the form of a versus N curves and a versus da/dN plots, are given in Figures 6.5(a) - 6.5(d) and Figures 6.6(a) - 6.6(d) respectively. For air fatigue tests it can be seen that short cracks exhibit similar growth behaviour at cyclic frequencies of 10, 1 and 0.1 Hz, *i.e.*, all cracks grow at a high speed in the initial stages and then decelerate to a minimum growth rate at a certain crack length. At a frequency of 0.01 Hz the crack growth behaviour is slightly different due to the coalescence of a number of distributed cracks. The anomalous crack growth behaviour caused such coalescence events is indicated by arrows in Figures 6.5(d) and 6.6(d).

Short Cracks in Seawater

The first evidence of damage on smooth specimens of Q2N steel tested in artificial seawater is that of the formation of corrosion pits which develop rapidly during the early stages of the test. The development of pits shows a feature that is different to that of the growth of fatigue cracks in that the length of a fatigue crack usually increases constantly as the number of loading cycles increases, although, as previously discussed, it may exhibit a discontinuous behaviour under some circumstances [14] [15]. Pits however have been observed to develop to a certain size in the early stages of fatigue cycling and then show little further apparent growth. It has been observed that short cracks initiate at the edges of these pits. Figures 6.7(a) and 6.7(b) show two typical examples of cracks emerging from the edge of pits in the early stage of tests.

The number of multiple cracks observed during tests, as shown in Figures 6.8(a) and 6.8(b), was found to be dependent on the applied cyclic test frequency. The

relationship between the number of cracks and cyclic frequency is shown in Figure 6.9. From this figure it is apparent that the number of cracks increases sharply for cyclic frequencies above 0.1 Hz. Below this, *i.e.*, $f < 0.1\ Hz$, there is no apparent change in numbers of cracks. The experimental data presented in Figure 6.9 can be approximated by two straight lines on a $log - linear$ plot of frequency versus number of cracks. A plot of Equations 6.4 and 6.5 are also shown in Figure 6.9.

$$n = INT[13log(f)] + 17 \qquad (f > 0.1Hz) \tag{6.4}$$

$$n = 4 \qquad (f \leq 0.1Hz) \tag{6.5}$$

The development of the main cracks, that is when $a > 1mm$, at various cyclic frequencies are presented in Figure 6.10 to Figure 6.13. Nine main cracks were observed on the surface of one specimen tested at 10 Hz. The majority of these cracks were formed by the coalescence of randomly distributed individual sub-cracks, see Figure 6.10. Similar results have been found at a cyclic frequency of 1 Hz although the total number of cracks found was fewer than for tests at 10 Hz, see Figure 6.11. Similarly crack growth data obtained at the lower test frequencies of 0.1 and 0.01 Hz is shown in Figure 6.12 and 6.13. These figures show that crack coalescence events are fewer in number and only occur late in terms of the lifetime of the test. It appears therefore that any enhancement in crack growth rates for this material - environment system, attributable to crack coalescence, occur only at higher cyclic frequencies.

In order to demonstrate the difference of crack growth behaviour under different test frequencies data from the dominant cracks, for all the tests, are compared in Figure 6.14. Here the ordinate denotes the dominant crack length a_d and the abscissa is the number of loading cycles. It is clear from this figure that,

at progressively lower frequencies, cracks develop at an earlier stage in terms of the number of applied cycles, consuming fewer cycles to reach a certain length. Dominant crack growth rates determined from the data in Figure 6.14 are compared in Figure 6.15. The main feature noted from this figure is that low test frequencies produce high crack growth rates in both the MSC and PSC regimes.

6.3.3 Crack Coalescence

Crack coalescence events were observed during corrosion fatigue for tests conducted at four test frequencies. Since relatively fewer cracks initiate at the lower frequencies of 0.01 Hz and 0.1 Hz the effects of the interaction and coalescence of multiple cracks, upon the crack growth behaviour and fatigue lifetime, appear less significant within this frequency range.

The coalescence of corrosion fatigue cracks observed from specimen surfaces are of the following two forms:

1. Two slightly misaligned cracks grow so that their closest tips pass beyond one another for a small distance before turning and growing towards the opposite crack, as shown in Figure 6.16.

2. New subcracks initiate between the closest tips of two adjacent cracks. These cracks then grow rapidly to connect the two adjacent cracks, as shown in Figure 6.17.

Clearly a detailed understanding of the mechanism of crack coalescence would involve a solution of the local stress between the tips of two adjacent cracks, and for short cracks, a knowledge of the effect of microstructure around the crack

tips. Determination of the local stress conditions at each crack tip, as shown in Figure 6.8(a), would be extremely difficult and it is considered that such a detailed analysis of this problem is beyond the scope of the present study. It is however acknowledged that further work is needed in this area.

6.4 Modelling of Frequency Effect on Short Crack Growth in Seawater

In Chapter 5 a short crack growth model has been proposed for corrosion fatigue loading at cyclic frequency of 0.1 Hz. In this model it was assumed that short crack growth can be represented by the relationship $da/dN = C(\Delta r_p)^m$, where the plastic zone size, Δr_p can be calculated by adopting continuously distributed dislocation theory and the coefficient C and exponent m are functions of both the material and environment.

In order to consider the effects of loading frequency in this model, it is necessary that the coefficient C and exponent m are expressed as functions of the cyclic frequency, f, *i.e.*, $C = C(f)$ and $m = m(f)$. Accordingly the short crack growth model which accounts for the influence of loading frequency may be represented by the following equation:

$$\frac{da}{dN} = C(f)(\Delta r_p)^{m(f)} \tag{6.6}$$

In this section Equation 6.6 will be applied to quantify frequency effects on short crack growth. The analysis presented here will mainly focus on PSC type cracks due to the lack of data in the pit growth regime.

The values of $C(f)$ and $m(f)$ in Equation 6.6 were determined from the cor-

responding experimental data for different cyclic test frequencies as shown in Figures 6.14. The analytical procedure used to determine $C(f)$ and $m(f)$ is the same as that described in Chapter 5, that is, (i) a calculation of the plastic zone size Δr_p corresponding to each crack length by adopting continuously distributed dislocation theory; (ii) determination of C and m for each cyclic frequency by performing a best fit regression analysis of the data set (da/dN, Δr_p). The values of $C(f)$ and $m(f)$ obtained are given in Table 6.3 and also are plotted in Figure 6.18 and Figure 6.19.

Frequency (Hz)	C	m
0.01	2.704×10^{-4}	1.202
0.1	1.028×10^{-4}	1.306
1	8.750×10^{-5}	1.266
10	2.818×10^{-5}	1.332

Table 6.3: C and m for different test frequencies

From Table 6.3 it can be seen that the value $m(f)$ shows little dependence upon the applied test frequency over the range of the frequencies investigated. The value of $m(f)$ can therefore be given as an average value as in Equation 6.7. This is also shown in Figure 6.19.

$$m(f) = 1.276 \tag{6.7}$$

In contrast to this the value of $C(f)$ increases as the cyclic frequency decreases, which indicates that the increase in the rate of short crack growth is proportional to time. From Figure 6.18 it can be seen that the relationship between $C(f)$ and f exhibits a inverse linear function on this $log - log$ plot. The equation representing this relationship was obtained by using a least - squares regression

analysis.

$$C(f) = 6.427 \times 10^{-5} f^{-0.3016} \tag{6.8}$$

The frequency effect on short crack growth under the environmental and loading conditions studied may be obtain by substituting $C(f)$ and $m(f)$ into Equation 6.6 as shown in Equation 6.9

$$\frac{da}{dN} = 6.427 \times 10^{-5} f^{-0.3016} (\Delta r_p)^{1.276} \tag{6.9}$$

6.5 Discussion

For comparison of the short crack growth rates at different frequencies in air, crack growth rates versus crack lengths at all the frequencies were replotted together in Figure 6.20; 2nd order regression lines corresponding to each frequency have also been determined and are shown in Figure 6.21. Although it is acknowledged that short crack growth can not be fully modelled using a 2nd order regression analysis it has been found to be useful in showing the main difference in short crack growth at different frequencies. From these figures it can be seen that there is no significant difference in the short crack growth rates between the frequencies 10, 1 and 0.1 Hz. However the initial crack growth rate at $f = 0.01$ Hz is faster when compared to those at other frequencies for cracks length upto 100 μm. After the initial stage, the main difference between crack growth behaviour at 0.01 Hz and at other frequencies is the anomalous growth rate changes caused by crack coalescence. If the crack coalescence, causing a 'jump' in the crack growth rate, is excluded, the expected crack growth rate at this frequency will be similar to those at other frequencies.

Fatigue lifetime results as shown in Figure 6.2, indicate that fatigue lifetime in air

exhibits a slight decrease at very low frequency ($f = 0.01$ in current test). There are two factors which may contribute to this behaviour. Firstly the early stages of short crack growth may be related to crack initiation sites, *i.e.* cracks initiate at persistent slip bands which appear to accelerate the initial microcrack growth rate. Secondly, the corrosive effect of the atmosphere should not be ignored at such low frequencies as 0.01 Hz. Surface corrosion was observed on the specimen and multiple cracks were initiated at these sites during the fatigue test, see Figure 6.22. These randomly distributed short cracks then coalesced with each other, as shown in Figure 6.4, eventually causing premature failure.

Comparison of the seawater crack growth rates (Figures 6.23(a) - 6.23(d)), determined from the $a_d - N$ data sets, with that of the in-air data shows that the seawater data exhibits higher crack growth rates when compared to those in air. It should be noted that the minimum crack growth rates in air are much lower than those in seawater, up to two order of magnitude lower, which suggests that the corrosion fatigue crack growth mechanism proposed in [16] [17], *i.e.* conjoint action of chemical and mechanical processes to overcome the strength of the microstructural barrier may be operative during the initial stages in the present tests.

6.6 Summary

1. Frequency has little effect on the air fatigue lifetime in the range 10 to 0.1 Hz. A slight reduction of fatigue lifetime was found at 0.01 Hz.

2. For air fatigue tests short cracks show very similar growth behaviour at frequencies 10, 1 and 0.1Hz. There appears therefore to be little or no frequency effects on the short crack growth behaviour in the frequency range

10 Hz - 0.1 Hz.

3. At a frequency of 0.01 Hz initial short crack growth rates are faster when compared to growth rates at other frequencies. This is considered as a possible reason for the reduction in fatigue lifetime observed at this frequency.

4. Multiple short cracks were observed on the surface of specimens tested at 0.01 Hz. Crack coalescence which occurred during such tests is considered to be responsible for the large changes in crack length and crack growth rate. This mechanism is considered as an additional factor causing a reduction in fatigue lifetime at this frequency.

5. The fatigue strength of Q2N steel in seawater is strongly dependent upon cyclic frequency, *i.e.*, the fatigue lifetime decreases significantly on reduction of the applied cyclic test frequency.

6. Multiple short fatigue cracks were observed on all seawater tests. The relationship between the number of total cracks n and the cyclic frequency f can be approximated by:

$$n = INT[13log(f)] + 17 \qquad (f > 0.1Hz)$$

$$n = 4 \qquad (f \leq 0.1Hz)$$

7. Crack coalescence which occurred during corrosion fatigue exhibited the following two forms:

   (a) two slightly misaligned cracks grow so that their closest tips pass beyond one another for a small distance before turning and growing towards the opposite crack.

   (b) new subcracks initiate between the closest tips of two adjacent cracks. These subcracks then grow rapidly to connect the two adjacent cracks.

8. The dominant short crack growth rates of this steel in seawater exhibit a large scatter, however it can be found that the dominant crack growth rate at a lower frequency is discernably faster than that at a higher frequency. A short crack growth model reflecting the influence of loading frequency can be represented by following equation:

$$\frac{da}{dN} = 6.427 \times 10^{-5} f^{-0.3016} (\Delta r_p)^{1.276}$$

6.7 References

[1] Forrest P.G. (1962) Fatigue of Metals. Pergamon Press, p124

[2] Ryder T.T. and Witzell W.E. (1985) Effect of low temperature on fatigue and fracture properties of Ti-5Al- 2.5Sn (ELI) for use in engine components. Fatigue at low temperatures, $STP857$. pp210-237.

[3] Lomas T.W., Ward J.O., Bait J.R. and Colbeck E.W. (1956) The influence of frequency of vibration on the endurance limit of ferrous alloys at speeds up to 150,000 cycles per minute using a pneumatic resonance system. Inst. Mech. Engrs. Int. Conference on Fatigue, p375

[4] Frost N.E., Marsh K.J. and Pook L.P.(1974) Metal Fatigue. Clarendon Press, pp264-265.

[5] McAdam D.J., Jr (1930) The influence of stress range and cyclic frequency on corrosion. Proc. ASTM, 30, pp411-447.

[6] Endo K. and Miyas Y. (1958) Effect of cycle frequency on corrosion fatigue strength. Bull. Japan Soc. Mech. Eng., 1, pp374-380

[7] Barsom J.M. (1971) Corrosion-fatigue crack propagation below K_{ISCC}. Engng. Fract. Mech., 3, pp15-25

[8] Scott P.M. (1979) Corrosion fatigue in pressure vessel steels for light water reactors. Metal Science, 13, pp396-401.

[9] Atkinson J.D. and Lindley T.C. (1979) Effect of stress wave form and hold-time on environmentally assisted fatigue crack propagation. Metal Science, 13, pp444-448.

[10] Holroyd N.J.H. and Hardie D. (1984) Corrosion fatigue of 7000 series aluminium alloys. Environment - Sensitive Fracture: Evaluation and Comparison of Test methods. ASTM STP 821. (Eds. Dean S.W., Pugh E.N. and Ugianshy G. M.) American Society for Testing and Materials, Philadelphia, pp534 - 547.

[11] Austen I.M., Walker E.F. (1977) Quantitative understanding of effects of mechanical and environmental variable on corrosion fatigue crack behaviour. The influence of environment on fatigue. I Mech. E. Conference Publications.

[12] Gangloff R.P. and Wei R.P. (1986) Small crack-environment interaction: the hydrogen embrittlement perspective. Proceedings of the Second Engineering Foundation International Conference, Small Fatigue Cracks, pp239 - 264

[13] Pao P.S. Wei, W. and Wei R.P. (1977) Effect of frequency on fatigue crack growth response of AISI4340 steel in water vapour. Environment - sensitive fracture of engineering materials (Eds Z.A. Foroulis), pp565 - 580

[14] Miller K.J. (1987) The behaviour of short fatigue cracks and their initiation part I - a review of two recent books. Fatigue Fract. Engng Mater. Struct., 10, pp75 - 91.

[15] Miller K.J. (1987) The behaviour of short fatigue cracks and their initiation part II - a general summary. Fatigue Fract. Engng Mater. Struct., 10, pp93 - 113.

[16] Akid R. and Miller K.J.(1990) The initiation and growth of short fatigue cracks in an aqueous saline environment. In Environment assisted fatigue, EGF publication 7 (Eds P. Scott and R.A. Cottis), pp415 - 434 (Mechanical Engineering Publications, London)

[17] Miller K.J. (1991) Metal fatigue - past, current and future. Proc. Instn. Mech. Engrs., 205, pp1 - 14.

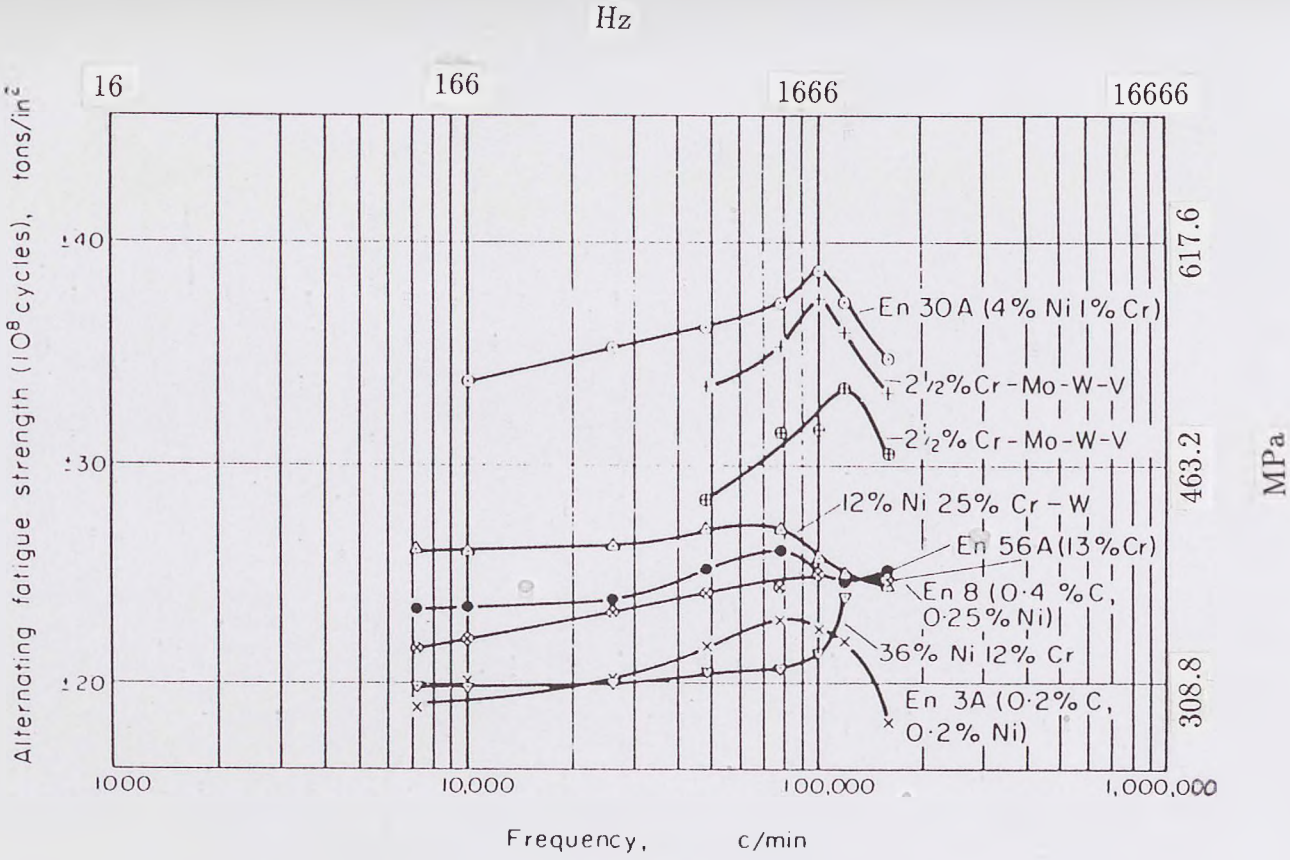

Fig.6.1 Effect of frequency on the fatigue strength of various steels [3].

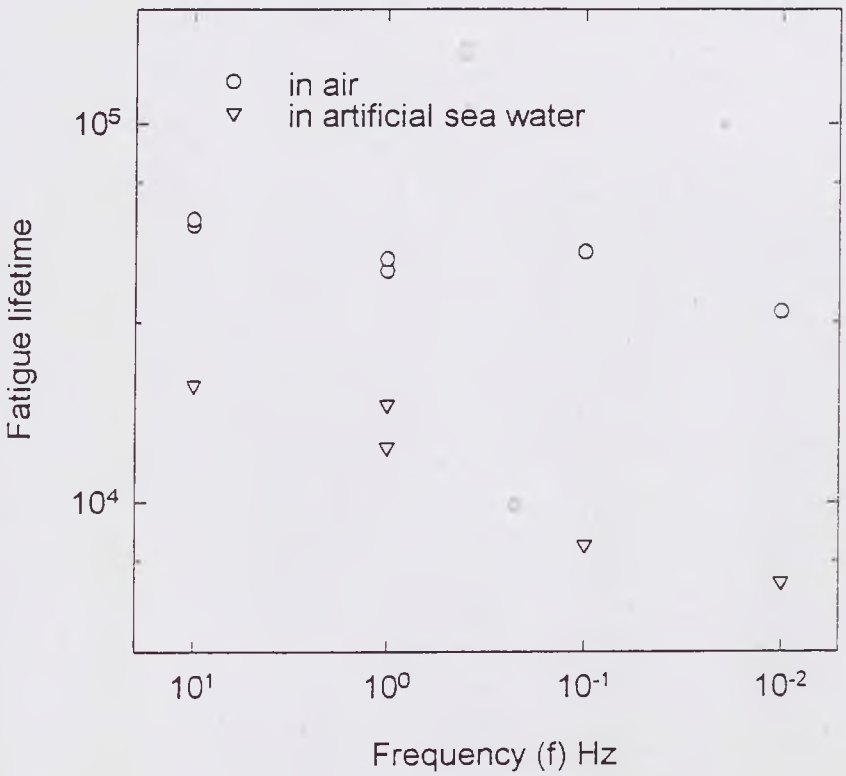

Fig.6.2 Fatigue endurance lifetimes of Q2N at different frequencies, $\Delta\sigma$ =1200 MPa.

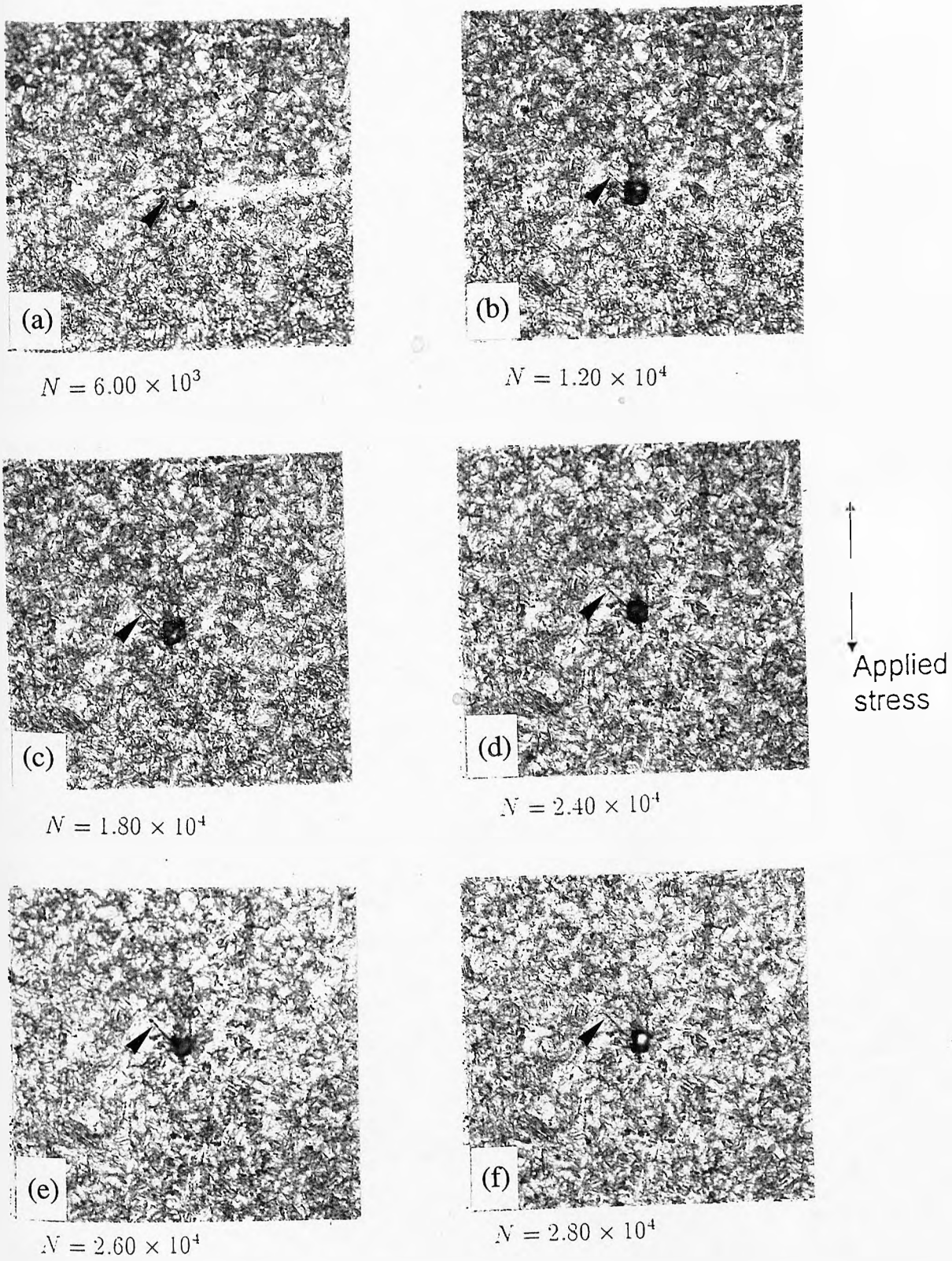

Fig.6.3 Micrographs showing crack growth behaviour in air, $f = 1$ Hz and $\Delta\sigma$ =1200 MPa.

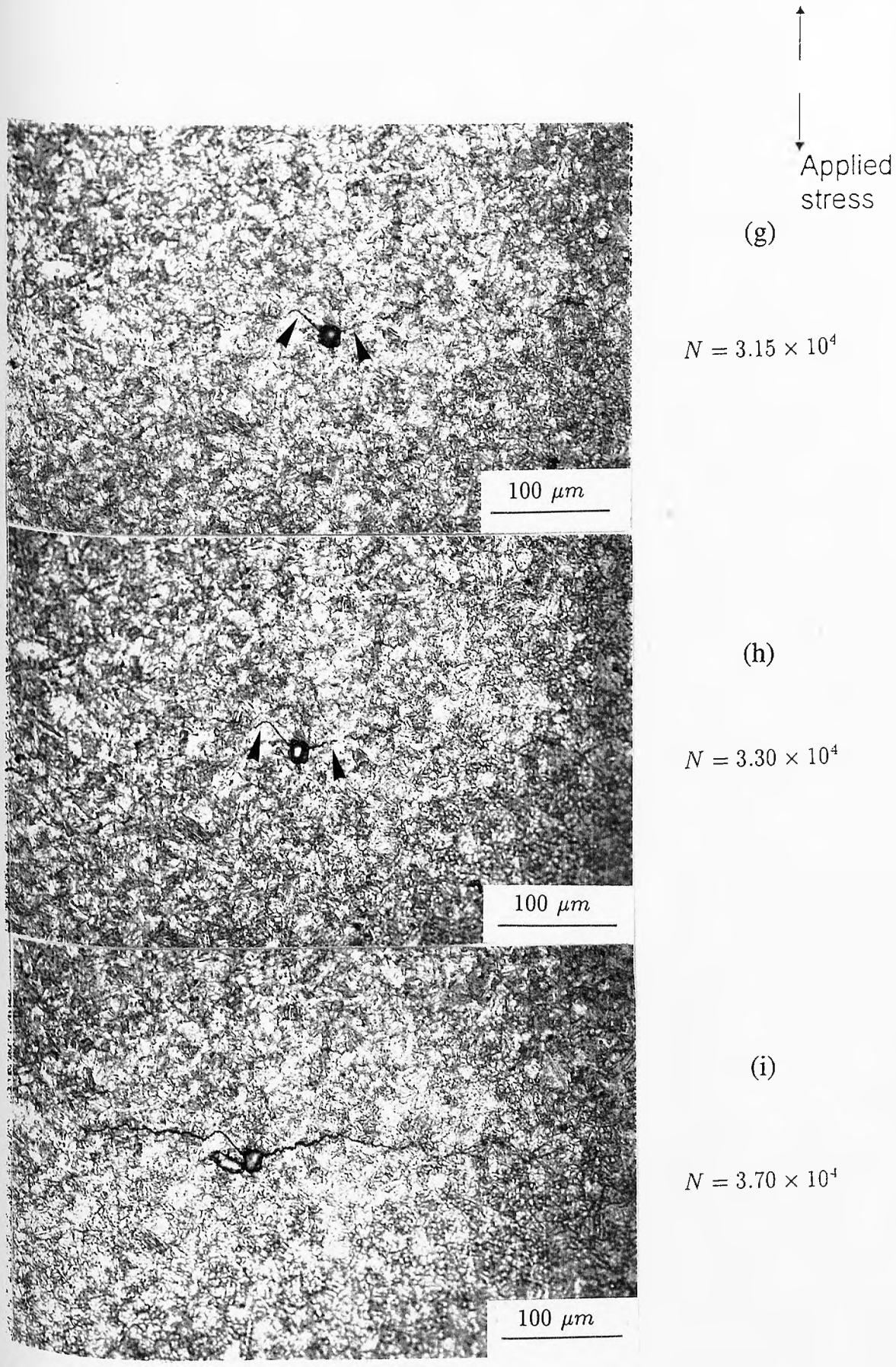

Fig.6.3 Micrographs showing crack growth behaviour in air, $f = 1$ Hz and $\Delta\sigma$ =1200 MPa.

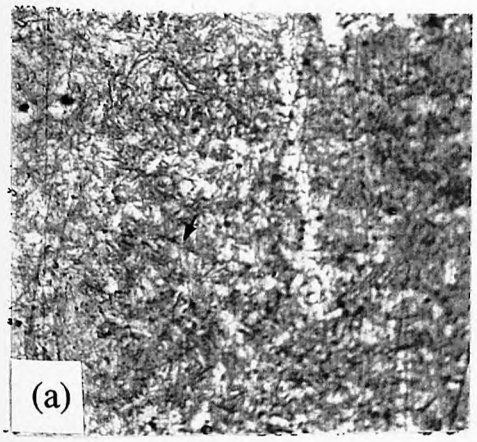

$N = 3.03 \times 10^3$

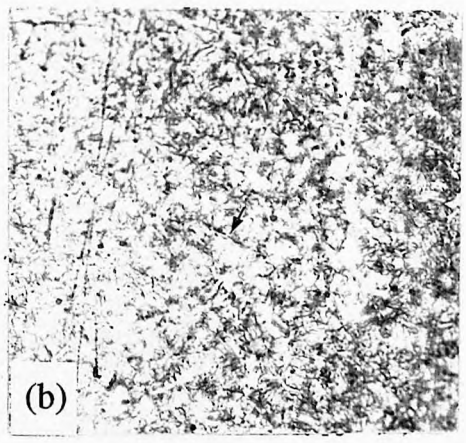

$N = 5.47 \times 10^3$

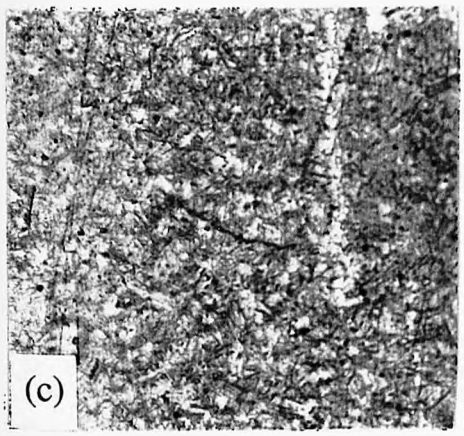

$N = 9.20 \times 10^3$

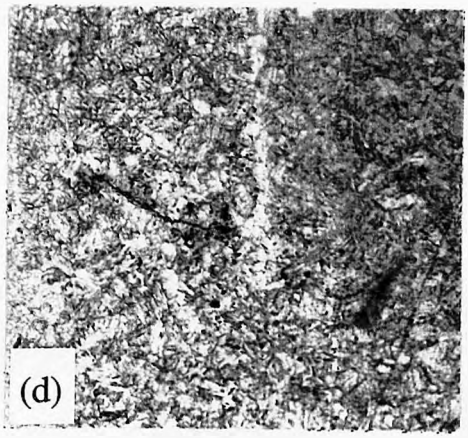

$N = 1.10 \times 10^4$

Applied stress

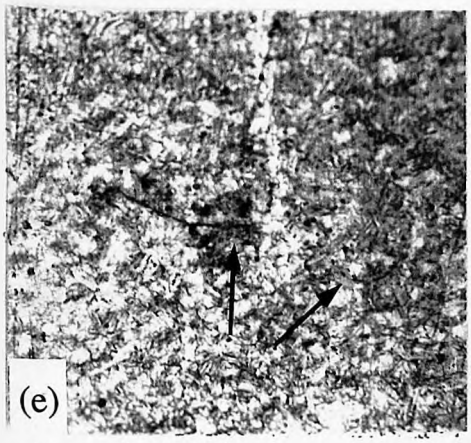

$N = 1.31 \times 10^4$

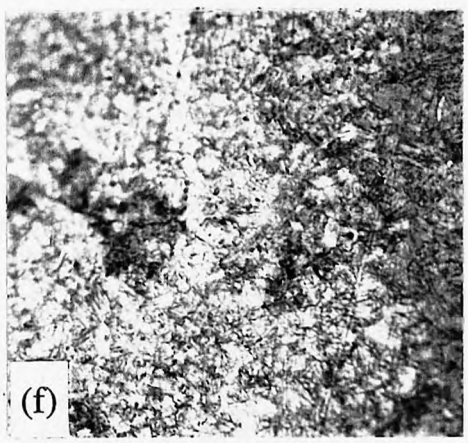

$N = 1.71 \times 10^4$

100 μm

Fig.6.4 Micrographs showing crack growth behaviour in air, $f = 0.01$ Hz and $\Delta\sigma$ =1200 MPa.

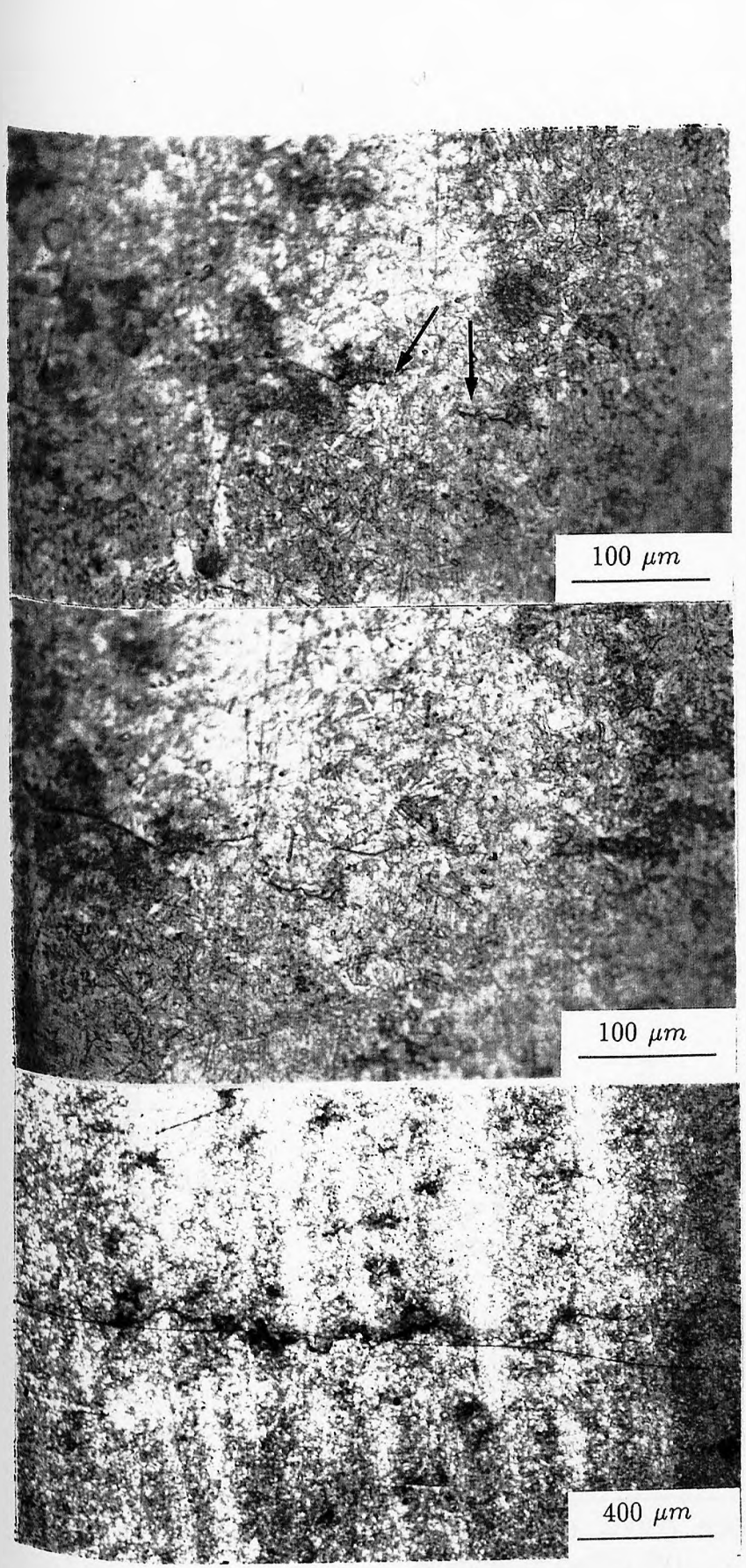

Fig.6.4 Micrographs showing crack growth behaviour in air.
$f = 0.01$ Hz and $\Delta\sigma$ =1200 MPa.

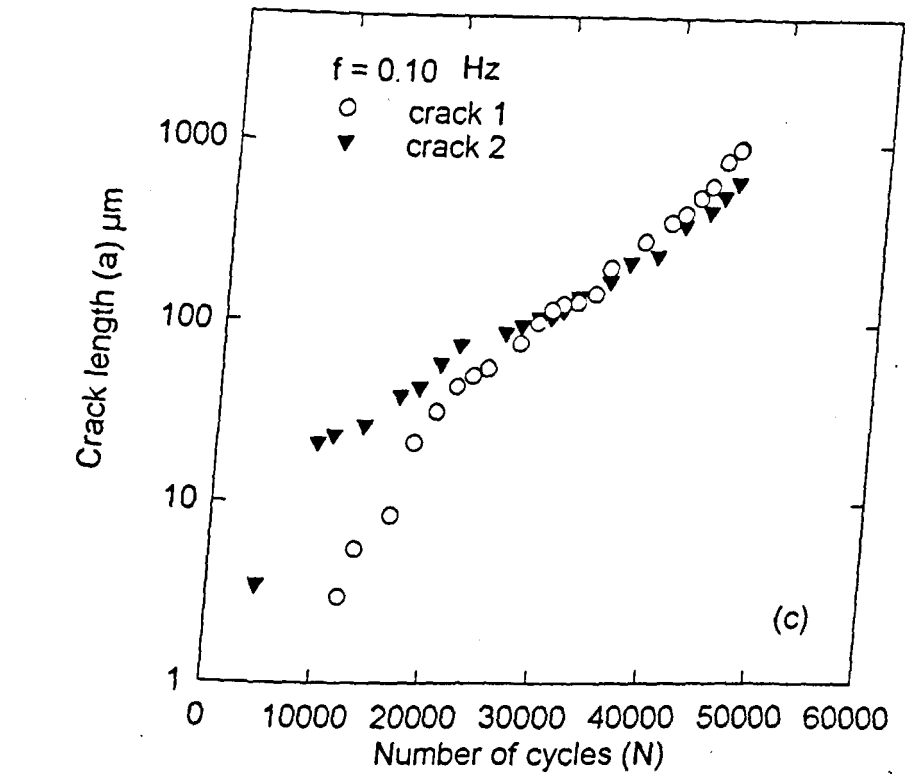

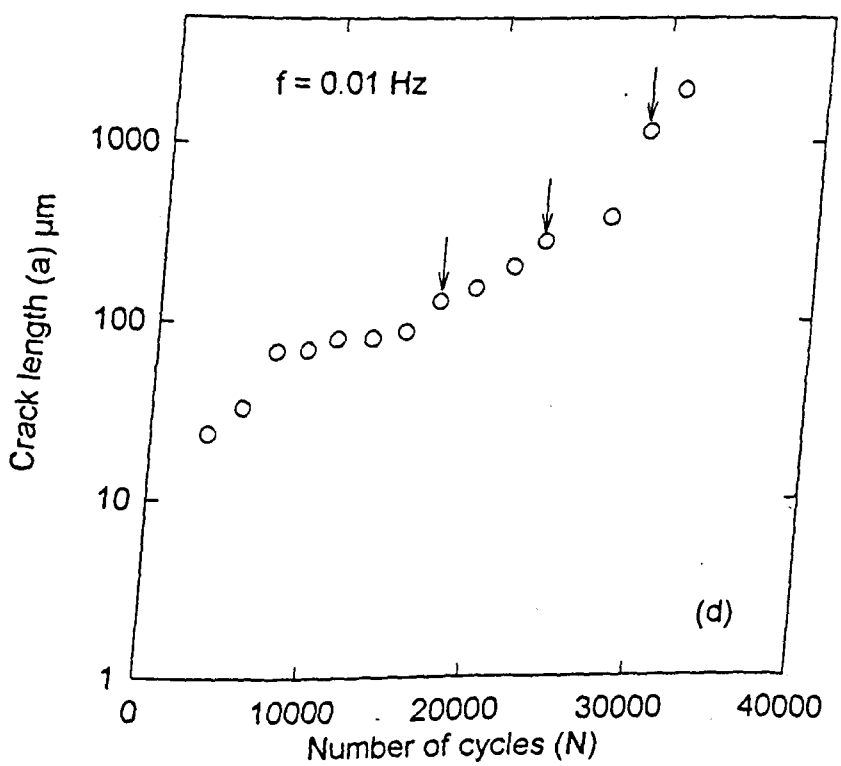

Fig.6.5 Short in-air fatigue crack growth behaviour; surface crack length versus number of cycles.

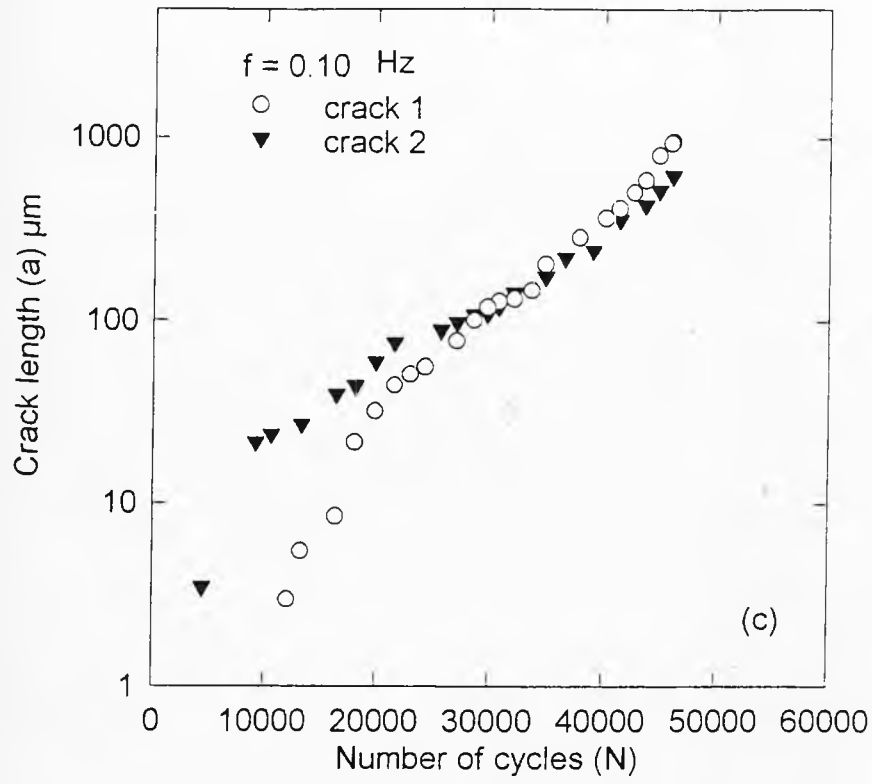

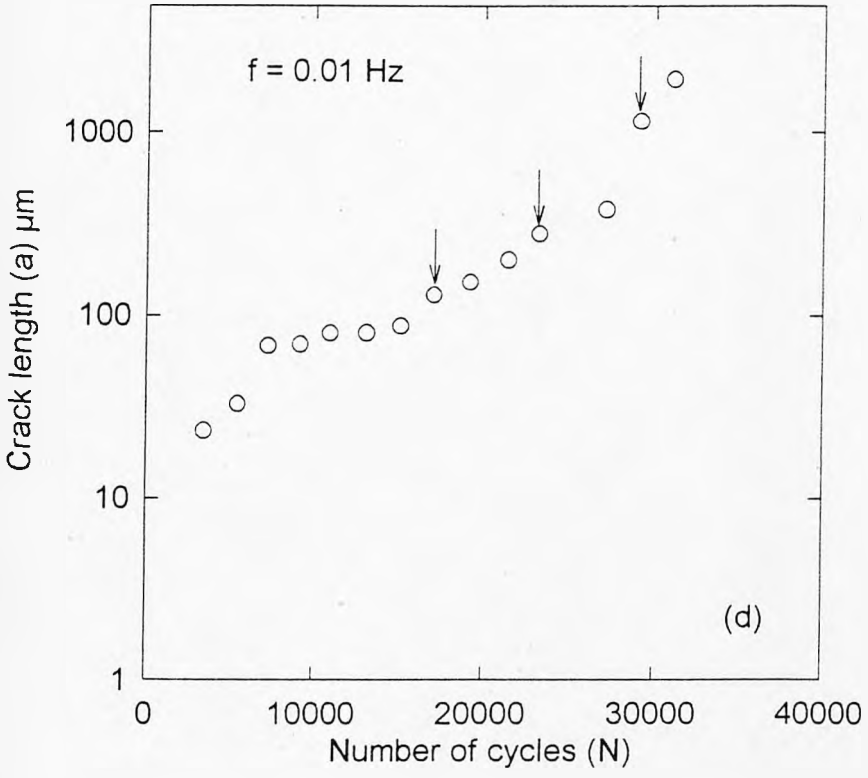

Fig.6.5 Short in-air fatigue crack growth behaviour; surface crack length versus number of cycles.

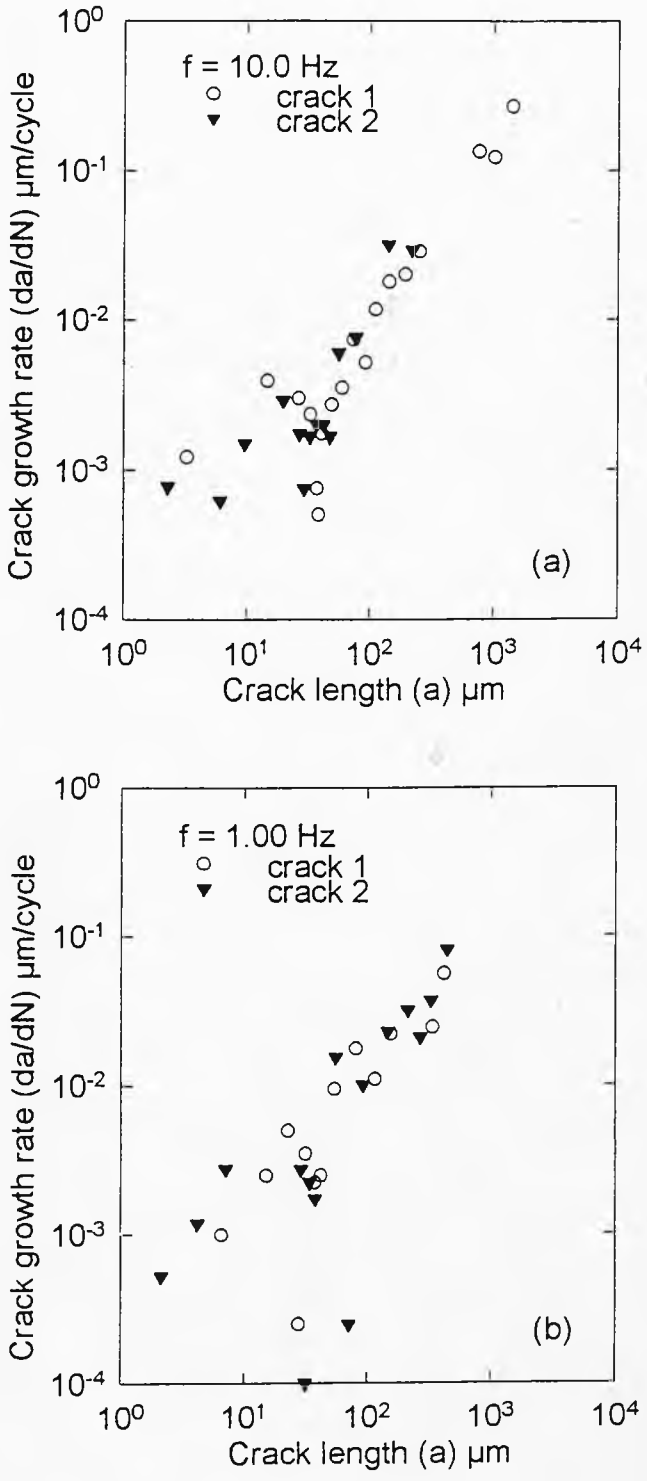

Fig.6.6 Short crack growth rate versus surface crack length for air fatigue tests.

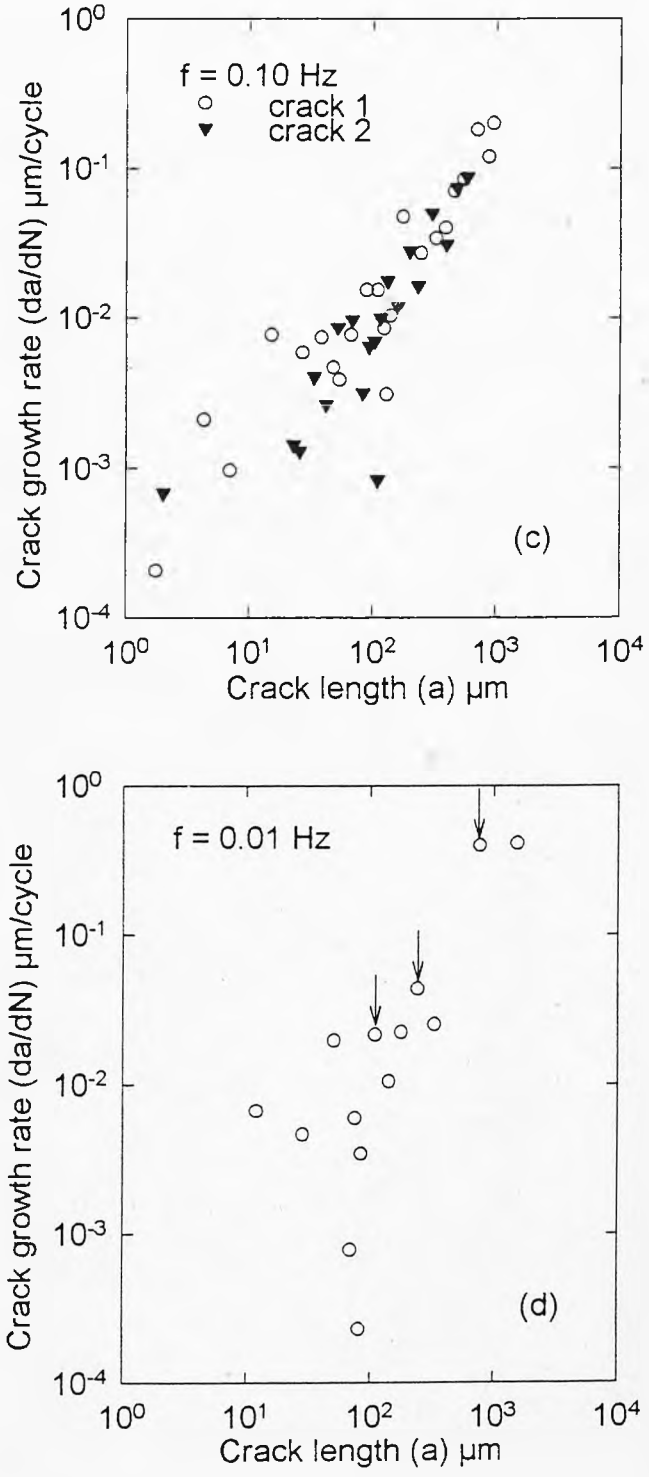

Fig.6.6 Short crack growth rate versus surface crack length for air fatigue tests.

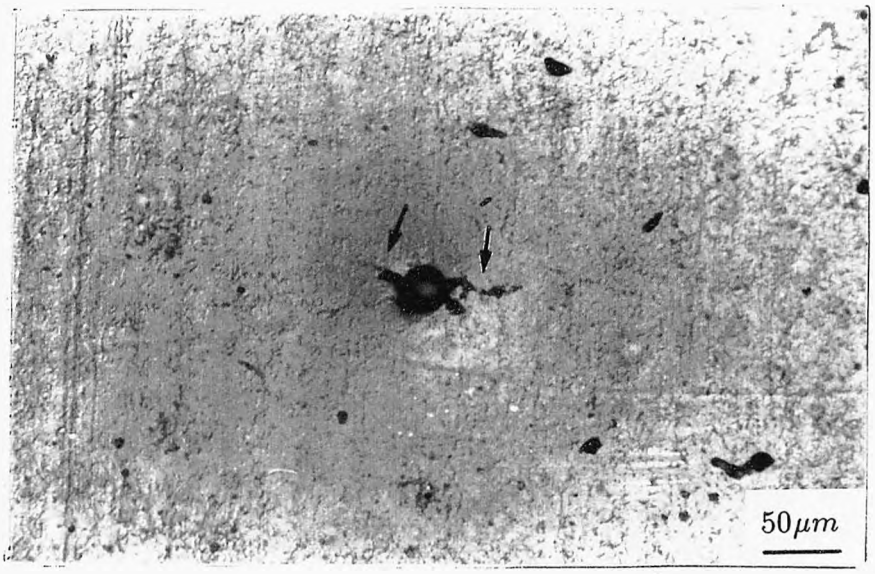

(a) $f = 10$ Hz, $N/N_f = 49\%$

Applied stress

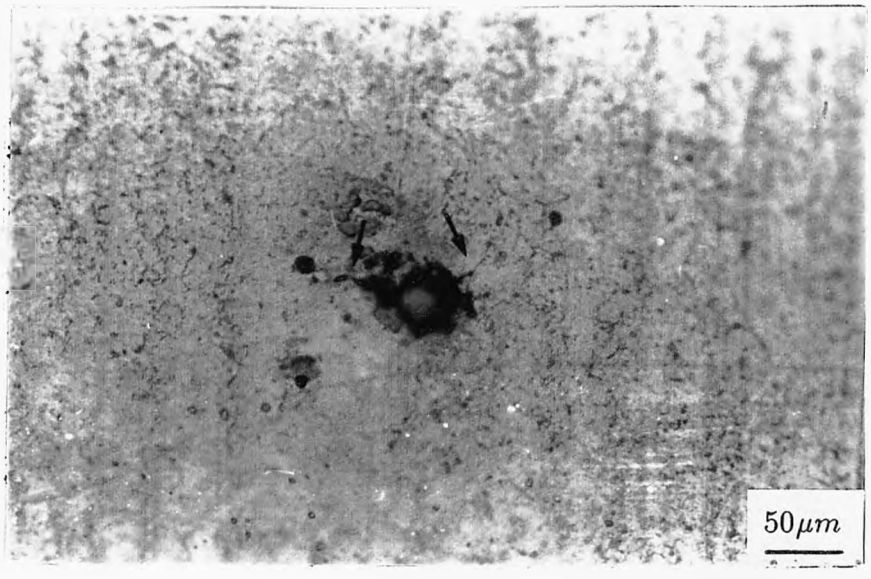

(b) $f = 1$ Hz, $N/N_f = 40\%$

Fig.6.7 Corrosion fatigue crack development at pit sites.

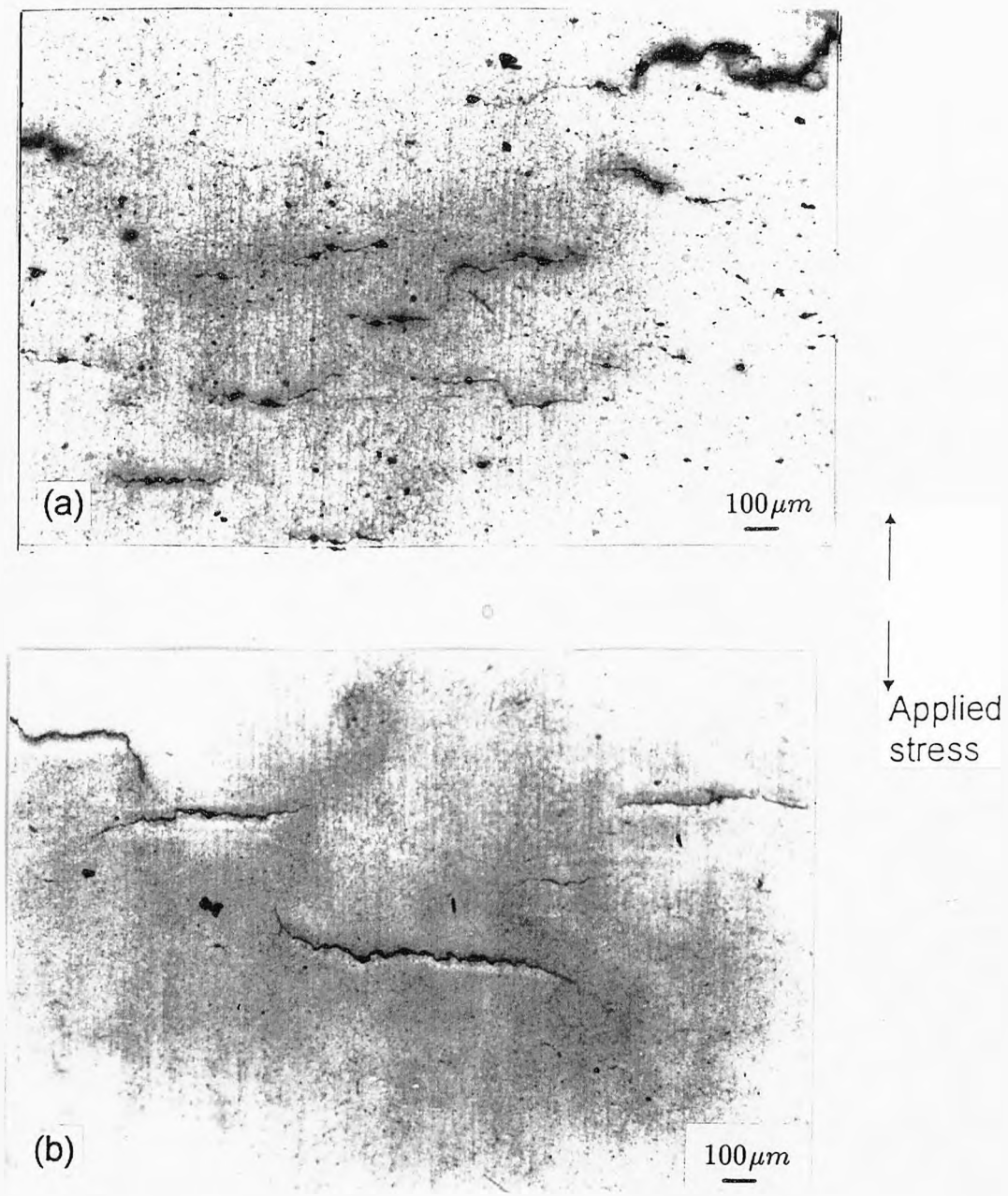

Fig.6.8 Specimen surfaces showing multiple corrosion fatigue crack development, $\Delta\sigma$ =1200 MPa.

(a) $f = 10\ Hz$. (b) $f = 1\ Hz$.

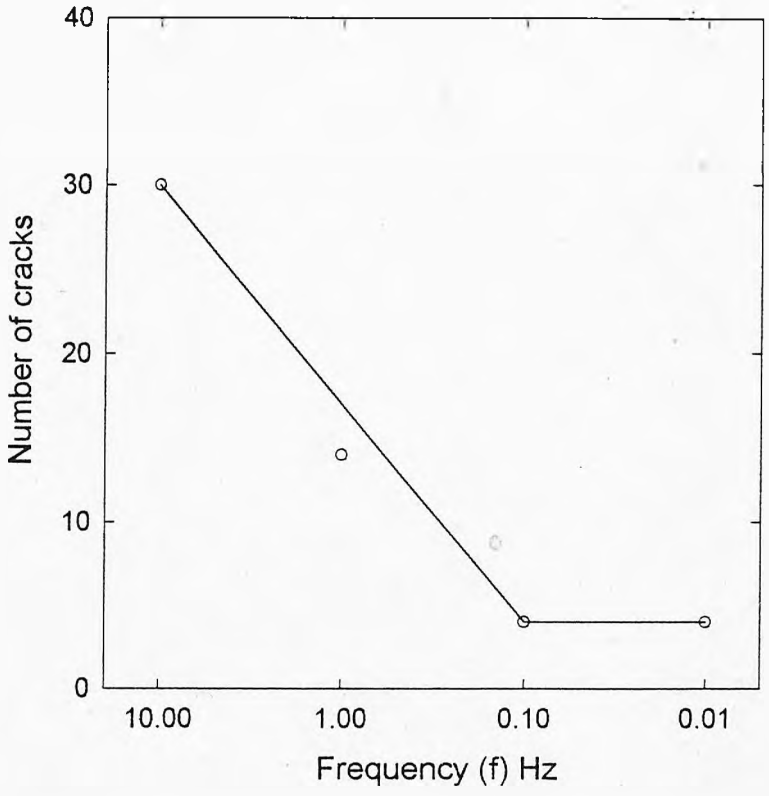

Fig.6.9 Number of surface cracks developed at different cyclic test frequencies.

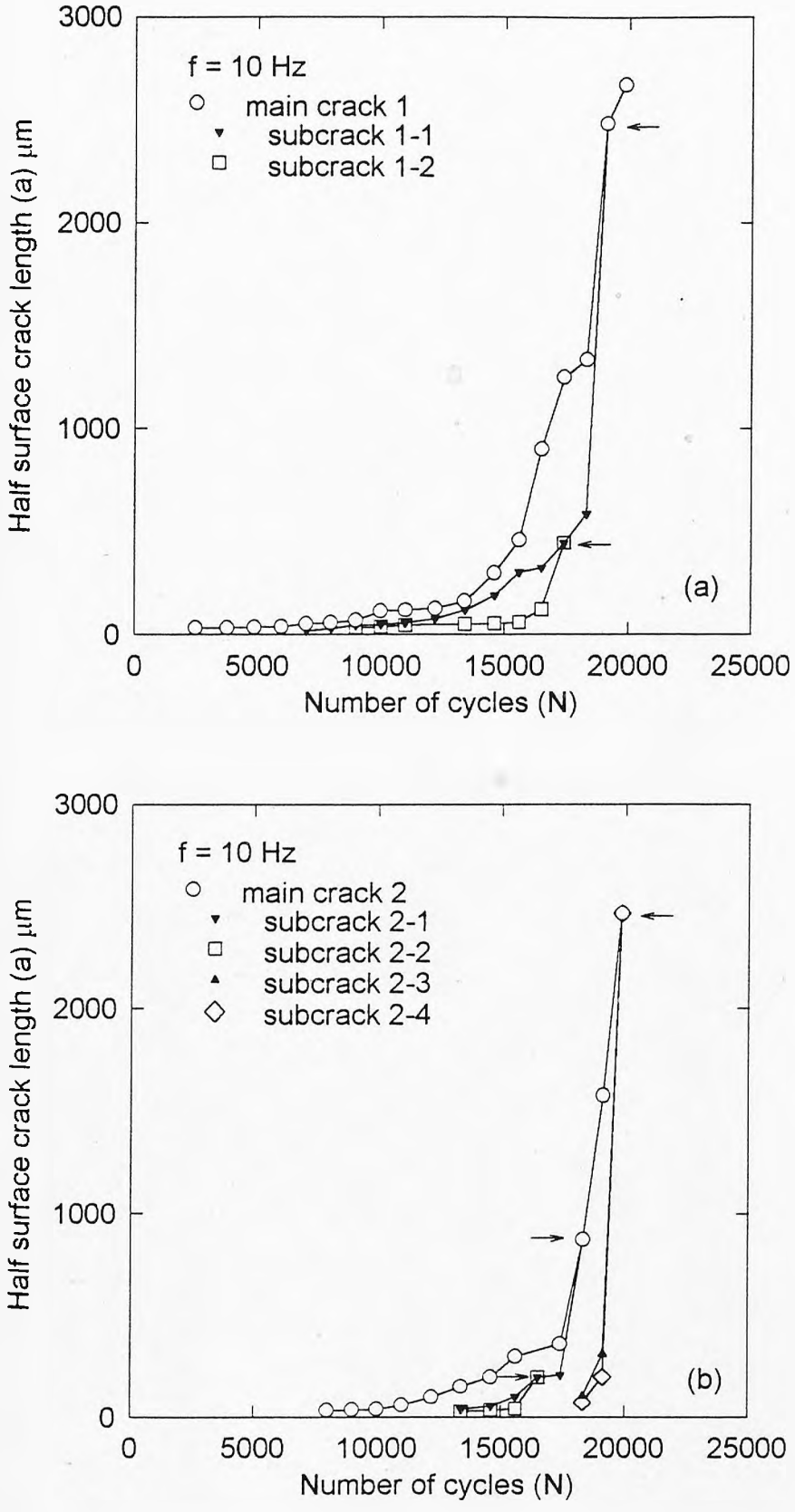

Fig.6.10 Crack length versus number of cycles at a test frequency of 10 Hz.

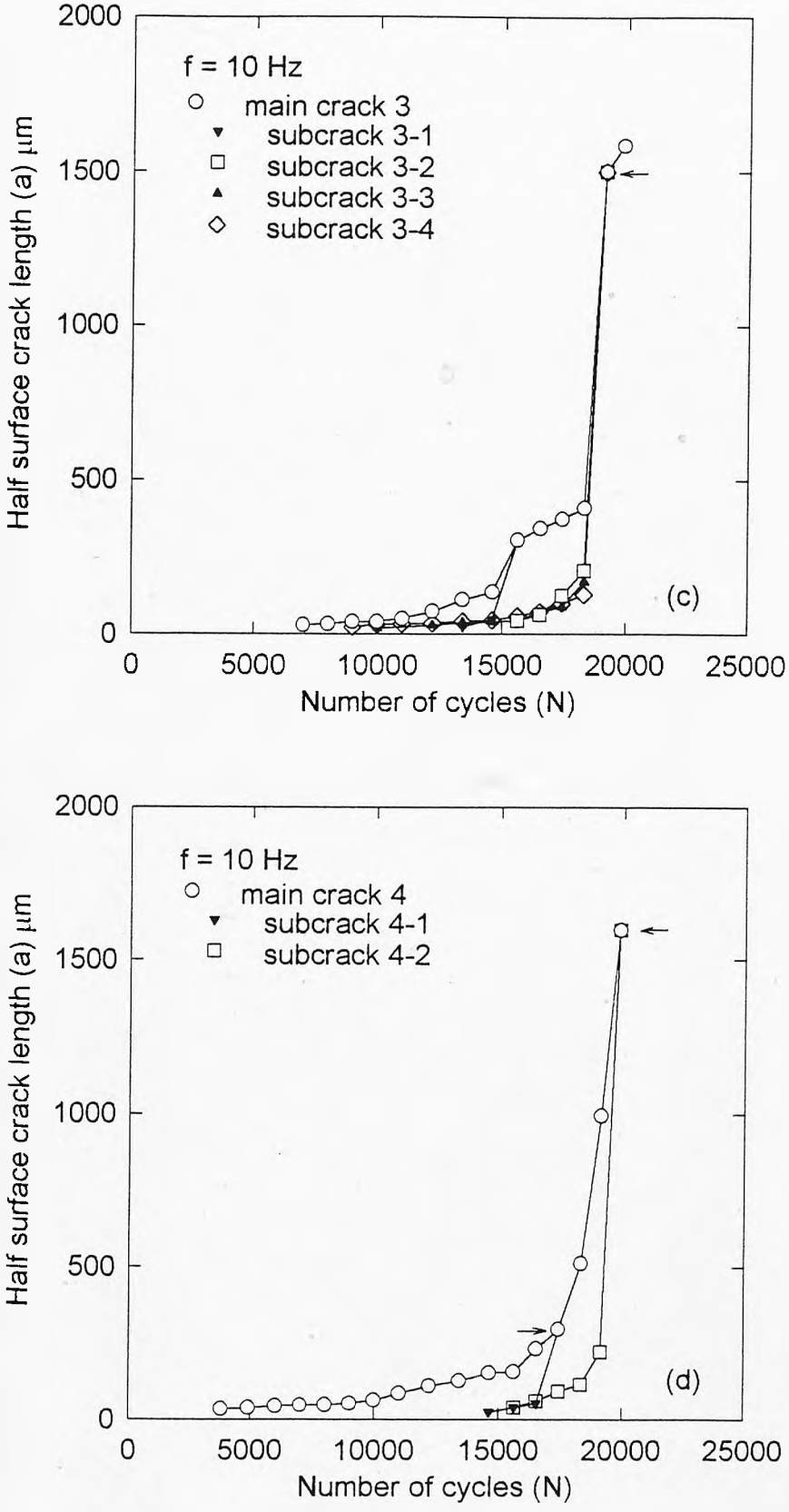

Fig.6.10 Crack length versus number of cycles at a test frequency of 10 Hz.

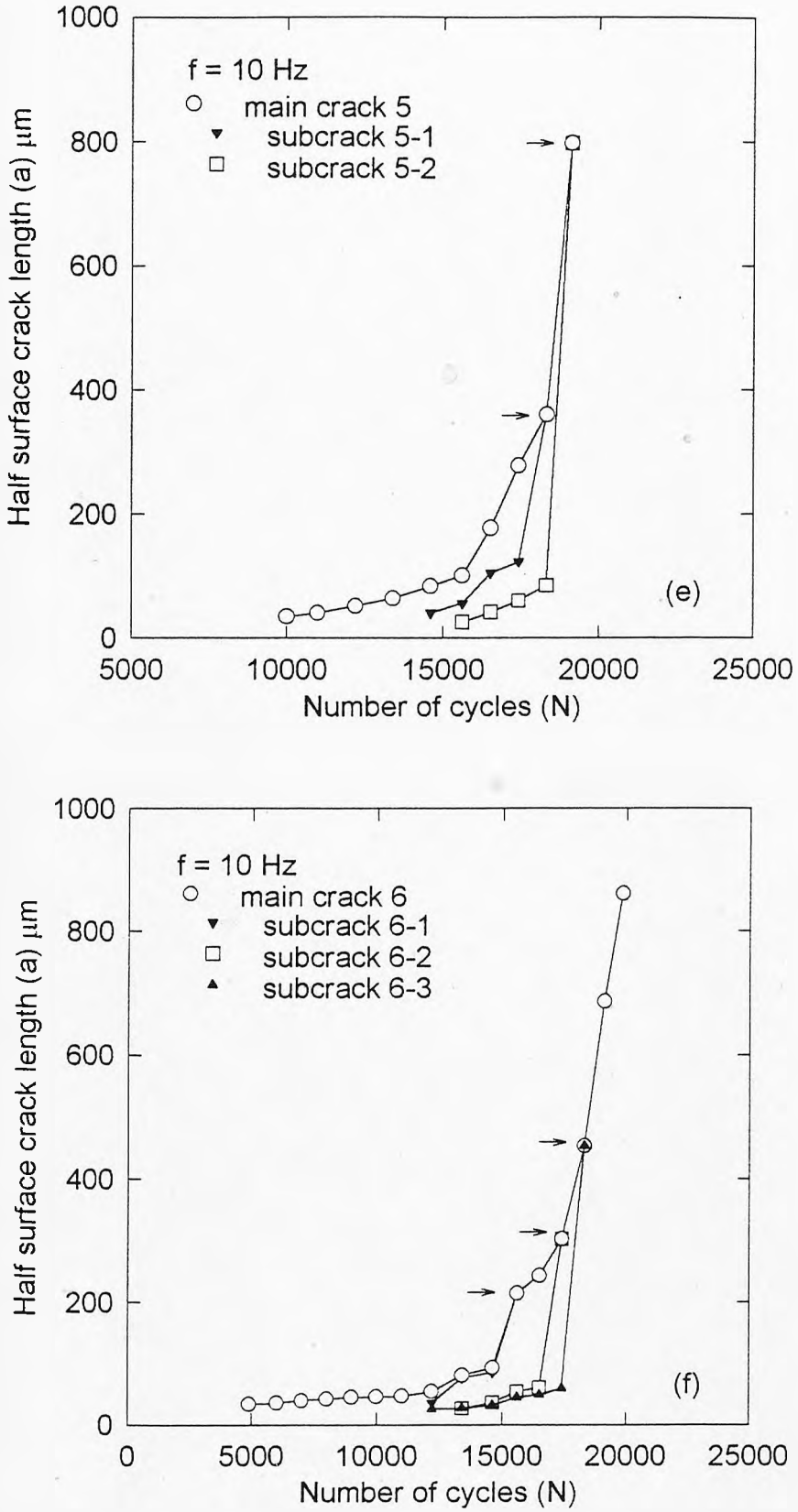

Fig.6.10 Crack length versus number of cycles at a test frequency of 10 Hz.

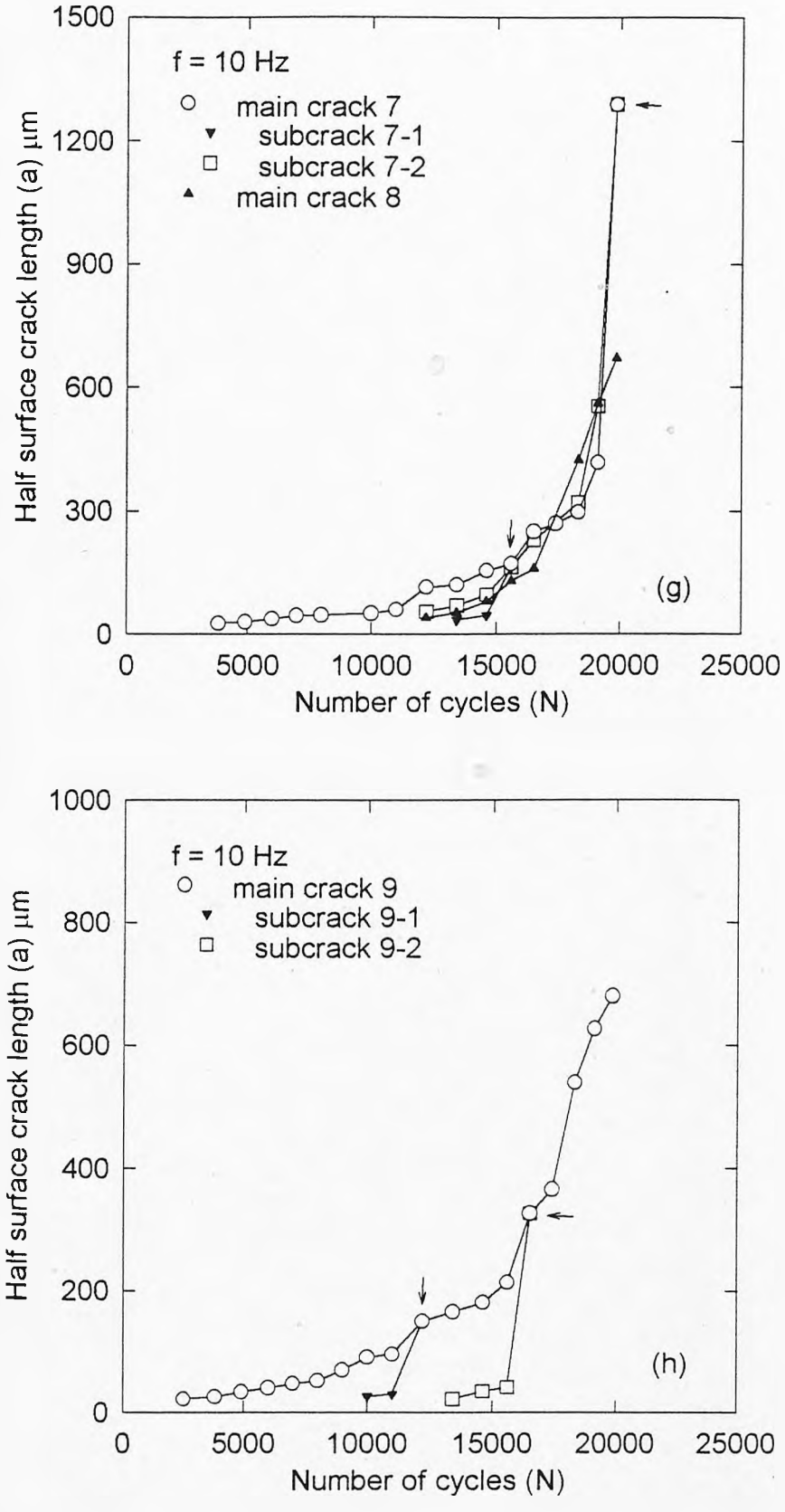

Fig.6.10 Crack length versus number of cycles at a test frequency of 10 Hz.

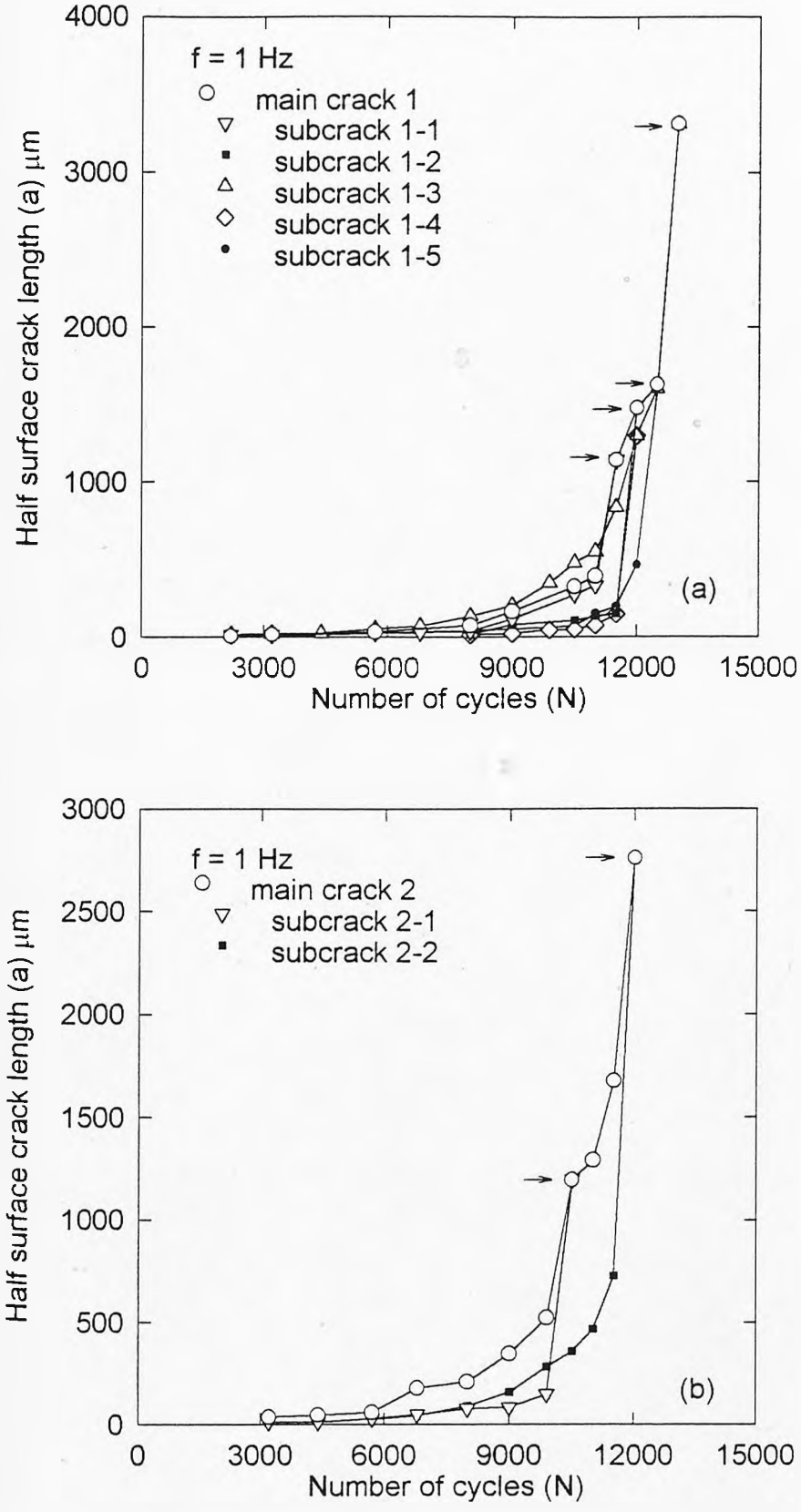

Fig.6.11 Crack length versus number of cycles at a test frequency of 1 Hz.

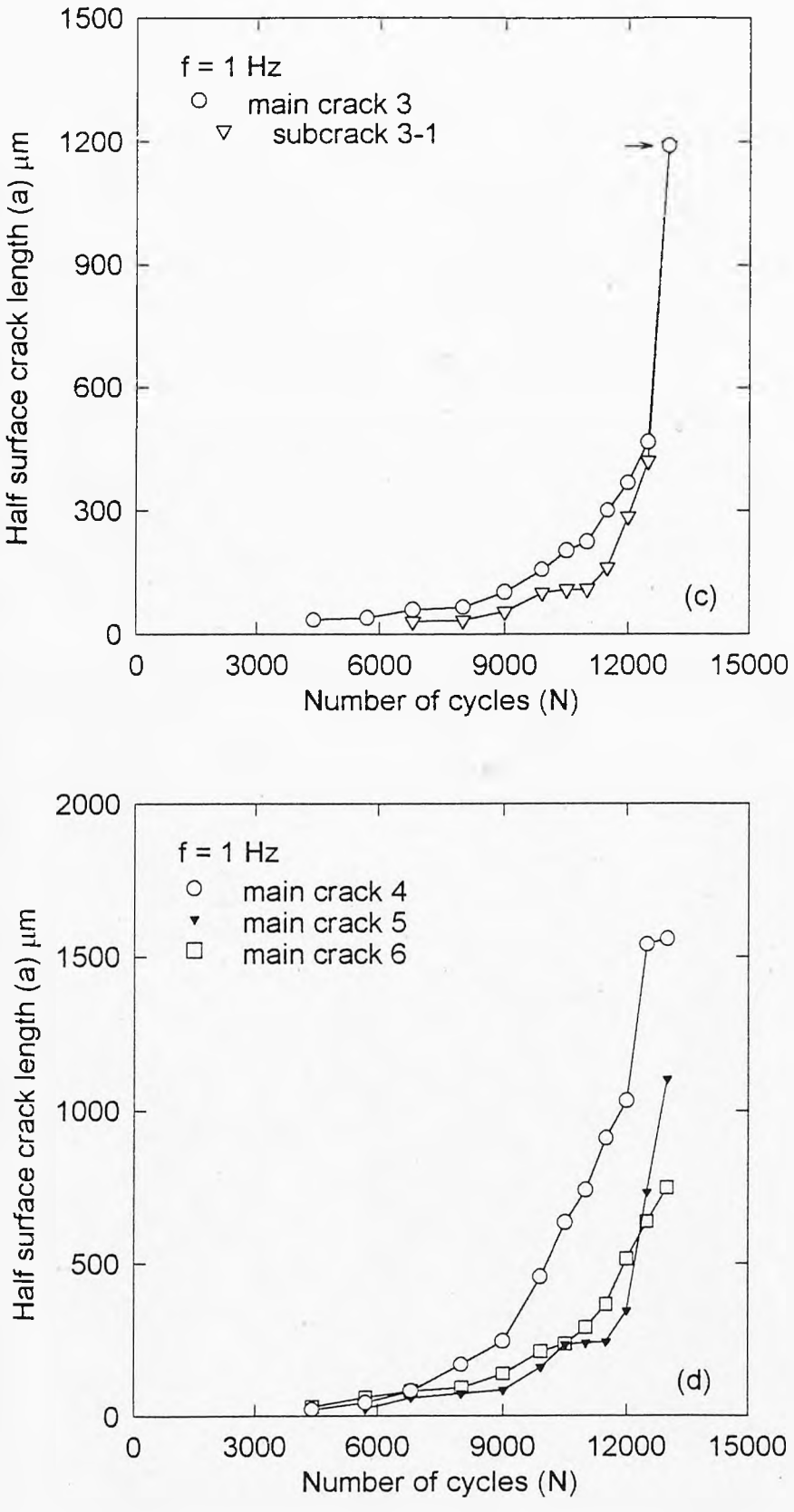

Fig.6.11 Crack length versus number of cycles at a test frequency of 1 Hz.

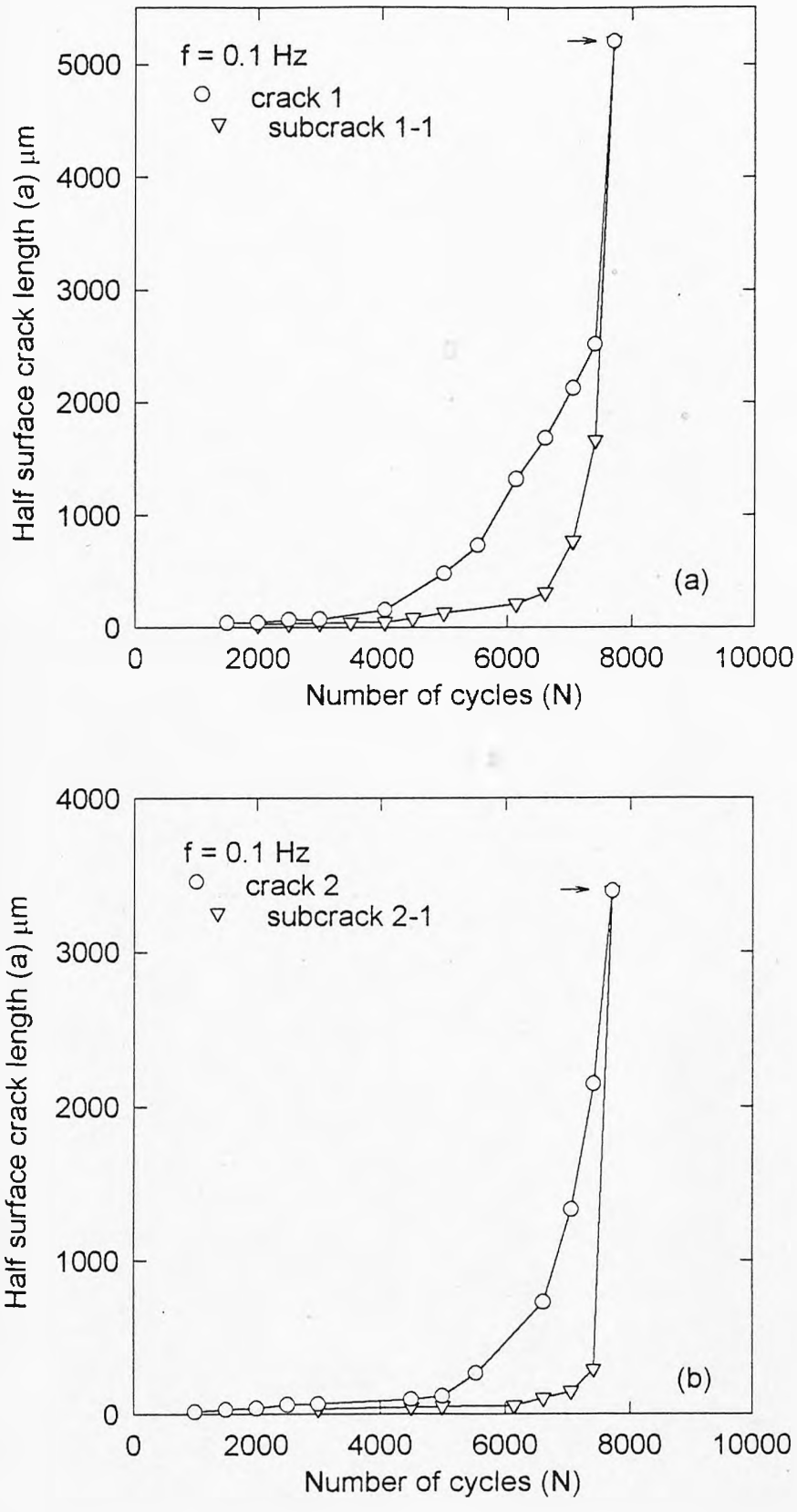

Fig.6.12 Crack length versus number of cycles at a test frequency of 0.1 Hz.

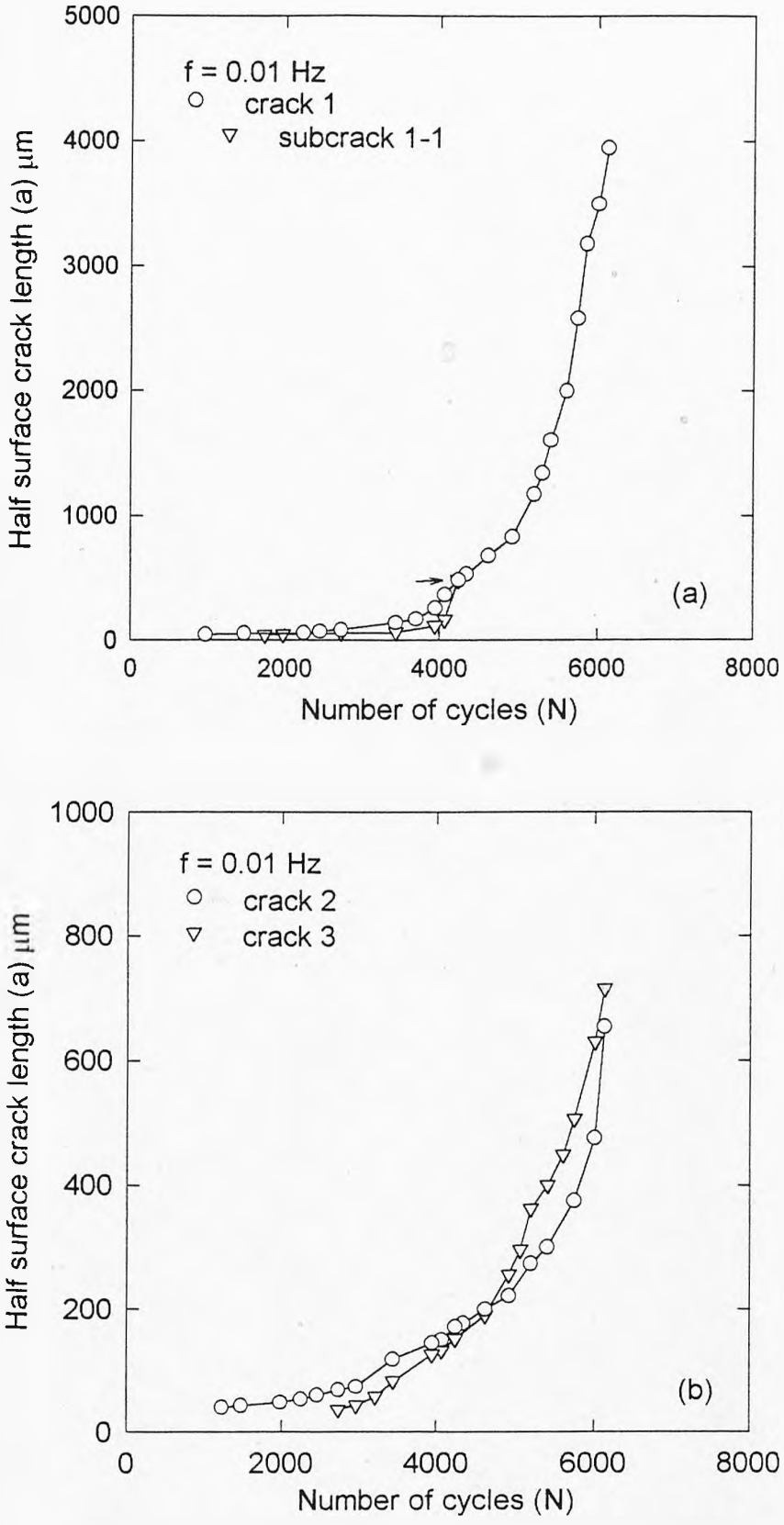

Fig.6.13 Crack length versus number of cycles at a test frequency of 0.01 Hz.

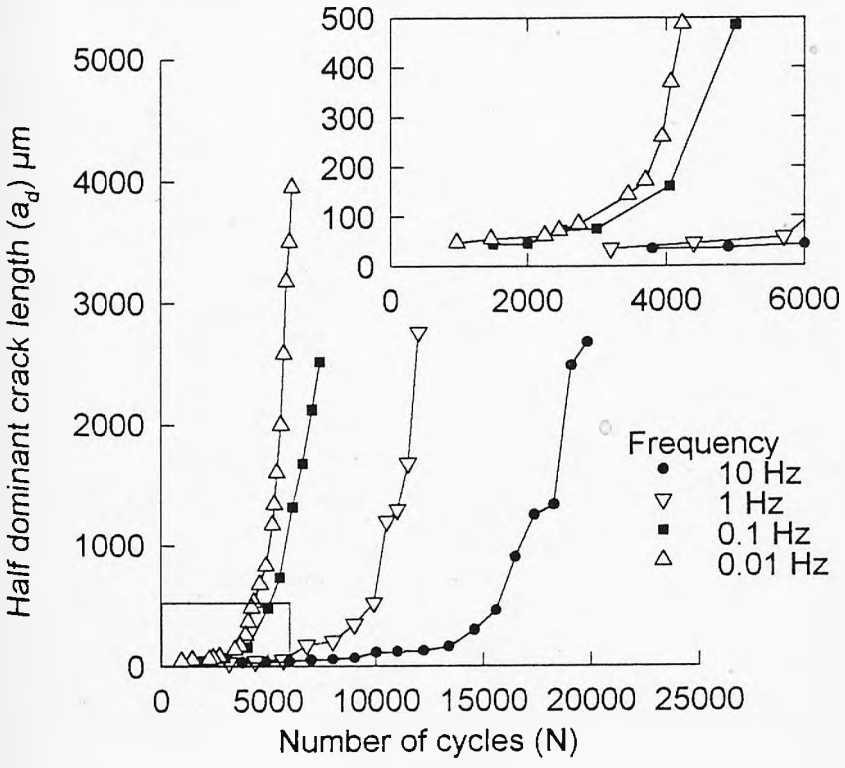

Fig.6.14 Comparison of crack growth behaviour at different test frequencies for tests conducted in seawater.

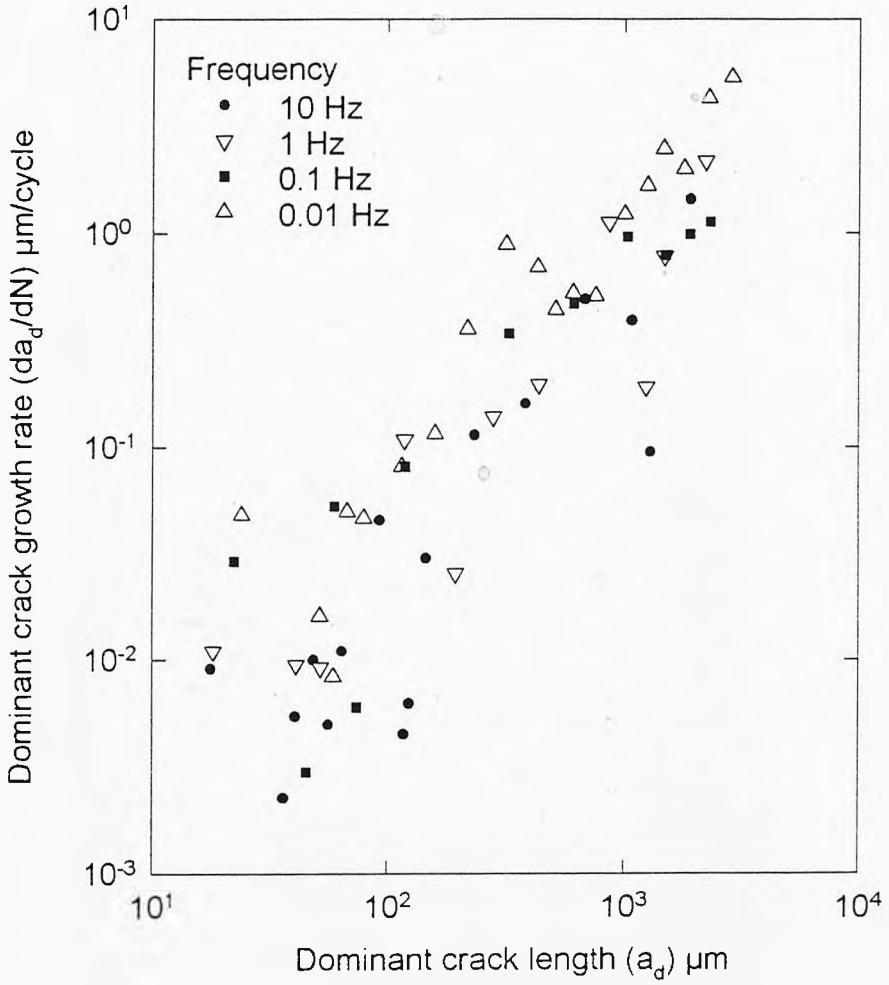

Fig.6.15 Comparison of crack growth rates at different test frequencies for tests conducted in seawater.

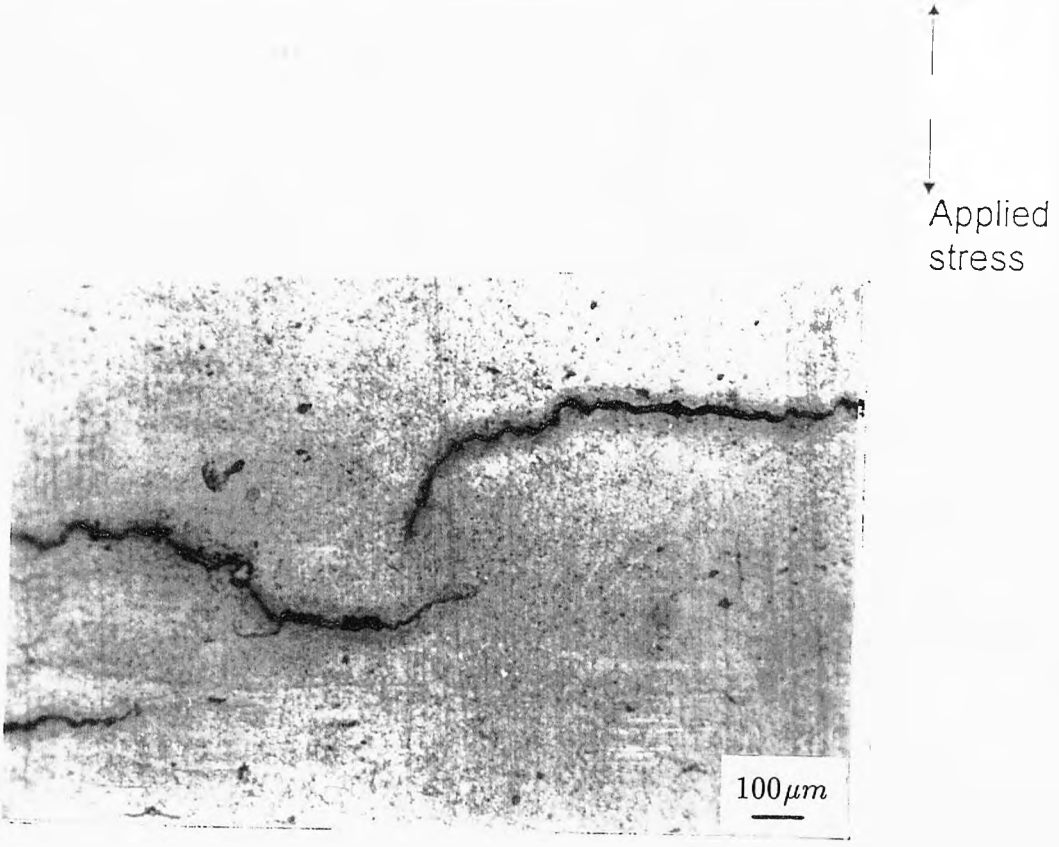

Fig.6.16 Typical example of crack coalescence achieved by the approach of two passing crack tips, $f = 1\ Hz$.

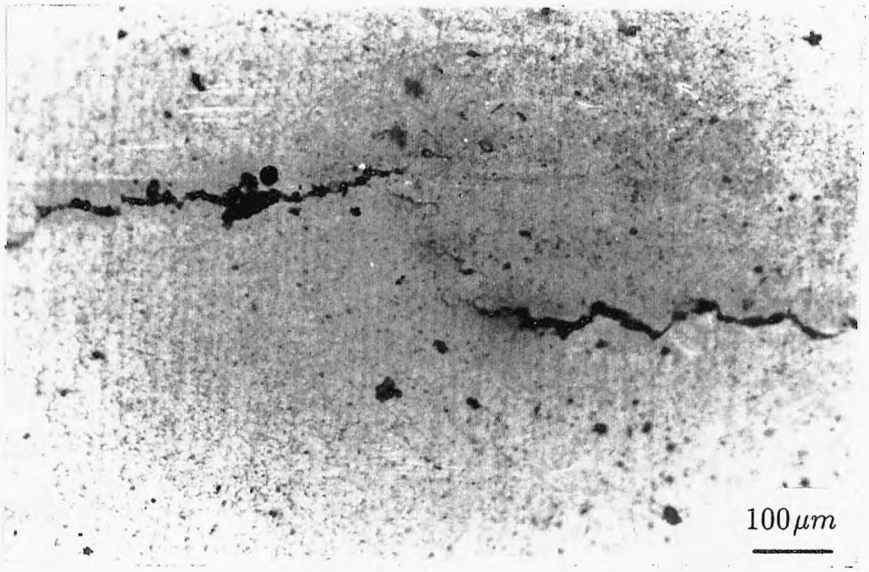

Fig.6.17 Typical example of crack coalescence achieved by the initiation and growth of new cracks between the tips of two adjacent cracks, $f = 1\ Hz$.

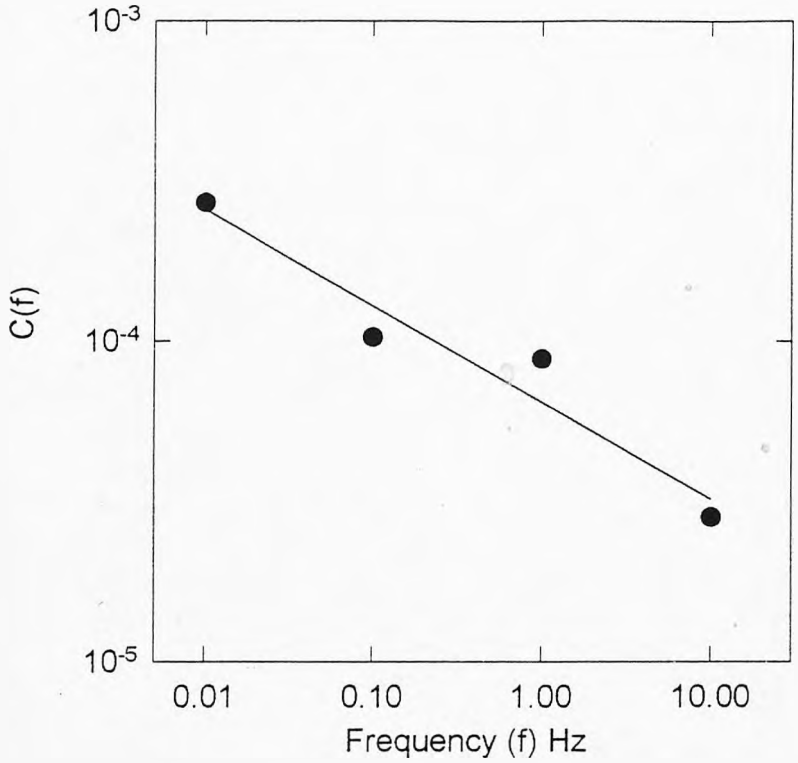

Fig.6.18 Crack growth parameter $C(f)$ as a function of testing frequency for tests conducted in seawater.

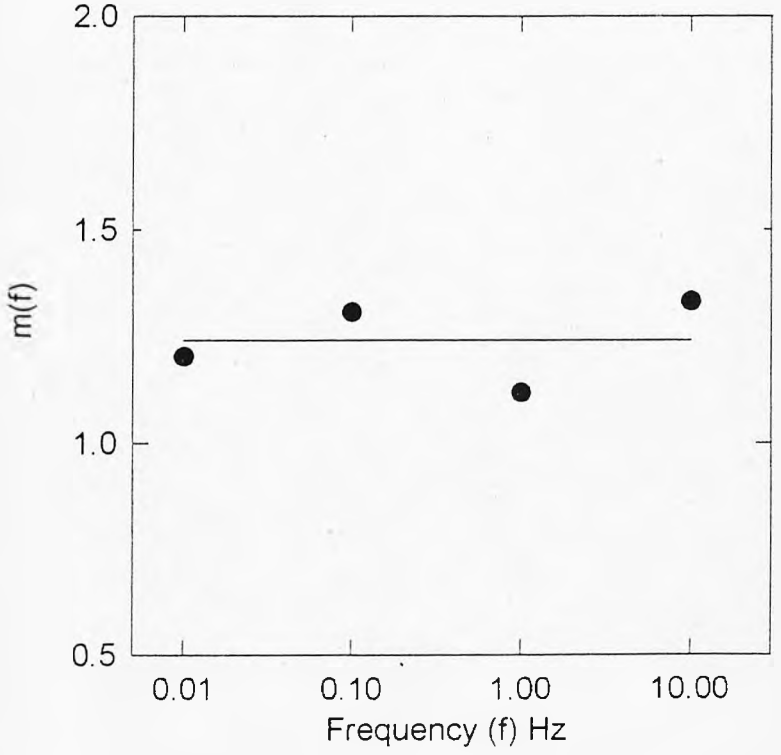

Fig.6.19 Crack growth parameter $m(f)$ as a function of testing frequency for tests conducted in seawater.

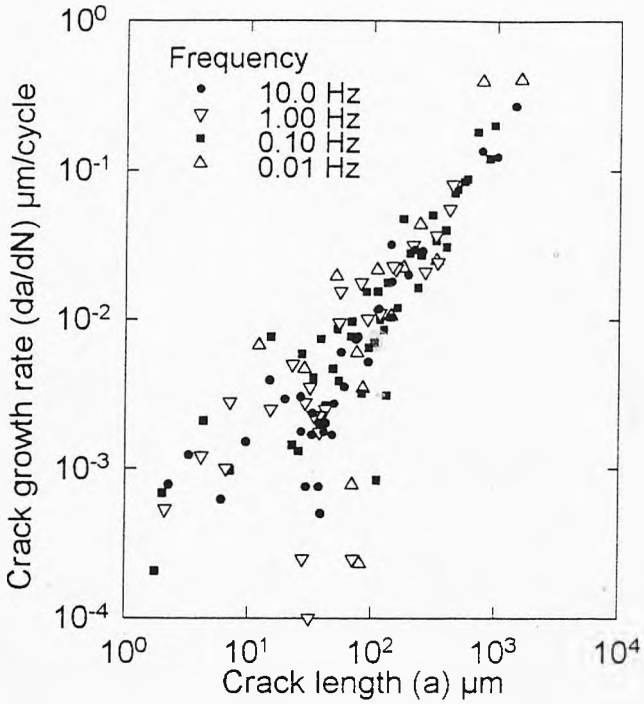

Fig.6.20 Comparison of short crack growth rates at different test frequencies for tests conducted in air.

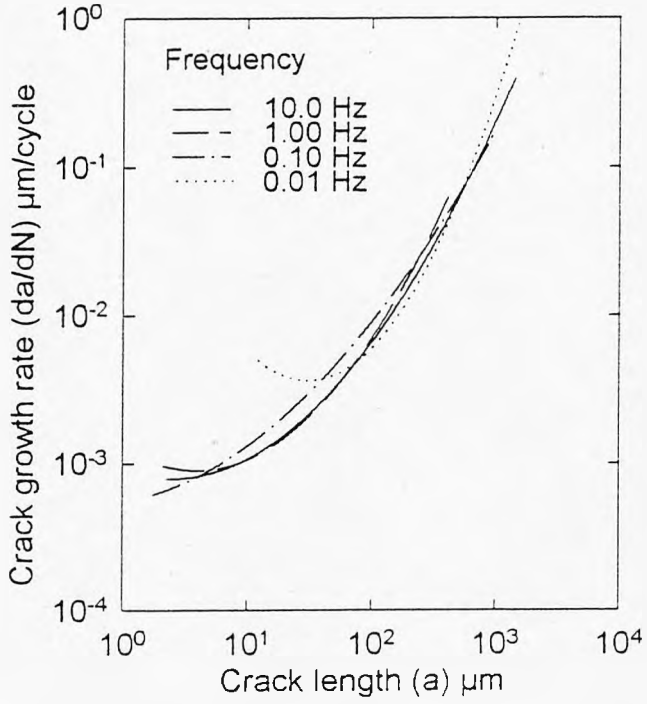

Fig.6.21 2nd order regression lines for in-air short crack growth data obtained at different test frequencies.

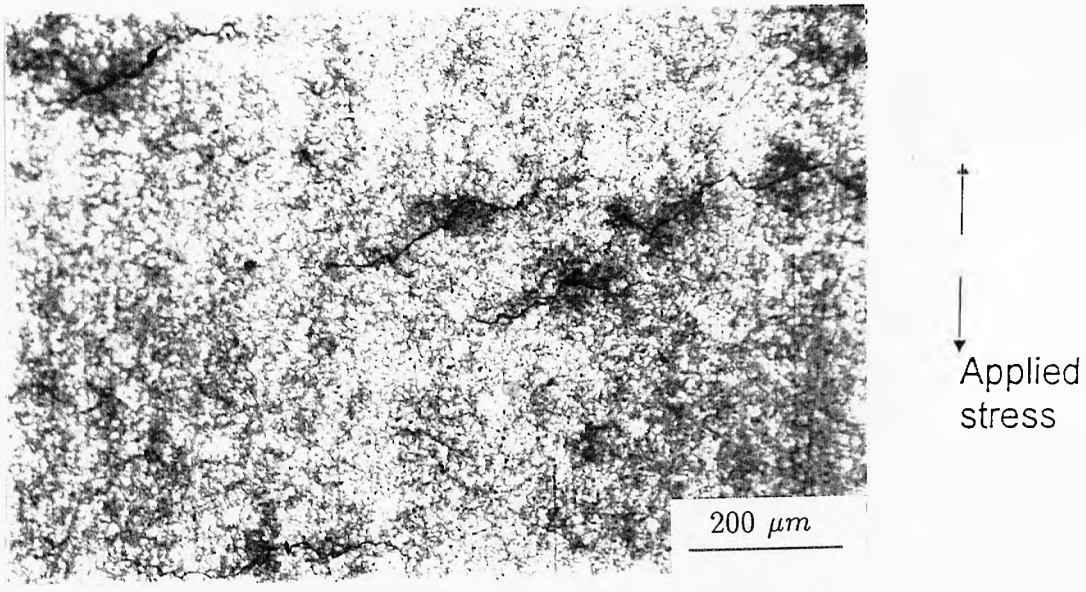

Fig.6.22 Multiple Short cracks on specimen surface at frequency of 0.01 Hz for tests conducted in air.

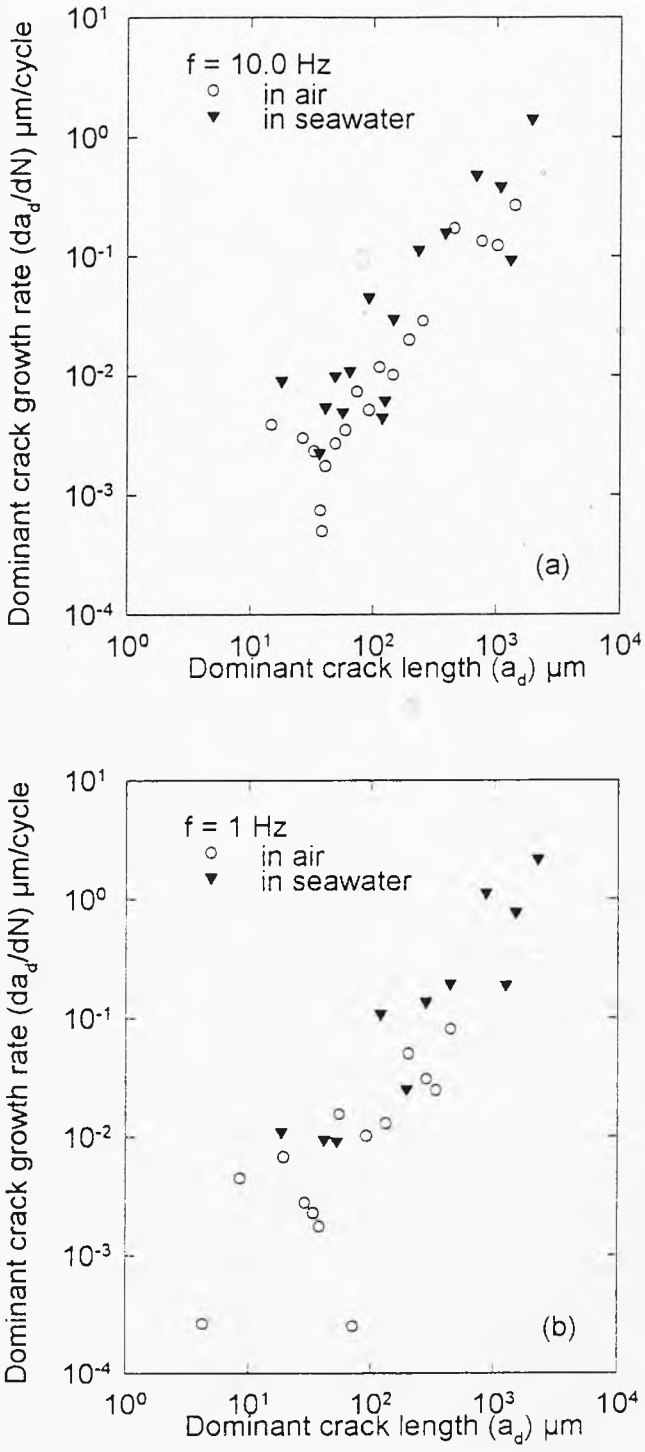

Fig.6.23 Comparison of short crack growth rates in air and in seawater.

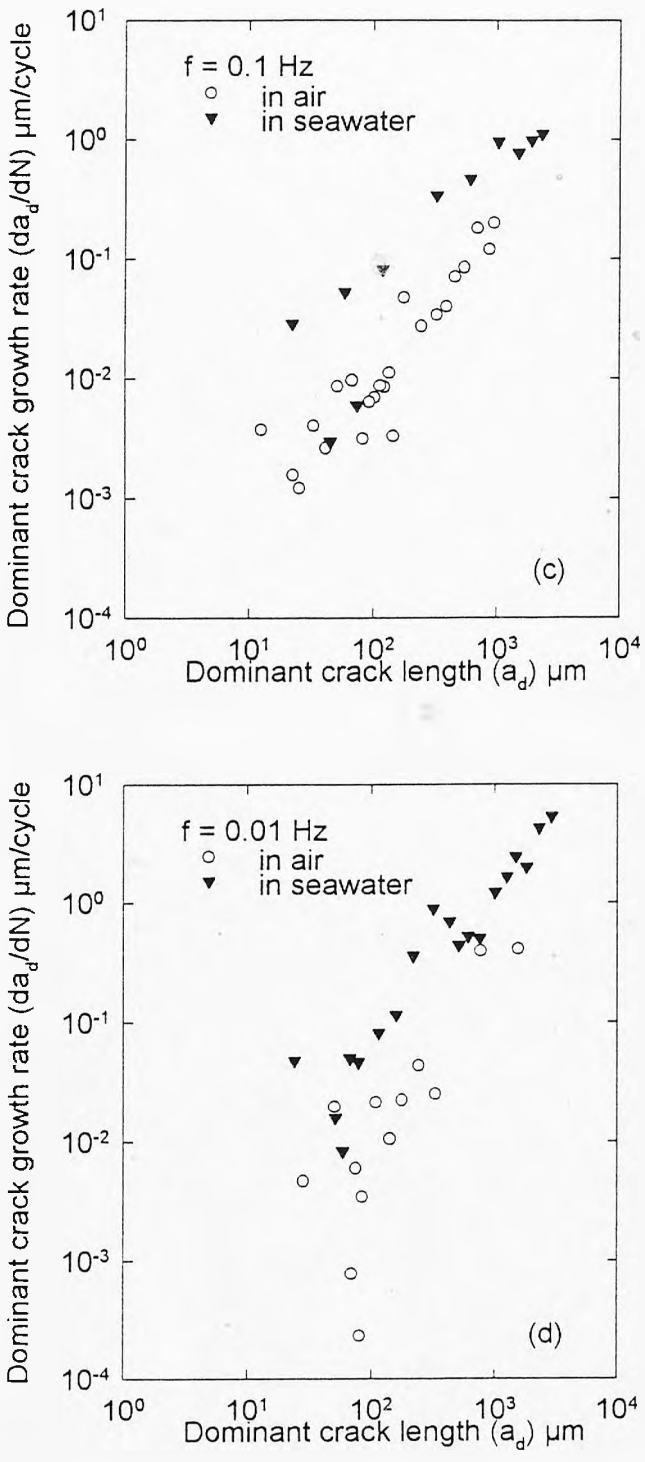

Fig.6.23 Comparison of short crack growth rates in air and in seawater.

Chapter 7

Conclusions and Possible Future Work

7.1 Introduction

Research on short fatigue cracks is becoming increasingly important as technological advances in manufacturing and surface engineering techniques are made and defect detection procedures improve such that smaller initial flaw sizes in critical components may be detected. An essential part of the research associated with that of short fatigue cracks is that of the development of short crack growth models which enable fatigue lifetime to be estimated with high levels of confidence. Furthermore it is necessary to understand the effects of operating environments and loading parameters on crack development in order to utilise laboratory data in real engineering applications. The first part of this chapter summarizes the progress made in this study towards achieving the above objectives, the final section of this chapter offers some recommendations for future work.

7.2 Conclusions

7.2.1 Air Fatigue Crack Growth Results

A series of in-air fatigue tests have been carried out during this study. Observations of the initial development of defects have revealed several main features of short crack growth. These included the initiation of short cracks at non-metallic inclusions, microstructural short crack (MSC) growth along crystallographic planes, physical small crack (PSC) growth cutting across martensite laths and crack growth retardation during the transition from the MSC regime to the PSC regime. Analysis of crack growth data in terms of stress intensity factor ΔK reveals that the initial growth rates of short cracks are faster than those of long cracks at all stress levels. Short cracks are seen to grow at a stress intensity factor range well below the threshold value for a long crack. These characteristics of short crack propagation provide essential information for modelling of short crack growth as discussed in Chapter 4.

7.2.2 Modelling of Short Crack Growth in Air

In order to establish a short crack growth model reflecting the characteristics of short crack growth in the microstructurally short crack (MSC) and the physically small crack (PSC) regimes the plastic zone emanating from the tip of crack is modelled for three cases: (A) a plastic zone that does not reach the PSC regime; (B) a plastic zone partially developed within the PSC regime and (C) a plastic zone entirely developed within the PSC regime. The theory of continuously distributed dislocations was applied to calculate the plastic zone size Δr_p for each

case.

The cyclic plastic zone size, Δr_p, may be used as a control parameter for assessing short crack growth. The short crack growth model obtained for Q2N steel can be expressed as:

$$\frac{da}{dN} = 2.948 \times 10^4 (\Delta r_p)^{0.472} \qquad MSC\ growth$$

$$\frac{da}{dN} = 7.112 \times 10^4 (\Delta r_p)^{0.852} \qquad PSC\ growth$$

Over a wide range of stress levels good agreement is observed between the present crack growth model and the experimental data.

7.2.3 Corrosion Fatigue Lifetime and Crack Growth Results

The corrosion fatigue endurance curve ($S - N$) obtained from tests conducted in seawater shows that the fatigue strength of Q2N steel is strongly influenced by the presence of a corrosive environment, *i.e.*, fatigue lifetime decreases significantly and the in-air fatigue limit was eliminated in the presence of seawater. Observations of the surface of corrosion - fatigue specimens provide evidence of the formation of corrosion pits from which short cracks develop. Short fatigue crack growth rates are significantly enhanced in the presence of seawater.

The minimum crack growth rates, observed from air fatigue tests, are much lower than those equivalent tests in seawater suggesting a corrosion fatigue crack growth mechanism consistent with the conjoint action of chemical and mechanical processes operating to overcome the resistance of the microstructural barrier.

7.2.4 Modelling of Corrosion Pitting and Short Crack Growth

Analysis of surface replicas obtained from corrosion fatigue test shows that corrosion pit growth appears to be the dominant defect growth process occurring during the initial stages of the corrosion fatigue lifetime. This type of defect growth is assumed to occur until the defect is of a size that it may be considered to be a physically small crack.

The corrosion pit growth and short crack growth for this material/environment system were modeled in terms of the time ratio of t/t_f and the size of the cyclic plastic zone at the crack tip respectively. Here t and t_f represent time and the time corresponding to the final fatigue failure.

Based on the model described above fatigue lifetime has been estimated. From the results of this modelling an acceptable estimation of corrosion fatigue lifetime is obtained.

7.2.5 Influence of Test Frequency on Fatigue Behaviour

Fatigue tests covering the loading frequency range of 0.01 to $10Hz$ have been conducted under both air and seawater conditions. The information obtained from this series of tests shows that in air frequency has little effect on the fatigue strength of this material although a slight reduction in fatigue lifetime was noted at the lowest frequency of 0.01 Hz. However the fatigue strength of this steel in seawater is strongly dependent on cyclic frequency, *i.e.*, the fatigue lifetime decreases significantly on lowering of the applied cyclic frequency.

As test frequency increases multiple short fatigue cracks are observed for the seawater tests. During the development and growth of these multiple cracks two forms of crack coalescence were observed, that is, (a) two slightly misaligned cracks grow so that their closest tips pass beyond one another for a small distance before turning and growing towards the opposite crack; (b) new subcracks initiate between the closest tips of two adjacent cracks and then grow rapidly to connect the two adjacent cracks.

A short crack growth model reflecting the influence of loading frequency has been proposed to estimate frequency effects on the short crack growth of Q2N in seawater.

7.3 Recommendations for Future Work

Several interesting points were derived from this study and recommendations for future work are summarized below.

Surface Finish

In the current study models of short crack growth in both air and seawater have been proposed based on the analysis of the experimental data obtained from highly polished specimens. However, many engineering components do not have a high standard of surface finish and the microstructural-dependent short crack growth behaviour associated with different surface finishes is still not fully understood. Further studies are required to quantify the effect of surface finish on initial defect development.

Loading Parameters

Loading modes such as push - pull, bending and torsion are known to have a large effect on short crack growth behaviour. Both experimental work and theoretical analysis are needed to develop a appropriate equivalent stress model in order to correlate the current model, based on bending tests, to other loading conditions.

Welding Effects

The material tested in this study, that is Q2N, is largely used in marine applications such as submarine hulls and warship hulls. A large majority of these structures are found in the welded conditions. Fatigue crack initiation and growth is likely to occur at such welded joints owing to (i) welding-induced tensile residual stresses remaining after the welding processes and (ii) the influence of the welding process on the adjacent parent microstructure. Fatigue tests on welded joints or simulated heat affected zone type microstructure would provide useful data which may be used to extend the current results to these realistic applications.

Frequency Effects

Frequency effects on short crack growth behaviour have been studied in both air and seawater conditions. However results obtained to date are limited at one relative high stress level. Further work is needed to gain an understanding of frequency effects at different load levels and hence lifetimes.

Crack Coalescence

It is well recognised that corrosion fatigue loading gives rise to multiple cracking and the development and subsequent coalescence of multiple cracks can significantly effect the lifetime of a component. In this respect the current work on short crack coalescence is worthy of extension. Such work

would aim to develop a new model which incorporates both continued crack nucleation and propagation with increasing number of cycles and crack coalescence. Specific criteria for coalescence events which contribute the formation of a major failure crack would form a necessary part of this revised model.